Variability of Equatorial Currents at 10°W and at 23°W

par

Lucia Gabriela Bunge Vivier

Composition du jury:

Président du Jury:	Claude Frankignoul, LOCEAN, Professeur Paris VI
Rapporteur:	Michael Mc Phaden, NOAA/PMEL, Senior Research Scientist
Rapporteur:	Yves Gouriou, IRD, Chargé de Recherche
Examinateur:	Lien Hua, Ifremer,
Examinateur:	Bernard Bourlès, IRD, Chargé de Recherche
Directeur de thèse:	Christine Provost, CNRS, Directeur de Recherche

Table des Matières

Résumé 1

Introduction 2

Chapitre 1: Variability of the Horizontal Velocity Structure in the Upper 1600 m of the Water Column on the Equator at 10º W 10

Chapitre 2: Variability in Horizontal Current Velocities in the Central and Eastern Equatorial Atlantic in 2002 44

Chapitre 3: Variability at Intermediate Depths at the Equator in the Atlantic Ocean in 2002-2005: Equatorial Deep Jets and Low-Frequency Meridional Flows 65

Chapitre 4: 13-Day Period Oscillations in Spring 2004 79

General Conclusions and Perspectives 101

References 104

Résumé

La variabilité de l'Atlantique équatorial en surface (premiers 300 m) et à profondeur intermédiaire (700-1700 m) a été examinée à partir des donnés courantométriques obtenues au cours de 6 années (2000-2005). Certains jeux des données proviennent du centre du bassin, à 23ºW, et d'autres de l'entrée du Golfe de Guinée, à 10ºW. Les donnes à deux régions différent on permis de comparer la cohérence de la variabilité entre régions ainsi comme de faire le suivi de la propagation de signaux.

Près de la surface, dans la bande de périodes intra-saisonnières, la variabilité au printemps est domine par des ondes a une période de 13-14 jours forcées par les vents. Selon l'année, cette oscillation peut montrer une signature en température de surface (SST). En 2004, le signal en SST a été particulièrement fort et cela nous a permis d'associer l'oscillation a 13 jours à une onde stationnaire du type mixte Rossby-gravité. En été et automne, la variabilité observe est principalement due a des ondes crées par le cisaillement entre courants zonaux. Ces ondes, mieux connues sous leur nom anglais de « tropical instability waves » (TIW), présentent une forte signature en température de surface (SST). Les images de SST ont permis l'observation de différent types d'anomalies de SST lies aux TIW, suggestive de différent types de TIWs.

L'analyse de la variabilité aux profondeurs intermédiaires montre le découplage entre les composantes horizontales de la vitesse. La composante méridienne de la vitesse présente des oscillations quasi-périodiques de 14 jours au printemps boréal et de 20-30 jours en automne boréal. La similitude dans la période et dans la saisonnalité de ces signaux avec celles observées près de la surface, suggère un lien entre les deux profondeurs. A 23ºW, la composante méridienne montre aussi des éventements de longue durée et faible amplitude. En effet, les donnes à 23ºW suggèrent que ces échanges interhémisferiques ont des périodicités de environ 10 mois, amplitudes de 5 cm/s et échelles verticales de 600 m.

La composante zonale aux profondeurs intermédiaires est caractérisée par la présence des jets équatoriaux profonds (EDJ), les quelles sont cohérent entre les deux régions. On trouve trois différentes échelles de temps pour les jets ; 7 mois, 18 mois et 5 ans. Superpose aux signaux des EDJ, on trouve aussi un cycle saisonnier avec une amplitude d'environ 8 cm/s et aux échelles verticales beaucoup plus larges en relation aux EDJ.

Introduction

The equatorial Atlantic region extends roughly from 10ºS - 10ºN and from 10ºE - 45ºW. The ocean is forced by the atmosphere through the Trade winds, northeasterly and southeasterly winds that converge in the equatorial region, generating Ekman divergence on the equator and downwelling to the south and north of it. In the atmosphere, where the Trade winds converge, there is a zone of strong convective activity, called the Intertropical Convergence Zone (ITCZ), which moves seasonally from around 3ºS in March-May to 10ºN in September-November. In the ocean, the equatorial circulation (Fig. 1) also exhibits strong seasonal variability and shows several zonal currents of small meridional and vertical scales (Stramma et al., 2003). The main near surface equatorial currents are the South Equatorial Current (SEC) flowing to the west between 3ºN and 8ºS, and the North Equatorial Counter Current (NECC) flowing to the east between 3ºN and 8ºN. Below the SEC, between 50 m and 300 m and centred at the equator, there is a strong eastward jet called the Equatorial Undercurrent (EUC). At intermediate depths, the mean currents are less documented. Nonetheless, intensive surveys at 35ºW have suggested the existence of a permanent westward current, the Equatorial Intermediate Current (Schott et al., 2003). The EIC is found below the EUC and extends to approximately 1000 m depth (Fig. 2).

The seasonal cycle is the largest atmosphere-ocean signal in the tropical Atlantic. At the equator, weak and variable winds prevail from January trough May when the ITCZ is in its southernmost position. As the ITCZ migrates northward, the south-easterly trade winds pick up and the winds along the equator intensify. Coupled with the wind velocities, the sea surface temperature (SST) along the equator also varies with a strong annual cycle. In the eastern tropical Atlantic, SSTs reach their maximum values in boreal spring, when the equatorial winds are weakest. As the year progresses, the trade winds along the equator intensify displacing

eastern surface waters to the west. The resulting zonal pressure gradient in the ocean and associated uplifting of the thermocline leads to the cooling of SST in the eastern region. The upwelling in the Gulf of Guinea is an ongoing subject of study, since the magnitude and phase of the cold tongue cannot be explained by the forcing of local winds only (Picaut, 1982). As expected, the intensification of the zonal winds also leads to the intensification of the main surface currents.

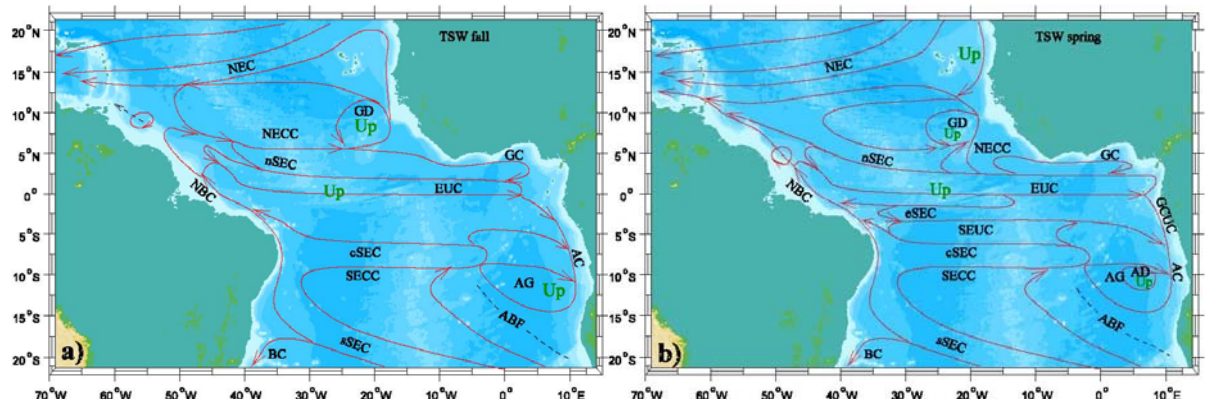

Figure 1: Schematic maps showing the horizontal distribution of the major tropical currents for the Tropical Surface Water layer at about 0-100 m depth for a) the northern spring and for b) the northern fall. Shown are the North Equatorial Current (NEC), the Guinea Dome (GD), the North Equatorial Countercurrent (NECC), the Guinea Current (GC), the South Equatorial Current (SEC) with the northern (nSEC), equatorial (eSEC), central (cSEC) and southern branches (sSEC), the Equatorial Undercurrent (EUC), the North Brazil Current (NBC), the Gabon-Congo Undercurrent (GCUC), the Angola Gyre (AG), the Angola Current (AC), the Angola Dome (AD), the South Equatorial Undercurrent (SEUC), the South Equatorial Countercurrent (SECC) and the Brazil Current (BC). The Angola-Benguela Front (ABF) is included as a dashed line. "Up" marks possible areas of upwelling. (after Stramma et al., 2003).

There are two modes of coupled ocean-atmosphere variability in the Tropical Atlantic affecting the weather in South America and Africa on annual and interannual time scales (Servain et al., 1998). The first mode is akin to the El Nino-Southern Oscillation (ENSO) in the Pacific, showing anomalous weak trade winds and warm SSTs during the warm phase and opposite conditions for the cold phase (e.g. Merle, 1980). The second mode is called the Atlantic

dipole and consists of a north-south interhemispheric gradient in SST, intimately related to the position and intensity of the ITCZ (Nobre and Shukla, 1996). To the extent that sea surface temperatures (SSTs) are primarily driven by changes in surface winds, interannual variability in the equatorial Atlantic is mainly due to variations in the surface winds. Those variations can be forced either remotely or locally. The main variations in the remote forcing can be associated to events or variability over extratropical regions in the Atlantic while variations in the local forcing are due to changes in the position and intensity of the ITCZ (e.g. Chiang et al., 2002).

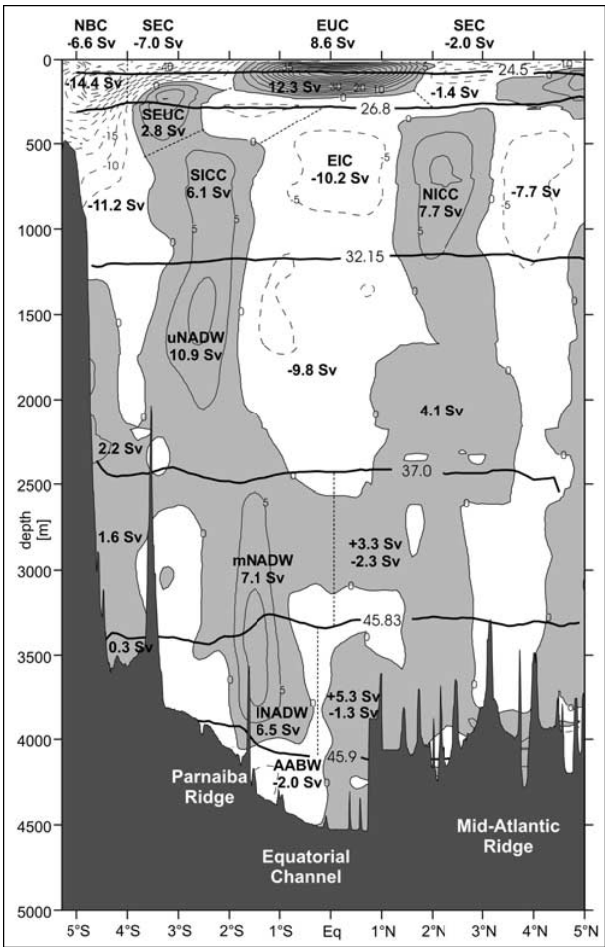

Figure 2: Mean zonal current distribution across 35ºW from the 13 sections, with transports (in Sv = 10^6 m^3/s) of the different current branches (from Schott et al., 2003).

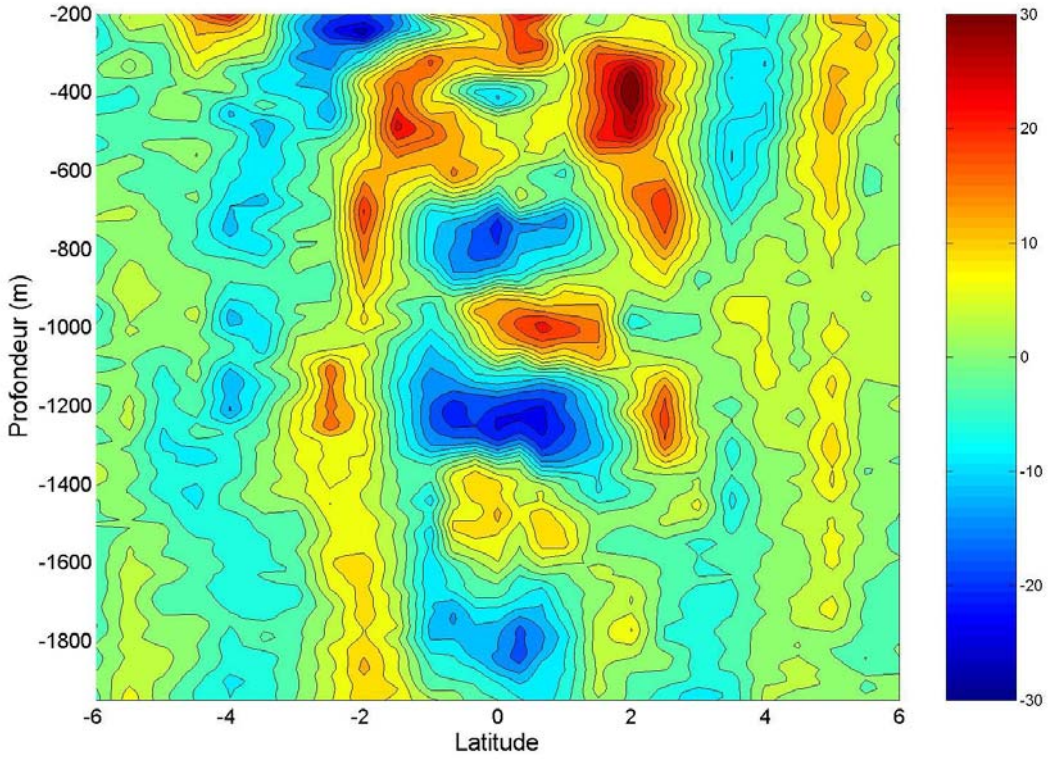

Figure 3: Meridional section of zonal velocity at 23ºW from EQUALANT campaign (Gouriou et al., 2001). Velocity units are in cm/s; positive values are eastward and negative values are westward. At the equator, Equatorial Deep Jets are easily detected and are confined between 2°N and 2°S. They have vertical scales of approximately 500 m and velocity magnitudes of more than 10 cm/s.

Near the surface, intraseasonal variability is due to many different processes. Among them are the forcing by intraseasonal winds and heat fluxes, and intrinsic mechanisms of the oceans like instabilities due to the velocity shear between zonal currents (Kessler, 2004). Although of smaller amplitude than the seasonal cycle, intra-seasonal variability can also play a role in climate variability. Results from Ocean General Circulation Model (OGCM) solutions suggest that intraseasonal atmospheric forcing acts to weaken the equatorial seasonal surface currents (Han, 2004) and that Tropical Instability Waves (TIWs) are potentially important in influencing the phase of the seasonal cycle and the position of the equatorial cold tongue and ITCZ (Jochum et al., 2003). In the Pacific Ocean, strong intraseasonal variability in the western Pacific is

observed at the onset stages of El Nino events (e.g. McPhaden and Yu, 1999) and there is an ongoing debate on the role of intraseasonal variability in the ENSO cycle. In part because of this debate, most of the work on oceanic intraseasonal variability has been done in the Pacific and Indian Oceans. The few recent observational studies of intraseasonal variability in the Atlantic Ocean have principally focused on TIWs. They show that TIWs have a fully three dimensional circulation sustaining an entire ecosystem in the region (Menkes et al., 2002); that TIWs are equally maintained by baroclinic and barotropic conversions (Grodsky et al., 2005); and that TIWs present strong interannual variations and have an impact on the ITCZ position and intensity (Caltabiano et al., 2005).

At intermediate depths, velocity snapshots in all three equatorial oceans have shown vertically stacked alternating eastward and westward jets with small vertical scales. In the Atlantic (Fig. 3), these jets present vertical scales of 400-600 m (Gouriou et al., 1999; Bourles et al., 2003), but their temporal nature is not well understood. For instance, some observational studies suggested a periodic nature with timescales of one year (Gouriou et al., 1999), or at least five years (Johnson and Zhang, 2002) and others suggested and intermittent behavior (Send et al., 2002). There is an annual cycle signal throughout the water column. An annual cycle at intermediate depths has been detected in drifters at 800 m and 1000 m in the entire basin (e.g. Schmid et al., 2003; Ollitrault et al., 2006), and it has also been inferred from repeated LADCP sections above 1000 m at 35ºW (Schott et al., 2003). An annual cycle was also observed in velocity time series at 1700 m and deeper at 15ºW (Mercier and Speer, 1998; Thierry et al., 2006). Models and velocity data indicate that the annual cycle is consistent with a downward-propagating odd meridional-mode Rossby beam (e.g. Brandt and Eden, 2005; Thierry et al., 2006), but there is no agreement on the phase of the seasonal signal at different locations. In

contrast with the zonal velocity component, the meridional velocity component at intermediate depths is dominated by intraseasonal oscillations. In the east of the basin, some of these fluctuations have been related to surface-forced mixed Rossby-gravity waves (Weisberg et al., 1979). In the west of the basin, intraseasonal oscillations have been related to fluctuations in the Deep Western Boundary Current (Richardson and Fratantoni, 1999).

Velocity time series near the surface in the equatorial Atlantic are scarce when compared to the available data in the Pacific. Since the FOCAL/SEQUAL experiment (1982-1984) in which 2-years of near surface velocity measurements were obtained at different locations (e.g. Weisberg and Weingartner, 1988), velocity observations have been sporadic and confined to single locations. Velocity time series at intermediate depths are scarce in all equatorial oceans. To our knowledge, excluding the datasets presented in this dissertation, only three other velocity time series datasets in the Atlantic at intermediate depths have been reported: one in the Gulf of Guinea by current meter moorings during a U.S.-French cooperative program which lasted from June 1976 to May 1978 (Weisberg and Horigan, 1981), a second from a mooring at 36ºW from 1992 to 1994 (Send et al., 2002), and a third at the Romanche fracture zone (Mercier and Speer, 1998; Thierry et al., 2006) also from 1992 to 1994

Since November 1999, the French program PATOM (Programme ATmosphère et Océan Multi-échelles) has provided funding for moorings at 23ºW and 10ºW at the equator in the Atlantic equipped with current meters at intermediate depths. The purpose of the PATOM program is to study Equatorial Deep Jets and the links between near-surface (upper 200m) and intermediate-depth (600-1700m) variability. The fine vertical resolution at intermediate depths provided by these measurements allows for the proper sampling of the small vertical scales of EDJs.

Simultaneously to the PATOM moorings program, the Pilot Research Moored Array in the Tropical Atlantic (PIRATA) project (http://www.brest.ird.fr/pirata/piratafr.html) also collected velocity measurements at the equator. The measurements were gathered at 23ºW and near the surface. The combined PATOM and PIRATA datasets, because of their simultaneity, permit to compare signals coherence and propagation (horizontal and vertical) at different locations. In this dissertation, we describe the variability observed in velocity measurements obtained from multiple mooring deployments at 10ºW and 23ºW, near the surface (upper 300 m) and at intermediate depths (600-1700 m) as part of the PIRATA and PATOM projects. The data were collected between the years 2000 and 2005. Near the surface, our focus is primarily on intraseasonal quasi-periodic oscillations. It is found that intraseasonal variability was dominated by two main types of waves, wind-forced and TIWs. The first ones are observed during boreal spring, when the ITCZ is in its south position. The second ones are observed during the summer and autumn, when the currents are stronger. At intermediate depths, our focus is on EDJs. Three different timescales for EDJs were found, 7-months, 18 months and 5 years.

This manuscript is organized following the chronological order of the velocity datasets. Chapter 1 describes data at 10ºW at the surface and at intermediate depths during the year 2000, classifying variability in period bands and comparing it between depths. Chapter 2 focuses on TIWs, 7-day and 14-day period oscillations and compares near surface velocity data at 10ºW and 23ºW. Satellite SST and surface wind velocities are also to support the interpretation of the current velocity observations. Chapter 3 analyzes velocity data at intermediate depth at 10ºW and 23ºW for the years 2002 to 2005, addressing EDJ timescales, structure, and coherence between locations, as well as the annual cycle at intermediate depths. Chapter 4 explores near surface velocity data at 10ºW and 23ºW and focus on a 13-day period oscillation occurring in the spring

of 2004 with a strong SST signature. Finally, the last section presents general conclusions and perspectives. Although we notice interannual variability in the data, the topic is not fully addressed and left aside as perspective.

Chapter 1 was published as

Bunge, L., C. Provost, J. M. Lilly, M. D'Orgeville, A. Kartavtseff and J.-L. Melice, 2006: Variability of the horizontal velocity structure in the upper 1600 m of the water column on the equator at 10°W. *J. Phys. Oceanogr*., **36**, 7, 1287-1304.

Chapter 2 has been accepted as

Bunge, L., C. Provost, and A. Kartavtseff, 2006: Variability in horizontal current velocities in the central and eastern equatorial Atlantic in 2002. *J. Geophys. Res*., in press.

Chapter 3 has been submitted as

Bunge, L., C. Provost, B. L. Hua, and A. Kartavtseff, 2006: Variability at intermediate depths at the equator in the Atlantic Ocean in 2002-2005: Equatorial deep jets and low-frequency meridional flows. *Geophys. Res. Lett.,* submitted.

Chapter 4 has not yet been submitted and a manuscript is under preparation.

Chapter 1: Variability of the Horizontal Velocity Structure in the Upper 1600 m of the Water Column on the Equator at 10ºW

Abstract

This paper (Bunge et al., 2006a) presents initial results from new velocity observations in the eastern part of the equatorial Atlantic from a moored current meter array. During the EQUALANT program (1999-2000), a mooring array was deployed around the equator near 10ºW which recorded one year's worth of measurements at various depths. Horizontal velocities were obtained in the upper 60 m from an upward-looking Acoustic Doppler Current Profiler (ADCP) and at 13 deeper levels from current meters between 745 and 1525 m.

In order to analyze the quasi-periodic variability observed in these records, a wavelet-based technique was used. Quasi-periodic oscillations having periods between 5 to 100 days were separated into four bands: 5-10, 10-20, 20-40, and 40-100 days. The variability shows a) a strong seasonality: the first half of the series is dominated by larger periods than the second one, and b) a strong dependence with depth: some oscillations are present in the entire water column while others are only present at certain depths. For the oscillations that are present in the entire water column, the origin of the forcing can be traced to the surface, while for the others, the question of their origin remains open.

Phase shifts at different depths generate vertical shears in the horizontal velocity component with relatively short vertical scales. This is especially visible in long duration events (>100 days) of the zonal velocity component. Comparison with a simultaneous Lowered Acoustic Doppler Current Profiler (LADCP) section suggests that some of these flows may be identified with

equatorial deep jets. A striking feature is a strong vertical shear lasting about 7 months between 745 and 1000 m. These deep current meter observations would then imply a few months duration for the jets in this region.

1.1. Introduction

Signals propagate much faster in the equatorial region than in the rest of the ocean. Tropical oceans therefore play an important climatic role at relatively short timescales. Velocity measurements at the equator have shown very high horizontal velocities, a wide range of variability, and different spectral contents for the two horizontal velocity components, with zonal motions being dominated by larger periods than meridional motions (e.g., Weisberg and Horigan, 1981).

In the equatorial Atlantic Ocean, velocity measurements are rather sparse in time and space. Near the surface, they come from ship drifts (e.g., Richardson and Walsh, 1986), drifting buoys (e.g., Lumpkin and Garzoli, 2005), as well as from numerous inverted echosounders and current meters deployed as part of the FOCAL-SEQUAL experiment (1982-1984) (e.g. Garzoli, 1987; Houghton and Colin, 1987; Weisberg and Weingartner, 1988). Intermediate depths were sampled in the Gulf of Guinea by current meter moorings during a U.S.-French cooperative program which lasted from June 1976 to May 1978 (Weisberg and Horigan, 1981). Deep velocity time series were also obtained from moorings at 36ºW (Send et al., 2002) and at the Romanche fracture zone (Mercier and Speer, 1998; Thierry et al. 2005) between 1992 and 1994. Additionally, some floats have documented the velocity field around 1000 m (e.g., Richardson and Schmitz, 1993; Molinari et al., 1999; Boebel et al., 1999; Schmid et al., 2003) and Lowered Acoustic Doppler Current Profilers (LADCPs) have returned velocity sections throughout the

entire water column during several hydrographic cruises (e.g., Gouriou et al., 2001; Bourlès et al., 2003).

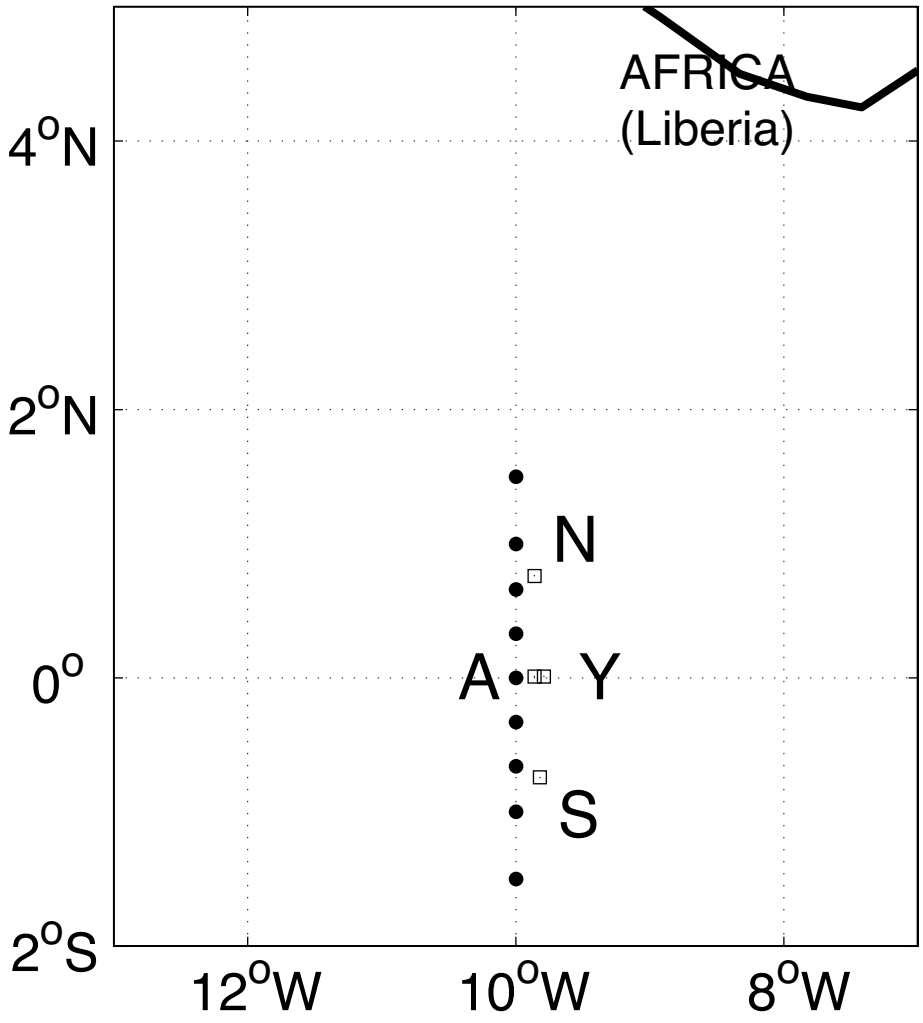

Figure 1: Study area. Squares indicate the position of the four moorings: Two are in the equator (A and Y), one at 0.75ºN (N) and the other at 0.75ºS (S). Mooring A has an ADCP to measure the subsurface and it is placed just next to a PIRATA Atlas buoy. The instruments were in the water from November 1999 to November 2000. Solid circles indicate the location of some of the Equalant LADCP sections used in this paper and made during the 30th of July and the 1st of August 2000.

Most studies of oceanic signals at the equator have tried to relate them to linear equatorial waves. One of the dominant periods in the meridional velocity component at the surface is about 30 days, associated with tropical instability waves (Weisberg and Weingartner, 1988). These waves are usually present from June to October (e.g., Grodsky et al., 2005) and their expression below the thermocline resembles that of linear Rossby-gravity waves (Weisberg et al., 1979). In the eastern part of the basin, energetic oscillations having a 14-day period are also observed in near surface oceanic records by Garzoli (1987) and Houghton and Colin (1987). Garzoli (1987) surmised that these oscillations are forced by wind fluctuations at the same period in the zonal wind component. The maximum amplitude of the 14-day signal was found to occur in the mixed layer at 3ºN which does not agree with equatorial wave theory which implies symmetry about the equator. Houghton and Colin (1987), on the other hand, attribute the forcing to the meridional wind velocity component and found that the thermocline displacements are nearly antisymmetric about the equator and that the structure of the oscillation resembles that of a second baroclinic mode Rossby-gravity wave.

At depth, the zonal velocity component is dominated by lower frequencies (~66 days, semiannual, annual and interannual oscillations) which**,** in some cases, have Rossby and/or Kelvin wave characteristics (e.g. Thierry, 2000; Schmid et al., 2003).

Among the most remarkable features of the deep equatorial scenario are the Equatorial Deep Jets (EDJ), present in the zonal velocity component between the thermocline and 2500 m. First discovered in the Indian Ocean by Luyten and Swallow (1976), they have been observed in the Pacific (Eriksen, 1985; Firing, 1987) as well as in the Atlantic (Ponte et al., 1990; Gouriou et al., 1999; Send et al., 2002; Bourlès et al., 2003). In the Atlantic Ocean, EDJ have vertical scales of around 400-600 m and a typical meridional extent of one degree (e.g., Gouriou et al., 1999).

There is no general consensus on whether EDJ are the result of equatorial Kelvin waves or first-meridional-mode equatorial Rossby waves, if any wave at all. Certain characteristics like the high zonal velocities are indicators of Kelvin wave behavior, but others, like the potential vorticity structure (Muench et al., 1993) or the off-equatorial maxima of vertical strain (Johnson and Zhang, 2002), suggest similarities with Rossby waves. In any case, the scales do not seem to match those of linear theory and thus nonlinearities have been suggested (Weisberg and Horigan, 1981; Philander, 1990; Hua et al., 1997). Another unknown is the temporal scale of these structures. Gouriou et al. (1999) suggest a seasonal reversal of the jets but, as other authors have recently remarked (e.g., Send et al., 2002), vertically propagating energy at large vertical scales could be responsible for such apparent jet-reversals. Based on linear wave theory, Johnson and Zhang (2002) propose periods of at least 5 years. Send et al. (2002) estimate similar periods, but also pointed out the possibility of an intermittent behavior.

Here we report the initial results from a mooring array deployed at 10ºW and the equator during the EQUALANT program (1999-2000). The year-long dataset consist of horizontal velocities in the upper 60 m obtained with an upward-looking ADCP, and the same at 13 deeper levels from current meters placed at depths between 745 and 1525 m. Despite the absence of data between 60 and 745 m, the EQUALANT current meter data set is unique because of its high vertical resolution between 745 and 1525 m. These depths are characterized by the presence of EDJ and by the interface between two important water masses, Antarctic Intermediate Water (AAIW) and North Atlantic Deep Water (NADW).

The objective of this paper is to provide a first description of these new data and to discuss the major features in comparison to previous observations and theory. Because the data clearly contain quasi-periodic fluctuations which may be modulated in time or may occur only in certain

portions of a time series, we use a wavelet-based technique (see Apendix) to isolate and extract individual component signals. It is found that energetic fluctuations occur both, at the surface and at depth, often with similar periods. These fluctuations are either distributed uniformly with depth or concentrated at a few distinct depth ranges. Finally, we find long duration events with vertical scales comparable to those of EDJ and temporal scales on the order of 7 months.

The paper is organized as follows: Section 2 describes the data and experiment, section 3 the wavelet method, section 4 the general spectral characteristics of the data and the main oscillations observed, and section 5 analyzes the vertical scales of long duration events. The results are summarized and discussed in section 6.

1.2. Data

Current meter data were obtained from 16 vector averaging current meters (VACMs) and an Acoustic Doppler Current Profiler (ADCP), 150 KHz narrow band, deployed at the Equator at 10ºW from November 1999 to November 2000 as part of the EQUALANT program (http://nansen.ipsl.jussieu.fr/EQUALANT**;** Kartavtseff, 2002). The array was initially designed with four moorings (fig. 1) of four VACMs each to sample the water column between 1000 and 1600 m depth. Two moorings were placed exactly on the equator (moorings A and Y), one at 0.75ºN (mooring N) and the other at 0.75ºS (mooring S). Mooring A at the equator was equipped with an ADCP to sample the surface and subsurface. It was deployed with a parachute to reduce the tension of the cable. This technique, while it made the mooring descend gently, also let the mooring drift to a somewhat shallower location than was originally planned. As a result, the ADCP was only able to continuously sample the upper 50-60 m (fig. 2). Mooring Y had VACMs at staggered depths with those of mooring A in order to increase vertical resolution. An

intermediate cruise was done in March 2000 to recover and re-deploy mooring Y. The recovery of the whole array was done in November 2000.

Table 1 reports the depth and duration of the current meters time series. Y_A and Y_B represent the two deployments of mooring Y and the numbers 1, 2, 3, 4 after the mooring's designation represent the current meters by order of increasing depth. Furthermore, series from Y_A at 1187 and 1420 m were merged with series Y_B at 1190 and 1415 m to form series Y2 and Y3, respectively, while Y_B at 930 was named Y1. From now on, we will use the 30 m depth ADCP time series, as a representation of near surface data. Because of technical problems with some of the VACMs, only 13 series were analyzed; the length of the longest time series being 380 days (see table 1 for details). In order to examine time scales of variability longer than one week, the hourly-data were averaged every 25 hours to remove tidal frequencies and resampled to daily resolution (fig. 3).

	Real depth (in m) and length of the time-series (in days)				
	S (0.75ºS)	N (0.75ºN)	A (equator)	Y_A (equator)	Y_B (equator)
1	840-380	745-375	825-234	1187-120	930-257
2	1110-42	1000-377	1060-339	1420-120	1190-258
3	1360-272	1120-294	1275-148	1645-120	1415-258
4	1525-248	1385-257	1460-378	1830-120	1635-12

Table 1: Depth and duration of the current meters time series. The moorings were deployed between November 11, 1999 and November 24, 2000. The location is given by the capital letters: N is 0.75ºN, S is 0.75ºS, A and Y is the very equator. Y_A and Y_B represent the two deployments of mooring Y. The numbers 1, 2, 3, 4 represent the instruments in each mooring in increasing order of depth. For each mooring, the depth in meters of the current meters is given in each column followed by the length of the time series in days. Only series longer than 120 days were used. The current meter A3 record has gaps for unclear reasons and therefore was not used.

The VACMs were calibrated both before and after deployment at the Institut français de recherche pour l'exploitation de la mer (Ifremer) in Brest, France. The reported accuracies are between ±1 to 2 cm/s for the various instruments, with the minimum measurable current speeds varying between 0.53 and 3.78 cm/s.

The analysis also makes use of Lowered Acoustic Doppler Current Profiler (LADCP) data collected during EQUALANT cruise in July and August 2000 (fig. 4), while the current meters were in the water. These data have been previously described in Bourlès et al. (2003).

To investigate possible forcing mechanisms for the variability observed, surface wind data were also analyzed. Wind data came from two sources: satellite scatterometer data from QuikSCAT (http://www.ifremer.fr/cersat/fr/data/overview/gridded/mwfqscat.htm) between July 20, 1999 and May 20, 2004 and from the ATLAS buoy of PIRATA (Pilot Research Moored Array in the Tropical Atlantic), at 10ºW (http://www.pmel.noaa.gov/pirata/display.html).

The satellite scatterometer data have a daily temporal resolution and a 0.5 degree spatial resolution. We examined the region comprised between 25.75ºW and 0.25ºW, and 7.25ºS and 9.25ºN. Because of the large size of this dataset, the analysis was performed with a multi-taper method (Thomson, 1982; Percival and Walden, 1993). We used the Singular Spectrum Analysis - Multi-Taper Method (SSA-MTM) toolkit (Ghil et al., 2002) with nine tapers: 9=2P-1, where P is the time band width product. The smoothing of the spectrum may be estimated by 2P/N, where N is the time length of the series (almost 5 years). This implies a smoothing in Fourier space over a region of approximately 2 cycles/year in width. The spatial distribution of the oscillations representing the "peaks" in the spectra (fig. 5b) shows maps of the spectrum amplitudes corresponding to some of those periods (fig. 5c and d).

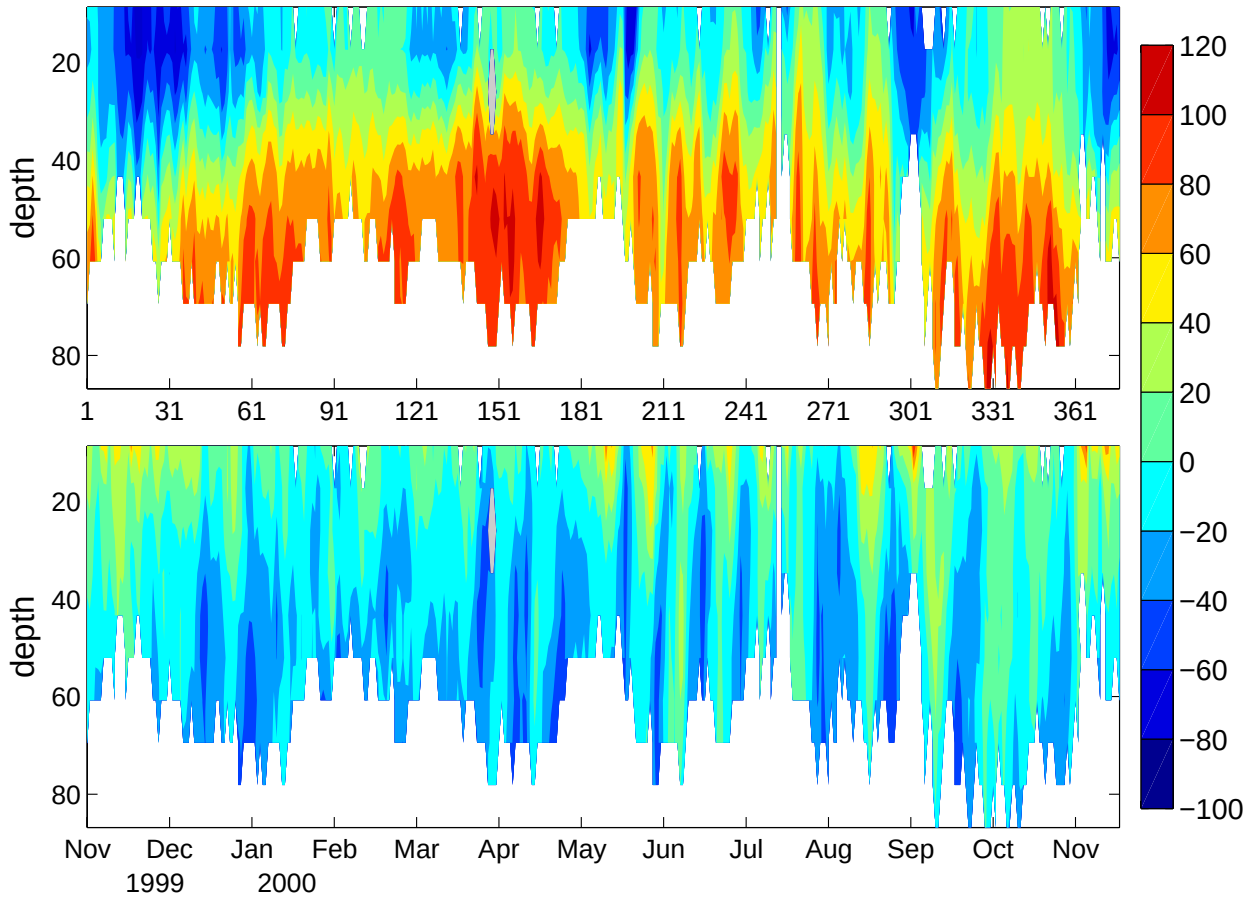

Figure 2: Zonal (top) and meridional (bottom) velocity components from the ADCP in mooring A. Velocity units are in cm/s. Time axis is in days (top) and in months (bottom), beginning November 12, 1999 and ending November 24, 2000.

The PIRATA wind data set has also a daily temporal resolution and a record length of 377 days. There are however big gaps in the record (fig. 6, top) and we therefore opted to perform a wavelet analysis (described in section 3) instead of the multi-taper method analysis.

1.3. Wavelet Analysis

In order to detect and extract quasi-periodic signals, we use a wavelet ridge analysis (Delprat et al., 1992; Mallat, 1999) together with a reconstruction scheme. Details can be found in the

Appendix; here we give a general overview, emphasizing practical considerations. The problem is to isolate and reconstruct signals of the form

$$x_1(t) = A(t)\cos(\phi(t)) \tag{1}$$

for the case in which $\omega(t) = d\phi/dt$, known as the "instantaneous frequency", varies with time. Such signals, which will be shown to be common in this dataset, are not well-represented using Fourier analysis.

The wavelet transform of a time series (defined in the Appendix) is a complex-valued function $W(t,s)$ of two variables, the time *t* and "scale" *s*. If a signal of the form (1) is present in a time series, its presence will be indicated by a curve $\tilde{s}(t)$, called a wavelet "ridge", on the time-scale plane. Ridges trace out the variations of the instantaneous frequency with time, under assumptions of slow variations of *A(t)* and *ω(t)* which are given explicitly in Delprat et al. (1992) or Mallat (1999). Such signals as (1) may be identified even if other variability is present at the same time, for example, sufficiently small-amplitude noise, or other quasi-periodic signals at other, sufficiently distant, frequencies. For our choices of normalization, discussed in the appendix, the ridge location reflects the instantaneous frequency of the signal (1) through $\tilde{s}(t) \approx 1/\omega(t)$, while the amplitude of the wavelet transform gives the signal amplitude $|W(t,\tilde{s}(t))| \approx A(t)$. These approximations hold under the slowly-varying assumptions, and become exact for a constant sinusoidal signal.

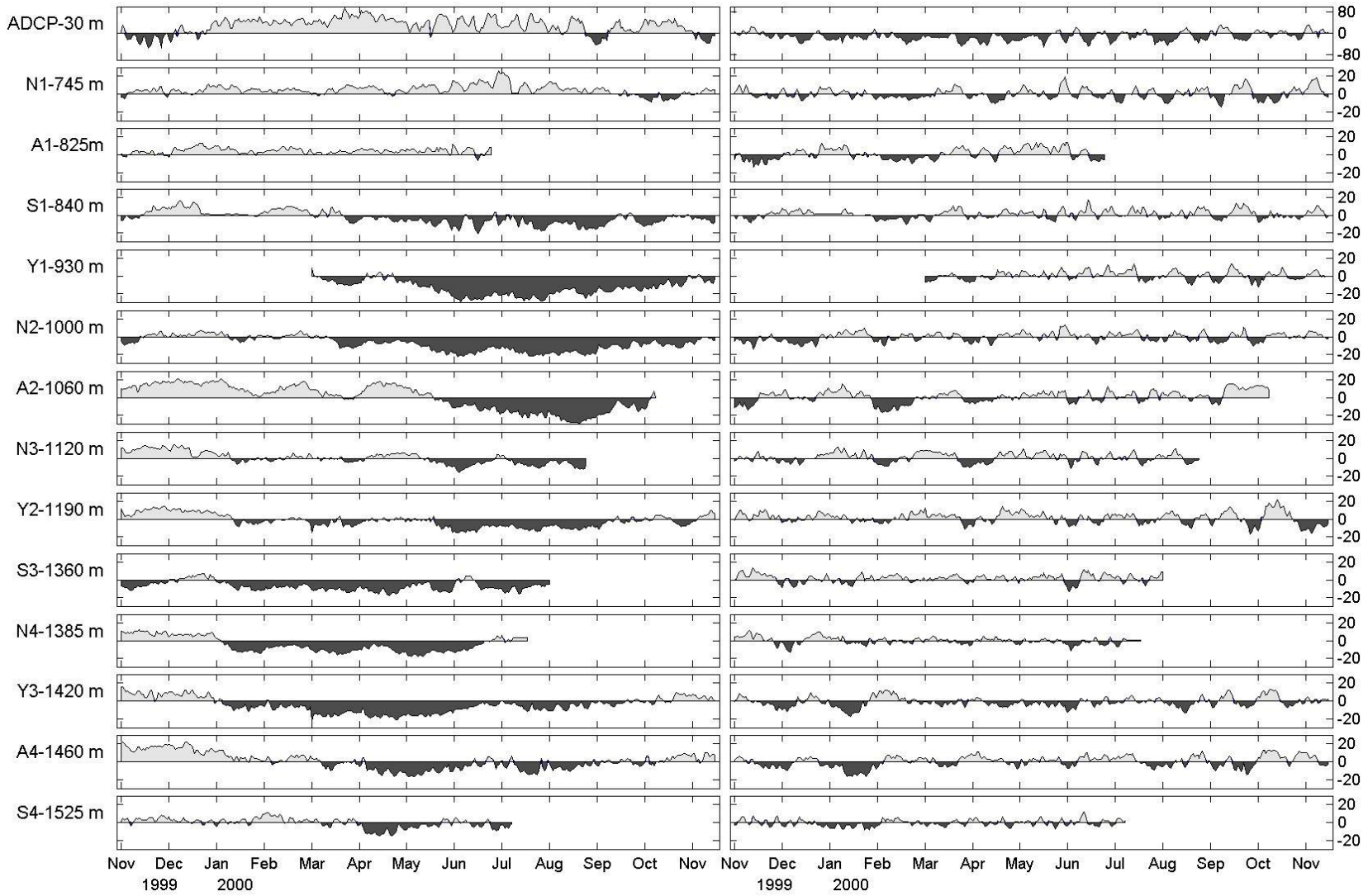

Figure 3: Zonal (left) and meridional (right) velocity components (in cm/s) obtained from the instrument array at 10ºW. The letters to the left identify the mooring. Negative velocities (blackened areas) are westward and southward directions respectively. Time line starts November 12, 1999 and ends November 24, 2000.

After locating such signals, we wish to reconstruct them. The simplest way is to use the wavelet ridge location and amplitude to determine $A(t)$ and $\omega(t)$. However, this approach leads to sudden starts and stops of the reconstructed signal components, giving the appearance of a discontinuous behavior. Instead we use a different approach, described in the Appendix, giving reconstructions which begin and end continuously and which are smoother overall than those of the direct method**.**

It is also important to mention the "edge effects". At either end of the time series, the wavelet will extend past the end of the data, leading to edge effect regions --- which widths are proportional to the scale s --- where the wavelet transform is contaminated. Edge effects are not problematic for this analysis because i) we are using time-localized wavelets and ii) there is not much low-frequency variability present near either endpoint of the time series. We tested the importance of the edge effects by using two different boundary conditions in the wavelet transform, in the first case setting the missing data to zeros, and in the second "reflecting" the data about either endpoint. The difference between these two cases was generally minor, even within the edge-effect regions. We have chosen to present the results of the reflecting boundary condition method.

After locating all ridges of each time series, we choose two criteria to eliminate ridges which are likely to result from "noise" or are otherwise spurious. The first criterion retains oscillations with ridge amplitudes larger than a measure of high frequency "noise-like" variability: for a ridge of temporal duration D_r and mean amplitude along the ridge $A_r = 1/D_r \int_{t_1}^{t_2} |W(t, \tilde{s}(t))| dt$, where t_1 and t_2 are the start and end points of the ridge, A_r must be larger than σ_H, where σ_H is the standard deviation of the time series accounted for by Fourier components having periods of less than 7 days. The second criterion rejects short-duration events, since we are interested only in quasi-

periodic features: only ridges with duration D_r greater than the period $1/\omega$ at the ridge point are selected.

This method was applied to each velocity component of the current meter data and PIRATA wind data. The wavelet transform and the significant ridges on wind data at 10ºW after extraction of the total mean (fig. 6) show that the method successfully detects signals, even though large gaps are present in the time series shown in figure 6. The edge effects can be minimized by eliminating the wavelet region with less than half the length of the wavelet, at each central frequency in each band (see dotted dark lines in figure 6).

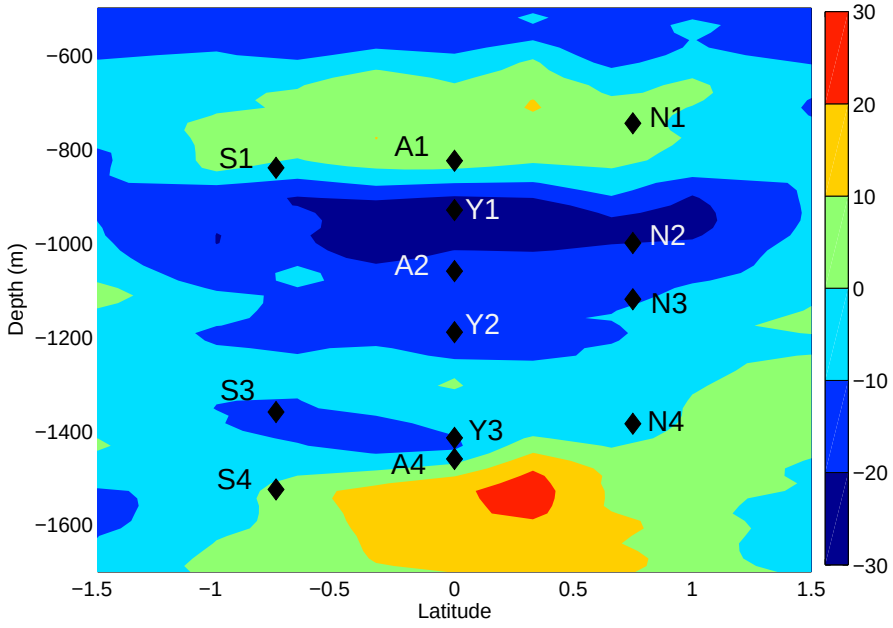

Figure 4: Section of zonal velocity (cm/s) at 10ºW. The section was made between the 30th of July and the 1st of August 2000 during an EQUALANT cruise. The vertical resolution is of 16 m and the spacing between LADCP stations is of 1/3º between 1ºS and 1ºN and half a degree elsewhere. The diamonds and labels correspond to the current meter positions and names. Three clear jet structures are observed: 1) an eastward jet centered at 750 m and with a meridional extension of 1º at each side of the equator, 2) a westward jet with maximum velocities at around 1000 m and a total meridional extension of 3º and 3) an eastward jet with maximum velocities at 1550 m and a total extension of 2º. Between 1200 m and 1400 m there is no clear signature of a deep jet structure.

In order to reconstruct the quasi-periodic signal in the band 5-100 days, we sum the reconstructions corresponding to the selected ridges in each time series. The results are displayed in figure 7: large amplitude variability in the meridional component is captured almost entirely, while the energetic large period events in the zonal component are not. Both components show a marked "seasonality" in the variability; in general, the first half of the series is dominated by larger periods than the second one.

The method is successful in isolating most of the organized quasi-periodic variability; the residuals (fig. 8) consist of high-frequency noise and of some isolated fluctuations that were excluded either for belonging to short ridges ($D_r \rangle 1/\omega$ - e.g. the meridional component of A1 and A2) or for having periods outside the band 5-100 days (e.g. very low frequency variability in the zonal component).

1.4. Observed Periods

The histograms in figure 9 show the most important periods found in the water column; they represent the number of days in which events of each period occurred, summed over all current meter series. This information comes directly from the selected ridges detected as described in section 3. The zonal component presents larger period variability than the meridional component; especially noticeable are oscillations around 70 days. The meridional component shows two distinctive "peaks", one at 14 days and the other at ~60 days. These histograms and previous information about the period of events found in the region (e.g., Garzoli, 1987) suggest distinguishing the following period bands: 5-10 for the 7-day period oscillations, 10-20 for the 14-day period oscillations, 20-40 for the tropical instability waves, and 40-100 for the 60- and 70-day period oscillations.

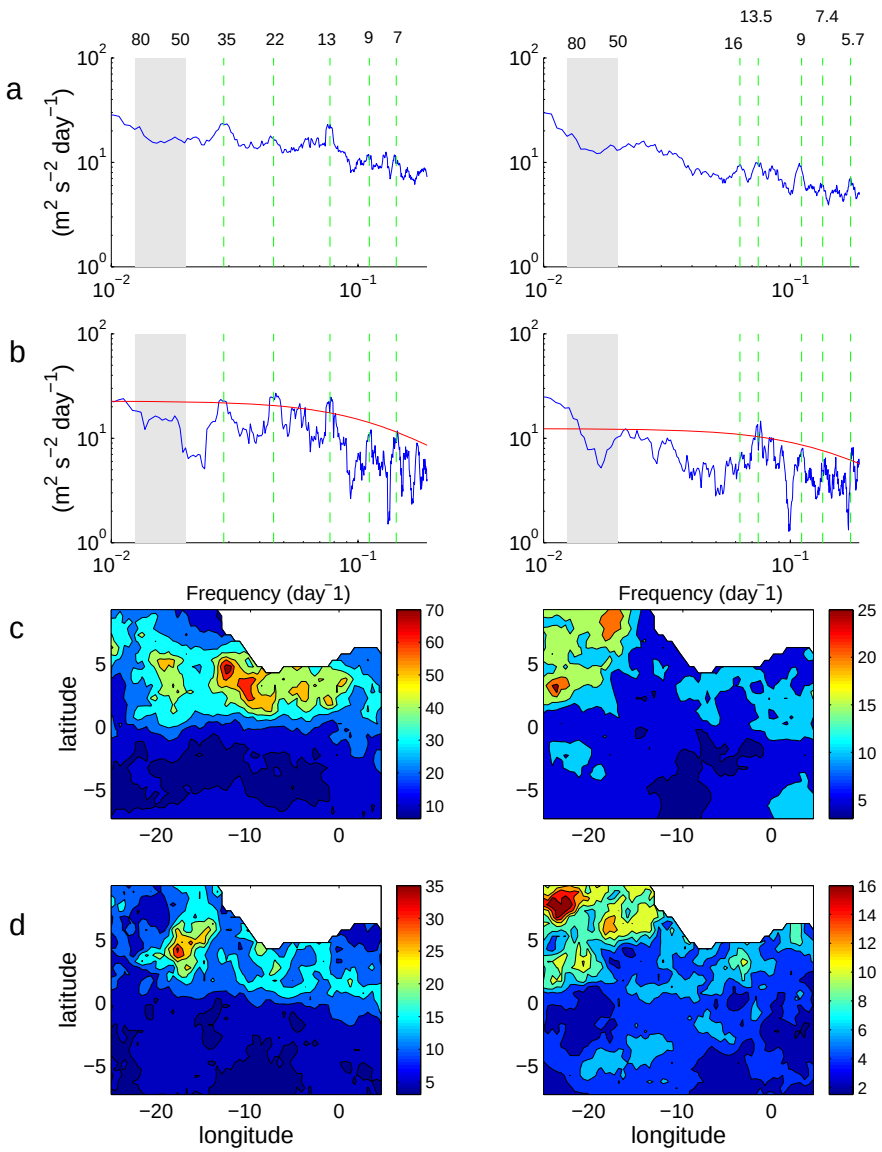

Figure 5: a) Mean velocity wind spectra of the zonal (left) and meridional (right) components from QuikSCAT. The mean is computed with the 2108 spectra corresponding to the grid points comprised between 25.75ºW and 0.25ºW, and 7.25ºS and 9.25ºN. The vertical lines from left to right indicate the periods of 35, 22, 13, 9 and 7 days (zonal component) and 16, 13.5, 9, 7.4 and 5.7 days (meridional component). Shadowed region indicates the 50-80 days band. b) Same as "a" but for a point located at 0.25ºN, 10.25ºW. The red curve indicates the 95% confidence interval. c) and d) Amplitude of the spectrum at 13 and 7 days for the zonal component (left) and for 13.5 and 7.4 days for the meridional component (right).

Figure 10 shows the signal corresponding to each period band for each velocity component. There is a marked seasonality, especially in the meridional component. Most time series can be divided in three parts: one with short periods in the middle, and two with longer periods before

and after. It is also observed that some oscillations are present in the entire water column while others appear exclusively at certain depths and/or have distinctive behavior depending upon latitude. Examples of these are oscillations of ~14-day period in the zonal component which are only seen at the surface and at around 800 m (between 200 and 270 days of the time series), and oscillations of ~60 day period in the meridional component which are only present around 1100 and 1400 m.

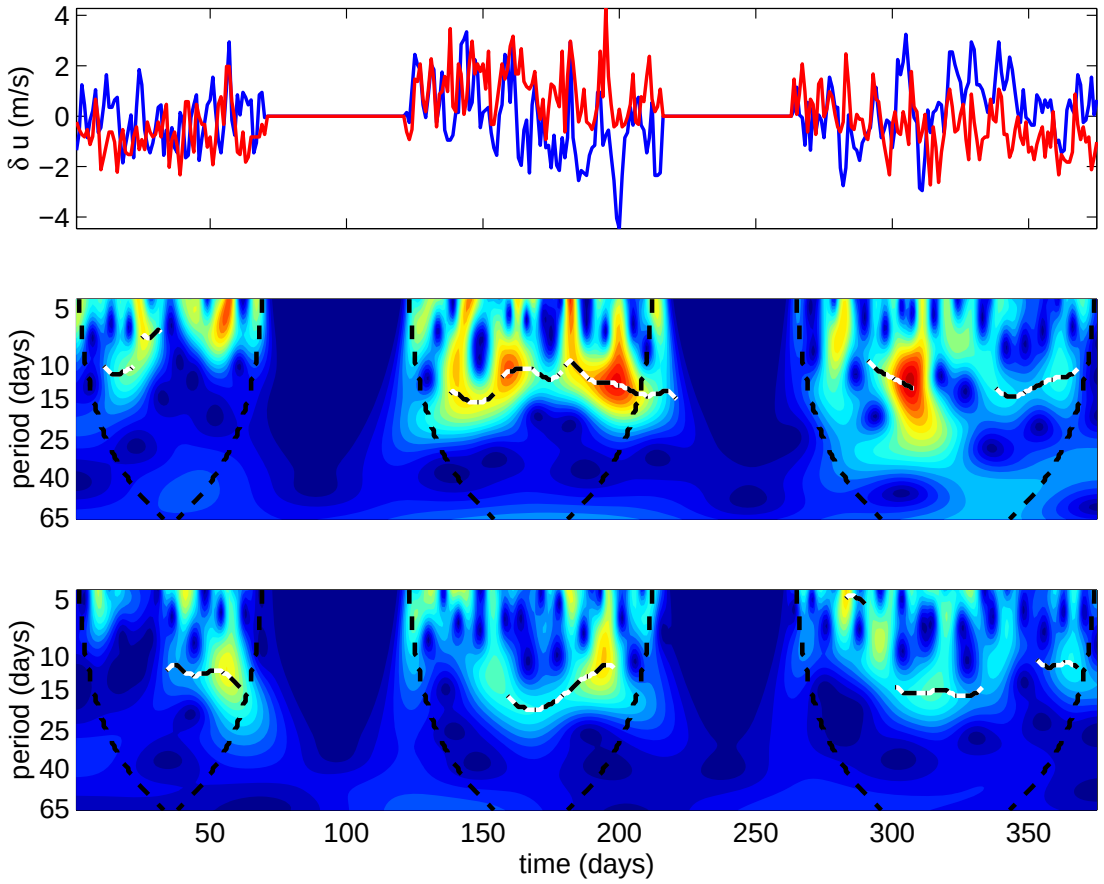

Figure 6: Top: Normalized PIRATA buoy anomalies time series of the wind horizontal velocity components at 10ºW (blue: zonal component and red: meridional component). Time line starts the 12 of November 1999, coinciding with the time line of current meter data. Data gaps are between 70 and 120 days (January 20th to March 10th), and between 214 and 264 days (June 12th to August 1st). Middle and bottom: Wavelet transform amplitude of the two series plotted above (middle panel: zonal component and bottom panel: meridional component). The black and white lines are the ridges of maximum amplitude from which the main components are extracted to reconstruct the signal, as shown in figure 7. The dotted black lines indicate the cutoff region to avoid edge effects.

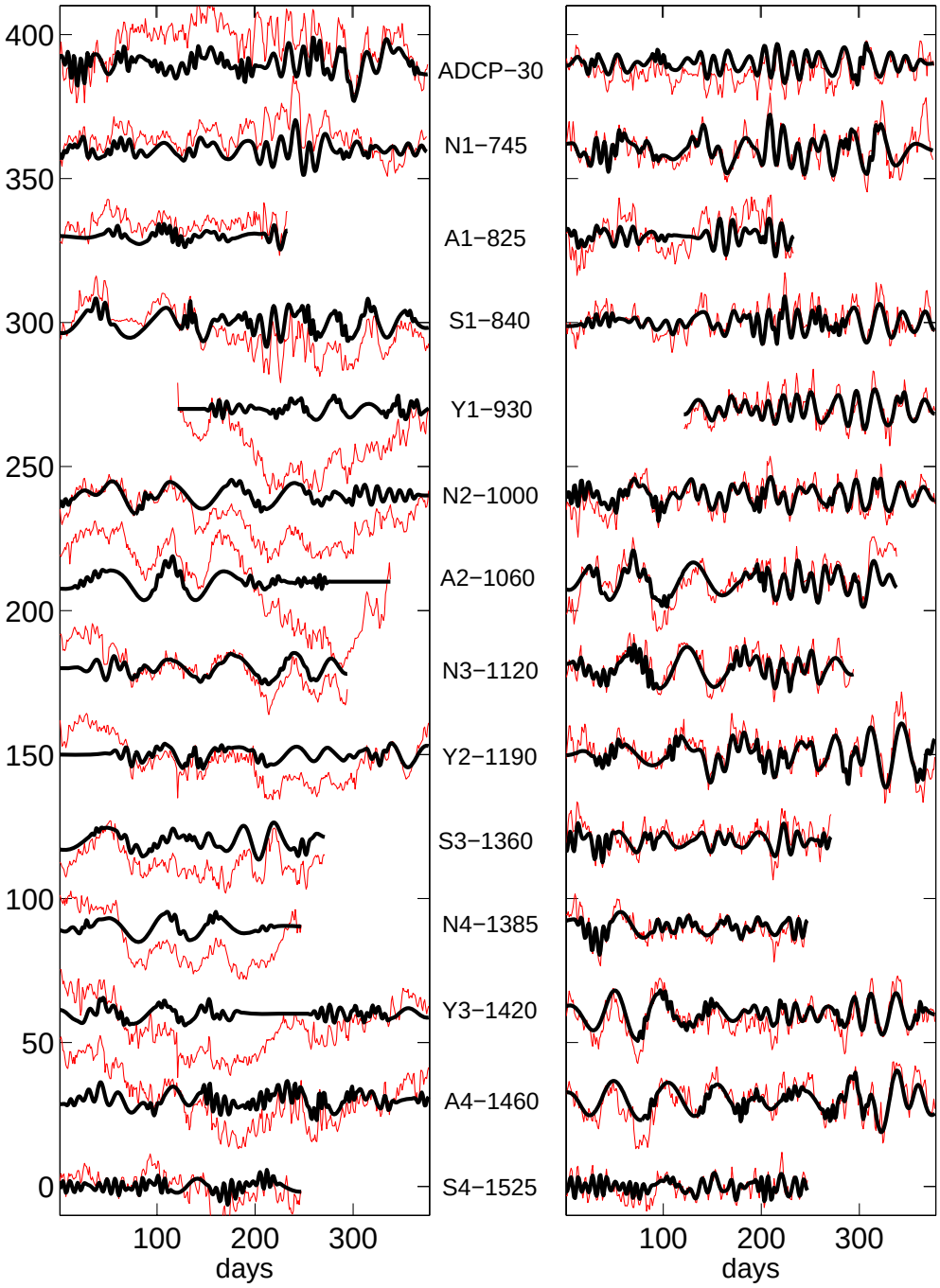

Figure 7: Zonal (left) and meridional (right) velocity components (in cm/s) obtained from the instrument array at 10ºW (red). In black (thick) is the reconstructed signal of the 5-100-day period band from the wavelet analysis. Series are offset by a factor of 30 and the values of series ADCP-30 are divided by 4. The name and depth of each instrument is specified between the two plots. Time line starts November 12, 1999 and ends November 24, 2000. It is observed that single isolated oscillations are not picked up, either because they do not fulfill our "ridge criteria" or because the period of the events is out of the period band that is being extracted (5 to 100 days).

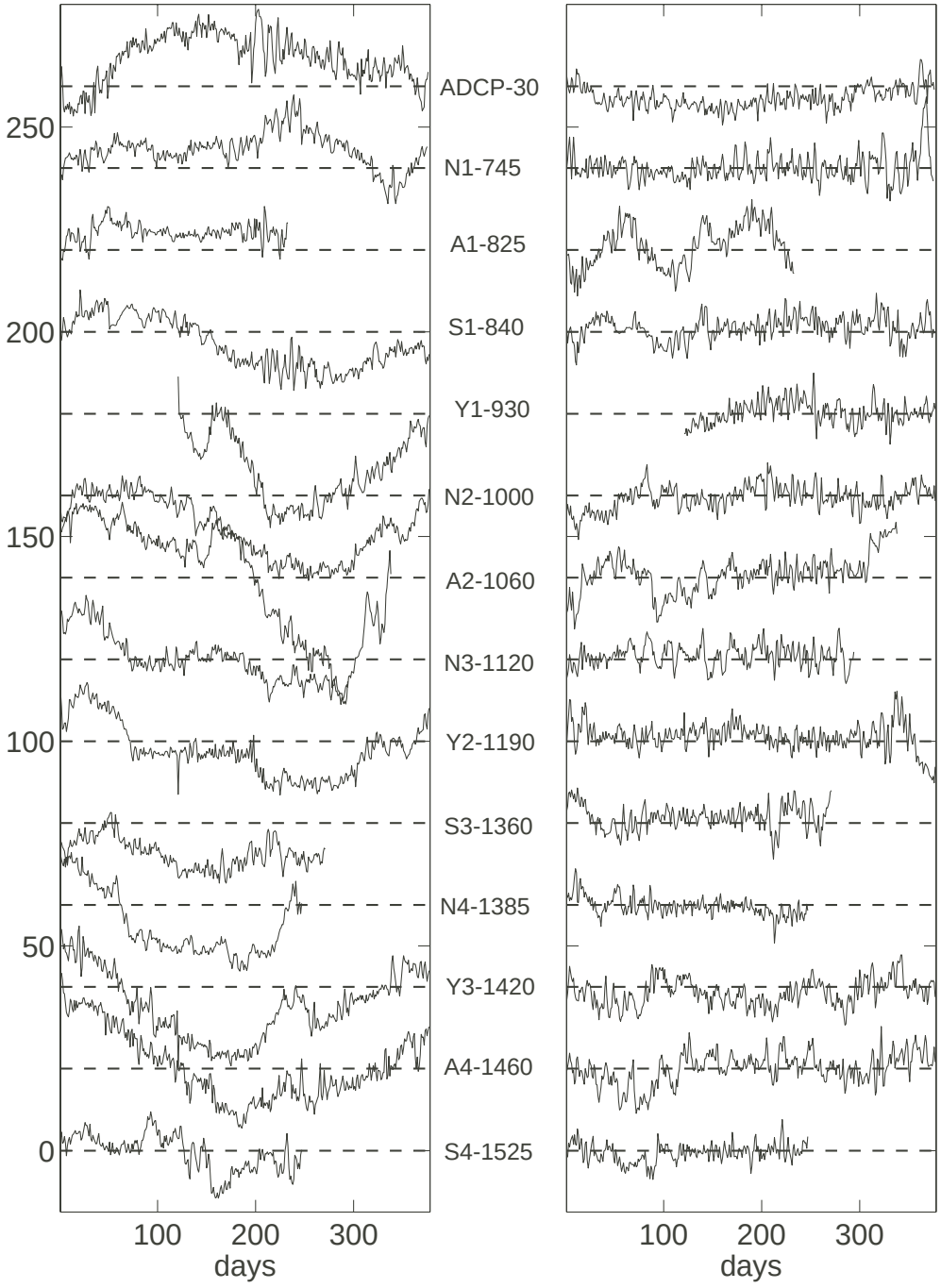

Figure 8: Residues of zonal (left) and meridional (right) velocity component time series after subtraction of significant quasi periodic oscillations with periods between 5 and 100 days. Velocity anomalies are in cm/s and the series are offset by a factor of 20. The values of series ADCP-30 are divided by 4. The name and depth of each instrument is specified between the two plots. Time line starts November 12, 1999 and ends November 24, 2000. Some isolated oscillations in the 5-100 day period band have not been picked up because they do not fulfill our "ridge criteria" (e.g. see meridional component of A1-825). In other cases, the periods of the events observed are out of the 5-100 days range (e.g. most zonal component series).

The 5-year satellite wind data were analyzed for the 5-100 day period band. The spectra present regional differences which explain why the mean of all spectra (fig. 5a) differs from the spectrum at 0.25ºN 10.25ºW (fig. 5b). For the zonal wind data component, the most important periods are 7, 9, 13, 22 and 35 days, and for the meridional component at 5.7, 7.4, 9, 13.5 and 16 days. Interestingly, the amplitude of the spectra for some specific periods presents different spatial distributions for each velocity component. For example, the amplitude of the spectrum at 13 days in the zonal component is maximum in a region located between 20ºW and 0ºW and between 0º and 6ºN (fig. 5c-left), while the spectrum of the 13.5 days in the meridional component shows most of its energy in a region comprised between 25ºW and 15º W and between 2ºN and 9ºN (fig. 5c-right).

We now systematically describe the variability of the current meter data in order of increasing period.

- **5-10 days:** Variability in this band presents a disorganized appearance, which in some cases can be defined as “noise”. Nevertheless, some features are worth mentioning. Near the surface, conspicuous events are only present in the zonal component (fig. 10). At depth, oscillations within this period band are common along the year in the deepest VACM (S4-1525) for both velocity components. In the meridional component, these oscillations also appear in the deeper southern and northern instruments (S3-1360, N4-1385 and S4-1525). During approximately the first 50 days of the records, they show opposite phases for northern and southern mooring locations creating a converging/diverging flow at the equator. This is interesting because of the implied up and down vertical velocities, in a region where deep waters should theoretically upwell. Unfortunatelly, there is not enough data to have a complete picture of the structure of the

velocity field corresponding to this period. The lack of continuity with depth and the different times of occurrence of the signal suggest that the events near the surface and at depth are not related. Moreover, the relation between components is not explainable in most cases in terms of a single phenomenon because they occur at different times of the year.

- **10-20 days:** The principal oscillation in the 10-20 day band has a period of approximately 14 days. These oscillations are very energetic near the surface and are mainly observed during the end of the spring to mid summer (fig. 10; 200-250 days). Near the surface, the signal is present in both velocity components at the equator, probably directly forced by the wind stress, which presents simultaneous fluctuations in the same period band (fig. 6).

  In the meridional component, 14 day oscillations are observed in almost all VACMs records with roughly the same seasonality (fig. 10). However, in the zonal component, they are only visible in the upper VACMs records (N1, A1 and S1). At those depths (~800 m), the structure of the signal is symmetric in the meridional component and antisymmetric in the zonal component (fig. 10, N1-745 and S1-845), reminiscent of Rossby-gravity waves.

  Assuming that the observed variability corresponds to a Rossby-gravity wave, a number of parameters can be estimated: The linear theory of equatorial waves (e.g., Gill, 1982) links the amplitude of the meridional velocity of the signal, v_0, to the amplitude of the meridional shear of the zonal velocity component, $\partial_y u$, through the relation $\partial_y u = \frac{v_0 \omega}{c}$, where ω is the frequency of the wave and c the phase speed of pure gravity waves of the vertical mode considered. According to the velocity records near the 800 m

depth level, characteristic values of v_0, $\partial_y u$, and ω are $v_0 \approx 6\,cm/s$, $\partial_y u \approx 6\times10^{-7}\,s^{-1}$, $\omega = 5.2\times10^{-6}\,s^{-1}$, and thus we obtain $c \approx 51\,cm/s$ which corresponds to a vertical mode 4 or 5 for the Atlantic. This value of *c* is almost constant throughout the records where this calculation can be performed. For this value of *c*, the linear dispersion relation of a Rossby-gravity wave with a frequency $\omega = 5.2\times10^{-6}\,s^{-1}$ shows eastward phase propagation. The Froude number, $Fr = \frac{v_0}{c}$, which compares the magnitude of the advection terms to the propagation velocity of pure gravity waves, is approximately 0.1, therefore suggesting a weakly nonlinear behavior.

The satellite wind data as well as the PIRATA wind data show high energy in this band, in both horizontal velocity components (fig. 5a and fig. 6). At 10ºW, satellite wind data shows that these fluctuations are stronger during spring and summer for both components and that the zonal component has, in general, larger amplitudes. In the zonal component, this signal has been associated with a near surface westerly jet close to the African continent, which latitudinal position varies with the meridional migration of the ITCZ (Grodsky et al., 2003). In the meridional component, satellite data show that this period is present in the western part of the basin, north of 2°N – but not as much in the Gulf of Guinea (fig. 5c).

- **20-40 days:** Fluctuations with this period are observed primarily in August and September (fig. 10). Near the surface, the periods of events are approximately 24 days. The zonal component has amplitudes up to 30 cm/s while the meridional component has maximum amplitudes of 22 cm/s. At depth, the most conspicuous events in the zonal component are observed simultaneously to those near the surface in records S1 and Y1. Their period is

approximately 34 days and therefore they cannot be directly related to near surface events. In the meridional component, 20-40 day period fluctuations are seen in almost all VACMs a month later than the near surface events. Periods are about 25 days in S1, Y1, N2, Y3 and A4, and 33 days in N1 and Y2 (fig. 10). Fluctuations in the 20-40 day period band occurring in August-September within the mixed layer have been associated with tropical instability waves (e.g., Weisberg and Weingartner, 1988).

- **40-100 days:** Near the surface, signals within this period-band are conspicuous only in the zonal component. At depth, oscillations with these periods are mostly present in the first half of the series (November 99 to April 2000) for both velocity components (fig. 10).

  The period of fluctuations observed in the zonal component at depth is mostly in the 60-80 day band. They are particularly important at intermediate depths (S1-840, N2-1000, A2-1060, and N3-1120) where they have amplitudes of 5-7 cm/s. The presence of these oscillations at 30 m in the first half of the series could suggest that the forcing of these waves comes from near the surface. Such variability is however not present in the satellite wind data analyzed here (fig. 5a, shadowed area) and the PIRATA wind records cannot be used for this period-band because of gaps in the time series.

  At depth in the meridional component, oscillations within this period band are found exclusively in the northern and equatorial moorings, around 1100 m and 1400m, with amplitudes from 4 to 8 cm/s (fig. 10), and a period of ~60 days. There is a clear opposition of phase between records at ~1100 m and those at ~1400 m. The phase relation between levels could be interpreted either as a vertical propagation or as a standing mode with a vertical scale of 600-800 m. The lack of signal in the southern mooring records implies that the geometry of the wave has no symmetry with respect to the equator, or that

the southern records coincide with nodes in the vertical. A possible forcing mechanism cannot be local and from the surface at the same time; there is no conspicuous signal in shallower records or in the wind field. However, variability with similar periodicities has been observed in northern tropics (15-25ºN) wind data (Foltz and McPhaden, 2004) and in subsurface eddies from the western boundary current in the tropical south Atlantic (Dengler et al., 2004). The potential link between all those observations, if it exists, is far from being understood.

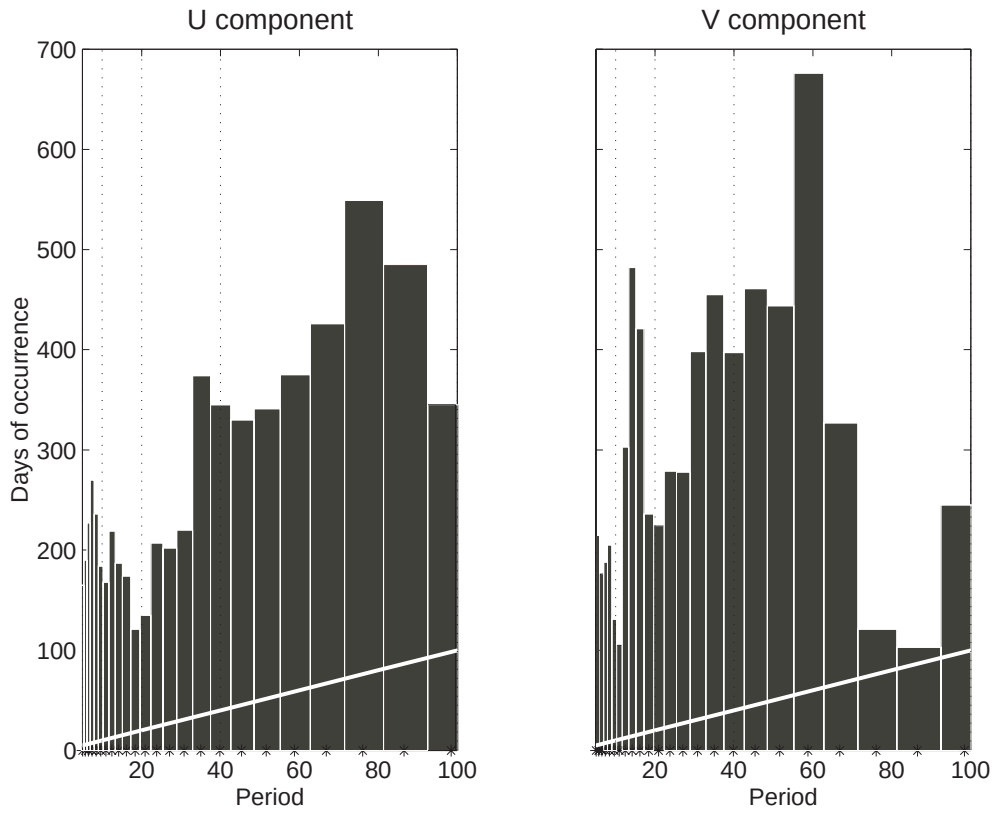

Figure 9: Ridge histograms for the zonal (left) and meridional (right) velocity components, of all current meter data. The bins were constructed by choosing the inverse of the central frequency of the wavelets used to calculate the wavelet transform. Central frequencies of the wavelets follow a logarithmic progression in such way that $\Delta(\log(f)) = \text{constant}$, therefore, bins from long periods are larger than those of short periods. The vertical dotted lines indicate the limits of period bands considered (5-10, 10-20, 20-40 and 40-100 days). The white line indicates the portion of the bars equivalent to one cycle.

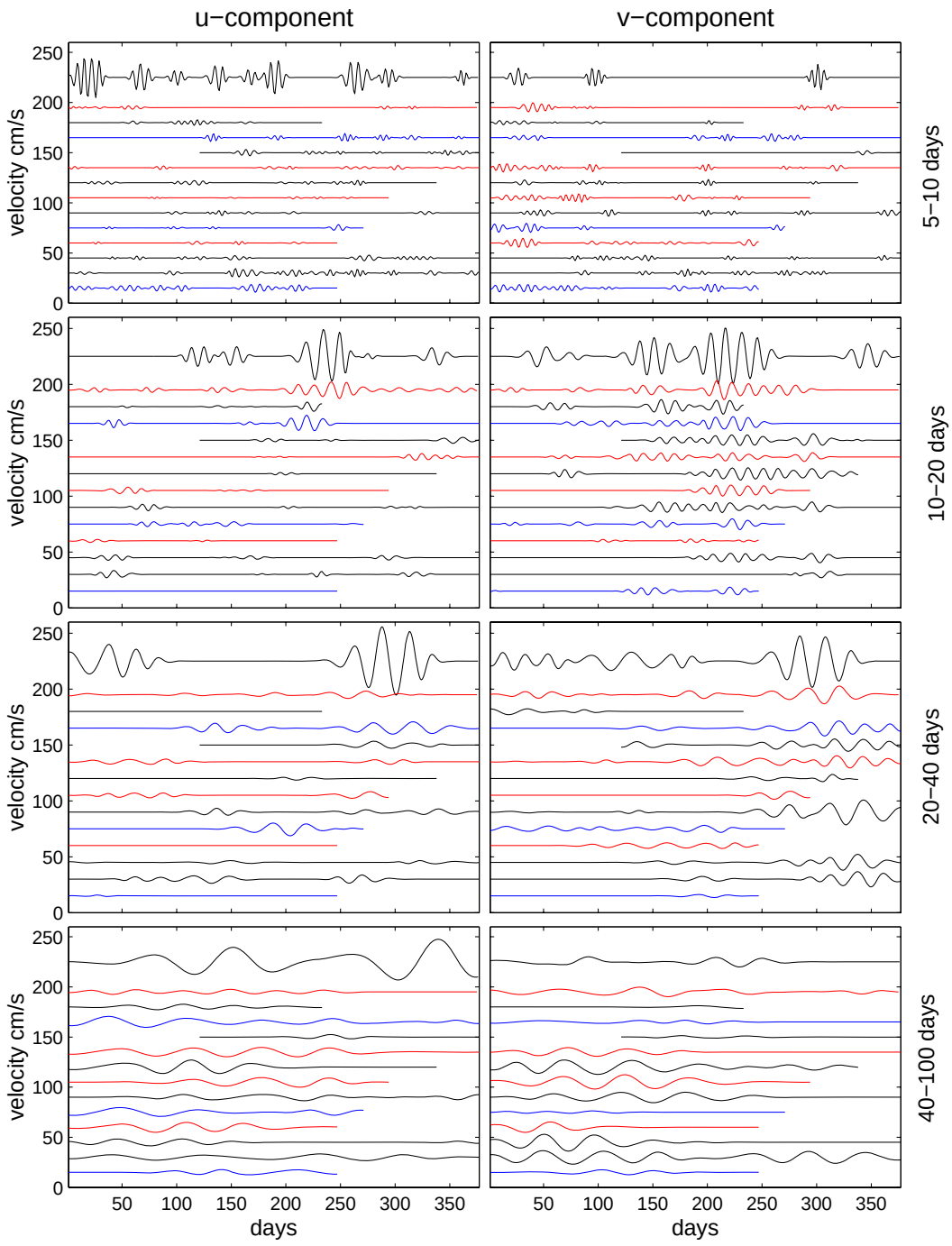

Figure 10: Signal extracted in the different period bands (5-10, 10-20, 20-40 and 40-100 days, up to bottom) for the zonal (left) and meridional (right) velocity components. The time series are in increasing order of depth (ADCP-30, N1-745, A1-825, S1-840, Y1-930, N2-1000, A2-1060, N3-1120, Y2-1190, S3-1360, N4-1385, Y3-1420, A4-1460 and S4-1525) and offset by 15 units, except for the surface where the offset is of 36 units. Northern location series are in red, southern location series in blue and equatorial locations series in black. Time line starts November 12, 1999 and ends November 24, 2000.

1.5. Long Duration Events: Evidence of EDJ

Because the annual cycle is so important in the equatorial Atlantic, at the surface as well as at intermediate and great depths (Mercier and Speer 1998; Schmid et al. 2003; Brandt and Eden, 2005; Böning and Kröger, 2005; Thierry et al., 2005), it is reasonable to hypothesize that the observed low frequency (fig. 8- zonal component) is the result of an annual signal plus the signature of other events of shorter vertical scale, like EDJ. The problem is to identify which variability corresponds to EDJ and which one to the annual signal. An annual signal suggesting a vertical mode 3 or 4 has been observed in current meter data at depth at 15ºW (Thierry, 2000). Moreover, energetic large vertical scale phenomena are often seen in LADCP profiles (e.g., fig 1, Ponte et al., 1990; fig. 3, Schott et al., 2003) and may be associated to this annual signal. On the other hand, EDJ are known to have small vertical scales (400-600 m) and strong amplitudes (~10 cm/s). This relation corresponds to strong nonlinear features characterized by large Froude numbers as estimated from published LADCP sections (e.g., Gouriou et al. 1999; Bourlès et al. 2003). The Froude number, $Fr = \frac{U}{c} = \frac{Um}{N}$, is calculated with a mean Brunt-Väisälä frequency of N=0.0023 s^{-1} (characteristic for those depths using data from the EQUALANT 2000 hydrographic data) and with the velocities and vertical wavelengths derived from the LADCP sections.

The vertical spacing between the current meters used in this study is small (90 m or less, with one exception between Y2-1190 and S3-1360 where the vertical spacing is 170 m) and therefore provides enough vertical resolution to study the EDJ and to answer the question as to whether the observed variability comes from the EDJ or larger vertical scale events. It is also important to consider the meridional spacing between current meters since current meters in the northern and

southern positions could be located outside the jets region. A change in the direction of the flow in that case would represent a meridional scale rather than a vertical scale. Examination of LADCP sections in the depth range of 745-1525 m (Gouriou et al., 1999; Send et al., 2002; Bourlès et al., 2003) shows, however, that EDJs extend to at least to 0.75ºS and N of the equator (with smaller amplitude on either side of the equator) and are therefore adequately sampled by the moored array. The annual signal latitudinal extent is also larger than the mooring array since it is associated with the lowest odd meridional mode Rossby beam (e.g., Brandt and Eden, 2005).

Most zonal component time series present low frequency variability (figs. 3 and 7) which clearly appears in the residues after the extraction of the significant high frequency signals (fig. 8). These large period fluctuations obey neither a standing mode pattern (where changes in phase are of 180 degrees) nor a vertical propagation pattern (changes in phase are not monotonic). Moreover the phase of the fluctuations seems to depend upon depth and not upon latitude.

At 745 m (N1-745), the residual zonal component has a maximum eastward velocity of 15 cm/s around mid July 2000. Approximately at the same time and 255 m deeper (N2-1000), the flow is westward with a maximum velocity of 20 cm/s. The vertical scales as well as the magnitude of the velocities correspond well with the signature of EDJ. Moreover, the depth, magnitude and direction of these flows compare well with the LADCP measurements made in July-August 2000 (fig. 6). The Froude number is calculated as above with a maximum amplitude for the jet velocity of 0.15 m/s and a vertical wavelength $m = \frac{2\pi}{510} m^{-1}$. It is approximately equal to 0.8, a value comparable to those estimated from the LADCP sections.

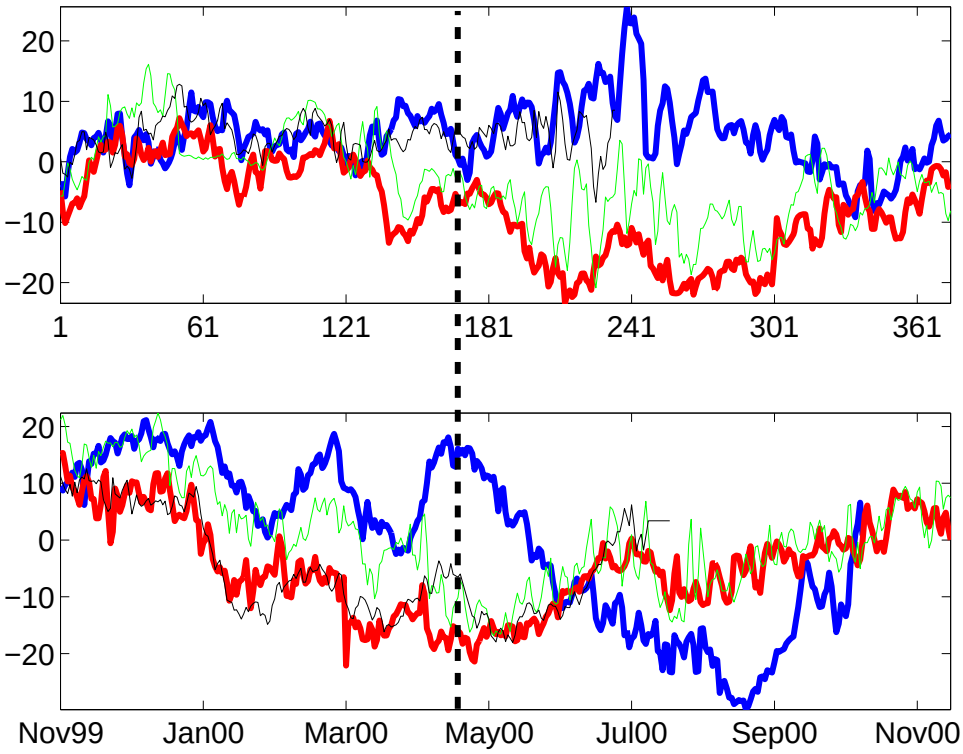

Figure 11: Daily zonal velocity component in cm/s. Top: VACM N1-745 (blue), A1-825 (black), S1-840 (green) and N1-1000 (red). Bottom: VACM A2-1060 (blue), N4-1385 (black), Y3-1420 (red) and A3-1460 (green). Thick lines indicate records from the same latitude with the higher opposite velocities. The black dotted line shows the time of maximum shear between A2 and Y3, discussed in the last section of the manuscript. The x-axis on top is in days (starting November 12, 1999 and ending November 24, 2000) and the one in the bottom indicates the month and year.

These two depths (745 and 1000 m) do not always have zonal flows in opposite directions. At the beginning of the measurements, from mid November 1999 to mid February 2000, the flow at both depths (as well as at A1-825, S1-840) is eastward with a velocity of 3 cm/s (fig 11, top). Then the two series show zonal velocities in opposite direction for approximately 220 days and then again in the same direction by mid October until the end of the record. The data records from instruments at intermediate depths between N1 and N2 (A1-825, S1-840 and Y1-930**)** exhibit the same behavior: A1-825, although lacking some data, suggests a node around that depth (fig. 11-top, cyan line); S1-840 shows a similar pattern than N2 slightly shifted to more positive velocity values, probably because of its shallower depth (fig. 11-top, green line); Y1-930

shows stronger westward flow than N2 (fig. 8), probably because of its location at the equator, where the jet velocities are stronger (fig. 4). All these records (N1, A1, S1, Y1 and N2) present similar zonal velocity values at their beginning (November 1999 to February 2000) and at their end (October and November 2000). One possible explanation is that these two EDJ have an intermittent behavior and a lifetime of around 7-8 months, a time scale much smaller than those estimated in the western tropical Atlantic (at least 5 years according to Johnson and Zhang (2002)). The observations of Weisberg and Horigan (1981) in the eastern tropical Atlantic between 600 and 1800 m suggest similar vertical and temporal scales for the zonal component to those of our observations: 365 m and 4 to 8 months.

Between the records at the equator A2-1060 and Y3-1420, there is also a vertical shear of the zonal component over 360 m depth, lasting 7-8 months (November 1999 to June 2000, fig 8 and 11-bottom). This shear is modulated by ~70 day oscillations and may be as strong as 40 cm/s in 360 m of depth in April 2000 (fig. 11-bottom). The implied vertical scale, 720 m, is larger than the 400-600 m scale of EDJ in the Atlantic. Nonetheless, the Froude number is high ($Fr \approx 0.8$), like in EDJ structures.

1.6. Summary and Discussion

New velocity data from surface and intermediate depths are presented. We analyze these data using a wavelet-based method to extract quasi-periodic variability in the 5-100 day band. The results were classified in four bands: 5-10, 10-20, 20-40 and 40-100 days, for both horizontal velocity components.

Near the surface, the 7-day period oscillations are most probably forced by the wind stress. The satellite wind data shows a peak of energy at around 7 days (fig. 5a and b) and the wavelet

transform for the 1-year PIRATA wind data at 10ºW shows energy at those periods during December 1999 - January 2000 (fig. 6). This period was also observed by Colin and Garzoli (1988) in wind time series taken at 1ºN, 29ºW and 0ºN, 4ºW and was associated with a harmonic of a biweekly signal. The amplitude of the spectrum of the wind zonal component for this peak has a spatial distribution that resembles that of 13 days (fig. 5c and d), with a maximum in the latitudinal band 0º to 6°N, which supports Colin and Garzoli's (1988) findings.

Biweekly fluctuations are present simultaneously near the surface and at depth. Although such fluctuations are present in the wind velocity field, there is no clear pathway to the deep ocean. 14-day period oscillations are especially present in the Gulf of Guinea at the surface (Houghton and Colin, 1987) and have been observed at depth on the continental slope off the Angola coast (Vangriesheim et al., 2005).

Oscillations with periods of approximately 24 days are observed near the surface during August and September. These periods and their timing in the year correspond well with the signature of tropical instability waves in the Atlantic (e.g., Grodsky et al., 2005). A month later, at depth, oscillations with the same period are observed in the meridional component. However, it is not clear whether 24-day period oscillations near the surface can be directly related to the fluctuations at depth. Model studies did however find a variety of short period fluctuations forced by instabilities of zonal currents in the equator (e.g. McCreary and Yu, 1992) and we can therefore surmise that part of the variability found at depth is forced by similar instabilities. This could also explain the marked seasonality observed in the time series with the different period fluctuations along the year resulting from changes in currents strengths.

40-100 day period oscillations are very energetic at intermediate depths and are responsible for important vertical shears in the velocity components. In the meridional component, periods

are approximately 60 days and the resulting shears due to opposite phase of the signal between depths can be as large as 15 cm/s over 360 m. In the zonal component, examples are the 50-day period oscillations present at the start of the 510 m vertical scale 8-month-event, and the 70-day period oscillations observed in A2-1060 (fig. 11). Whether these 50- and 70-day period oscillations are dynamically linked to EDJ or not, they can drastically change the vertical shear between two depths. According to the current meter data, a LADCP section made during April 2000 would have shown a totally different picture of the jets than the one from August 2000 shown in figure 4 (see black-dotted line in fig. 11): in April 2000, there would be no vertical shear in the zonal component between 745 and 1000 m, and strong opposite flows between 1060 and 1420 m.

Despite recent works by Thierry et al. (2005) and Brandt and Eden (2005), the structure of the annual signal in the water column and its variation with longitude remains poorly known. In all these studies, the phase of the annual signal is observed to change monotonically with depth. The low frequency observed in the records presented here does not fit this behavior and, on the contrary, suggests that, if an annual signal is present, it is masked by the presence of EDJ.

Events of long duration show two particularly interesting vertical scales: one of 510 m and another one of 720 m, both defined by the moorings vertical spacing. The first vertical scale is likely related to EDJ since comparisons between the current meter velocity measurements and LADCP data taken around the 1st of August 2000 (fig. 4) show that the amplitudes, directions, and positions associated with the 510 m vertical scale agree with each other: both datasets exhibit an eastward jet at 745 m and a westward one at 930-1000 m. In that case, the current meter time series suggests that the EDJ at 10^{o}W are intermittent with time scales of approximately 7 months. In the case of the 720 m vertical scale, the velocities from both data sets also coincide, but there

is no obvious jet at 1420 m in the August 2000 LADCP data. Despite the fact that the suggested vertical scale of 720 m is larger than commonly accepted (i.e., 400-600m), the strong nonlinearity of the event ($Fr \approx 0.8$ in April 2000) is indicative of a jet-like structure. It is more difficult to estimate a time scale for the 720 m vertical scale since there are large uncertainties associated with the vertical sampling between Y2-1190 and S3-1360: some vertical displacement of the jets may have not been sampled by the array. However, as for the 510 m vertical scale, the zonal velocity shear reversal between time-series A2-1060 and Y3-1420 suggests a time scale of around 7-8 months (fig. 11-bottom).

The information content in the current meter time series therefore suggests that EDJ at 10ºW have shorter time scales than those estimated by Johnson and Zhang (2002) and Send et al. (2002) for the western tropical Atlantic and have similar time scales to those estimated by Weisberg and Horigan (1981) in the eastern Atlantic. The methods used in estimations of EDJ time scales vary considerably, even in the cases where current meter data were used: Weisberg and Horigan (1981) performed a statistical analysis of their measurements and obtained a temporal scale of 4-8 months and a vertical scale of 365 m. However, at first glance, it is difficult to identify any jet-like structure in their data. Send et al. (2002) fit an a-priori model consisting of jets with a fixed vertical scale of 550 m to their mooring data, checked for the vertical phase of the jet system afterwards, and then found an interannual temporal scale for the EDJ. Nonetheless, vertical shear corresponding to shorter time scales can be observed in their figure 11. In this paper, the high vertical resolution of the mooring array allowed us to make direct observations of the duration of vertical shears between two given depths. When comparing the three approaches, it is clear that the results depend greatly on the chosen method of analysis: the measurements of Send et al. (2002) may have yield the same range of time scales if the statistical method of

Weisberg and Horigan (1981) had been applied and vice versa. This raises the question of how one truly defines the time variability of the jets. Should all the jets in the water column be coherent in time? Should a jet be considered the same one if the vertical shear between two depths disappears for a while and then reappears in the same direction? Until the mechanism for the formation of EDJ remains unknown, it is not easy to provide an answer.

Appendix: Signal Detection and Reconstruction

The wavelet transform of a time series *x(t)* is a function of time *t* and "scale" *s*

$$W(t,s) = \int \overline{\psi}_{t,s}(t')x(t')dt' \tag{2}$$

and is formed by projecting the time series onto a set of functions $\psi_{t',s}(t)$ called "wavelets"; here the over bar is the complex conjugate. The wavelets $\psi_{t',s}(t)$ are shifted and rescaled versions of a zero-mean, finite energy "mother wavelet" function $\psi(t)$

$$\psi_{t',s}(t) \equiv \frac{c}{s}\psi\left(\frac{t-t'}{s}\right) \tag{3}$$

where *c* is a constant chosen as

$$c = \frac{2}{\int \psi(t')e^{-2\pi i t'}dt'}. \tag{4}$$

The combination of this choice of *c* together with the scale normalization s^{-1} in (3) has the property that the wavelet transform of a unit-amplitude sinusoid of frequency f_0 has unit amplitude at scale $s=1/f_0$.

The wavelets used here are “analytic wavelets”, meaning their Fourier transforms vanish for negative frequencies. The wavelet transform is then complex-valued even for a real-valued time series *x(t)*, and so we write

$$W(t,s) = |W(t,s)|e^{i\theta(t,s)} \tag{5}$$

where $|W(t,s)|$ is the transform amplitude at the point *(t,s)* and *θ(t,s)* is its phase. Ridges are diagnosed directly from the wavelet transform phase *θ(t,s)* by finding connected curves such that

$$\frac{d}{dt}\theta(t,\tilde{s}(t)) = \frac{1}{\tilde{s}(t)} \tag{6}$$

which states that the rate of change of the wavelet transform phase at scale $\tilde{s}(t)$ is equal to the frequency associated with that scale.

Specifically, we use the generalized Morse wavelets of Olhede and Walden (2002), with parameter choices *β=2* and *γ=4* (defined therein), which control the behavior of the wavelet's Fourier transform at low and at high frequencies, respectively. This choice of parameters reflects a subjective assessment of which parameter settings best captured the variability present in the data.

To reconstruct a time series from its continuous wavelet transform involves integrating over the entire *(t,s)* plane. It is natural to attempt to reconstruct the quasi periodic components (1) by limiting the reconstruction integral to a wavelet ridge. This is motivated by the fact that the wavelet transform is a two-dimensional smoothing of a more fundamental quantity, the Wigner-Ville distribution, which represents any linear chirp as a delta-function (Mallat, 1999). Following this suggestion we write the “ridge reconstruction equation”

$$\hat{x}(t) \equiv \int W(t',\tilde{s}(t))\psi_{\tilde{s}(t)}(t'-t)dt' \tag{7}$$

which exactly reconstructs a sinusoid, and which performed well in our numerical trials with slowly-varying quasi periodic signals.

Chapter 2: Variability in Horizontal Current Velocities in the Central and Eastern Equatorial Atlantic in 2002

Abstract

Near-surface current velocity data from the PIRATA buoy at 23ºW in the year 2002 were re-examined and compared to simultaneous unpublished velocity data at 10ºW, near the surface. Strong 7-day period fluctuations were observed in the zonal velocity component and in temperature records at 23ºW. The large temperature fluctuations near the thermocline depth suggest a vertical velocity component at the same 7-day period. The 7-day period signals occurred in June/July simultaneously with the seasonal upwelling.

The meridional velocity component presented similar spectral contents at 23ºW and at 10ºW. Two distinguishable quasi-periodic signals were observed in the meridional component at both locations: the first signal occurred in the spring, had a periodicity of about 14 days, was subsurface intensified, and had the characteristics of a mixed Rossby–gravity wave. The second signal occurred three times in the year, once in winter 2001-2002, another in summer, and another during fall 2002, had a periodicity of about 20 days, was strongest close to the surface, and was the result of the passage of tropical instability waves (TIWs). This can be confirmed through satellite SST data which show the same periodicities as the meridional velocity records, and spatial structure in accordance with the TIW–SST signature. The summer of 2002, showed different TIW-SST patterns depending upon location, suggesting the existence of different types of TIWs. Finally, the analysis of SST and surface wind data, suggests that variability in the

current meter data for the year 2002 was mainly due to current instabilities, except around boreal spring, where intraseasonal variability in surface winds was strongest.

2.1. Introduction

At intraseasonal time scales, velocity currents near the surface in the equatorial oceans are dominated by quasi-periodic fluctuations associated with the passage of equatorially trapped waves. During the FOCAL/SEQUAL experiment (1982-1984), ocean velocity time series were obtained at different locations in the equatorial Atlantic and allowed the documentation of propagating equatorially trapped waves, in particular of Tropical Instability Waves (TIWs) (Weisberg, 1984; Weisberg and Weingartner, 1988). Since then, velocity observations at the equator in the Atlantic have been rather scarce and confined to single locations (e.g. 23ºW in Grodsky et al. 2005; 23ºW in Brandt et al. 2006; 10ºW in Bunge et al. 2006).

In December 2001, within the Pilot Research Moored Array in the Tropical Atlantic (PIRATA) project (http://www.brest.ird.fr/pirata/piratafr.html), a mooring with an ADCP (Acoustic Doppler Current Profiler) was deployed near the surface at 23ºW. Simultaneously, a Vector Averaging Current Meter (VACM) was deployed at 10ºW by the French program PATOM (Programme ATmosphère et Océan Multi-échelles) at 154 m. The combined data set allows for comparisons of near-surface (upper 150 m) equatorial signals at two different locations, 10ºW and 23ºW during the year 2002.

Most intraseasonal current velocity oscillations in the equatorial oceans are either wind forced or are the result of instabilities produced by the shear of zonal currents (Kessler, 2004). In the eastern part of the basin, wind-forced oscillations having a 14-day period have been observed in near surface oceanic records by Garzoli (1987), Houghton and Colin (1987) and Bunge et al.

(2006). In the last two papers, the structure of the oscillation was surmised to be a Rossby-gravity wave. In the atmosphere, the 14-day period oscillation has been observed in both horizontal wind velocity components. The 14-day period wind oscillations occurred during spring at the equator, when the Intertropical Convergence Zone (ITCZ) is at its most southern position. This is consistent with Grodsky et al. (2003) who found a biweekly oscillation in the zonal wind component associated with a near surface westerly jet close to the African continent, which latitudinal position varied with the meridional migration of the ITCZ.

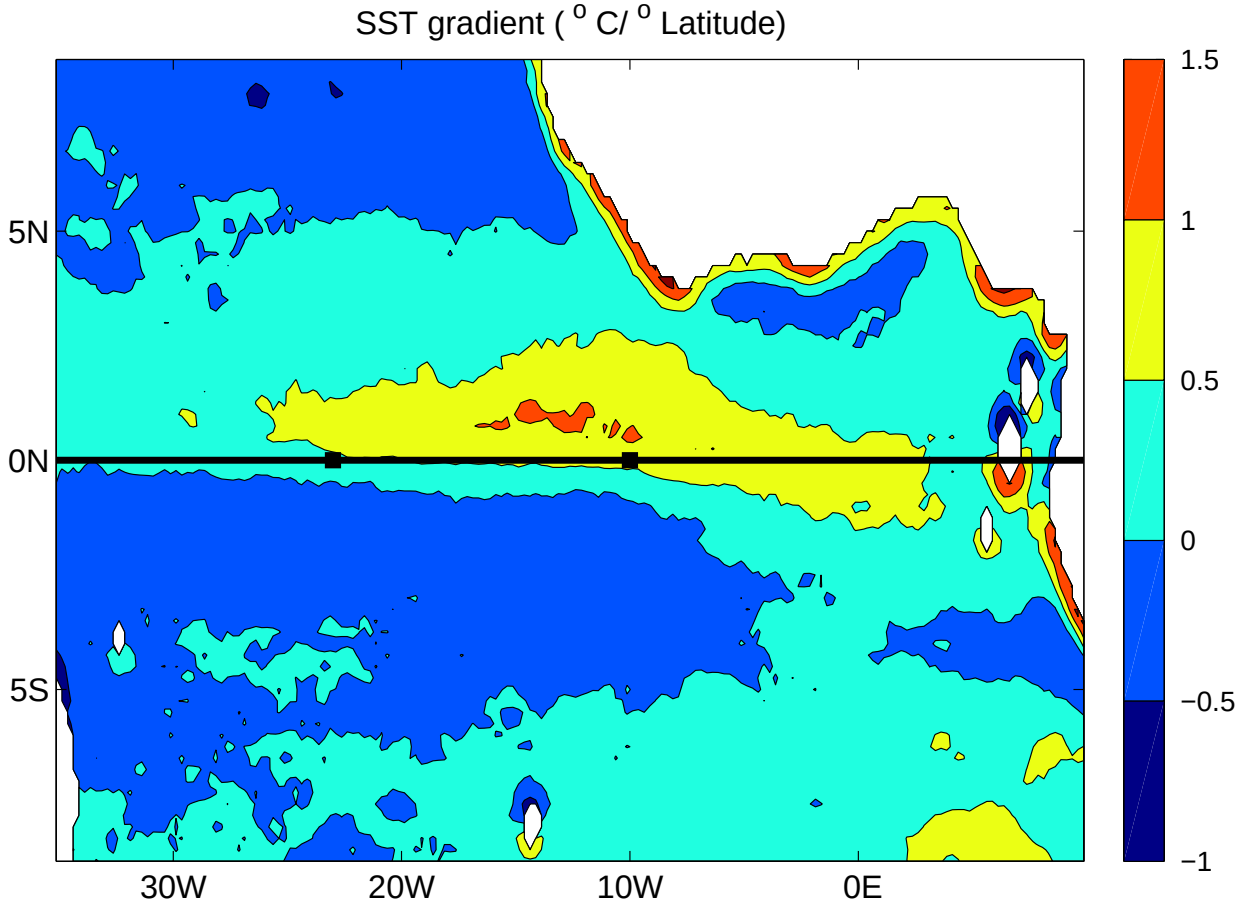

Figure 1: PIRATA/PATOM mooring sites (■) at 23°W and 10°W over a map of mean SST gradient distribution in 2002. The SST meridional gradient was estimated using satellite data described in section 2.

The oscillations resulting from zonal current shears are the TIWS. In the Atlantic Ocean, these oscillations occur mainly in summer, along with the intensification of the South Equatorial Current (SEC), but they can also be seen in late fall (e.g., Caltabiano et al. 2005). They have central periodicities of 25 days, zonal scales of around 1100 km, phase speed of around 0.5 m/s and are strongest in the center of the Atlantic basin (Weisberg and Weingartner, 1988). Their eastward limit is however not well established. Some observations suggest their presence as east as 4ºW (Weisberg et al., 1979), but east of 10ºW, the waves have been observed to have shorter zonal scales (~600 km) and smaller meridional displacements, and to be more transient (Legeckis and Reverdin, 1987). These differences in TIWs spatial-structure suggest the possibility of distinct TIWs depending on the region. In the Pacific Ocean, where TIWs have been most studied, different regions of TIW energy transfer have been detected (Luther and Johnson, 1990). Furthermore, Lyman et al. (2006) found two distinct TIWs presenting different periods, cross-equatorial structure, and dynamics. The first wave is better represented on meridional velocity measurements near the equator, has a central periodicity of 17 days, and a mixed Rossby gravity wave/surface trapped instability structure. The second wave has a strong signature on subsurface temperature data at 5ºN, presents a central periodicity of 33 days, and has the structure of an unstable first meridional mode Rossby wave.

The purpose of the present study is to further describe the intraseasonal variability (5 to 107-day period) in the Atlantic of near surface (upper 150 m) equatorial signals, by analyzing simultaneously velocity data from two different locations, 10ºW and 23ºW, together with satellite sea surface temperature (SST) and scatterometer surface wind velocity data. Since the FOCAL/SEQUAL years, satellite observations have improved with the development of microwave radiometry -which permits measurements of SST through clouds- and surface wind

velocity measurements. Satellite data bring information about the spatial structures of some velocity oscillations, their eventual propagation, their origin and fate, and therefore were useful to support the analysis of the current-velocity observations. Because the data clearly contain quasi-periodic fluctuations which may be modulated in time or may occur only in certain portions of a time series, we used a wavelet-based technique to isolate and extract the signals of interest.

The present paper is organized as follows: section 2 presents the data and data analysis; section 3 describes the near-surface velocity variability and compares it to signatures in SST; and the concluding section discusses and synthesizes the results.

2.2. Data and Data Analysis

Horizontal current-velocity data were obtained between December 2001 and December 2002 from two moorings in the equatorial Atlantic, one at 0ºN, 23ºW, the other at 0ºN, 10ºW (Fig. 1). At 23ºW, a PIRATA acoustic Doppler current profiler (ADCP, Workhorse Sentinel 300 kHz – 4-m cell size and time step of 1 hour) sampled the upper 120 m of the water column (see Fig. 1 in Grodsky et al., 2005), and at 10ºW, a PATOM VACM sampled the horizontal velocity at around 154 m (Fig. 2). Besides the velocity data, simultaneous temperature and salinity data from the upper 120 m of the water column were obtained from the PIRATA buoy at 23ºW (see Fig. 1 in Grodsky et al., 2005) but these data were not available at 10ºW in 2002.

The Vector Averaging Current Meter (VACM; Fig. 2) was calibrated at the Institut français de recherche pour l'exploitation de la mer (Ifremer) for velocity and pressure; details of the data calibration and validation can be found in Kartavtseff (2003). The hourly data were averaged

over 25 hours to remove tidal frequencies and re-sampled to provide daily resolution. Table 1 shows the location, depth and duration of the time-series.

Location	Depth	Starting Date	Ending Date	Days of good data
23ºW	ADCP (12-120 m)	13.Dec.01	21.Dec.02	372
10ºW	154 m	11.Dec.01	29.Dec.02	383

Table 1: Location, depth and number of days of good data of the current meters from PIRATA and PATOM moorings.

Data were analyzed using the wavelet-based technique described by Bunge et al. (2006). This technique isolates significant "ridges" (regions in the wavelet transform with high amplitudes and relatively long duration), and thus the time-varying period of the main components[1]. Once the main components of the signals were extracted, they were classified in period classes. The period range we observed was from 5 to 107 days. The period classes were chosen taking into account other equatorial Atlantic observations (e.g Garzoli, 1987) but also emphasizing that the main components found in these data would be represented by one of these classes. Those classes are: 5 to 10, 10 to 17, 17 to 38, 38 to 72 and 72 to 107 days. Figures 2 and 3 display the number of oscillations for each period band in each time series. The zonal component showed little quasi-periodic oscillations, except at 23°W where 5 to 7-day period oscillations were seen in the upper 120 m. The meridional velocity component was dominated by 10 to 17 and 17 to 38-day period oscillations at both locations. Temperature time series showed the same variability as the zonal velocity component while the salinity time series were well correlated with the meridional motions (Fig. 3). For all in-situ data, there were no quasi-periodic fluctuations in the periods between 38 and 107 days.

[1] Software tools for this analysis can be found at http://www.jmlilly.net/jmlsoft.html

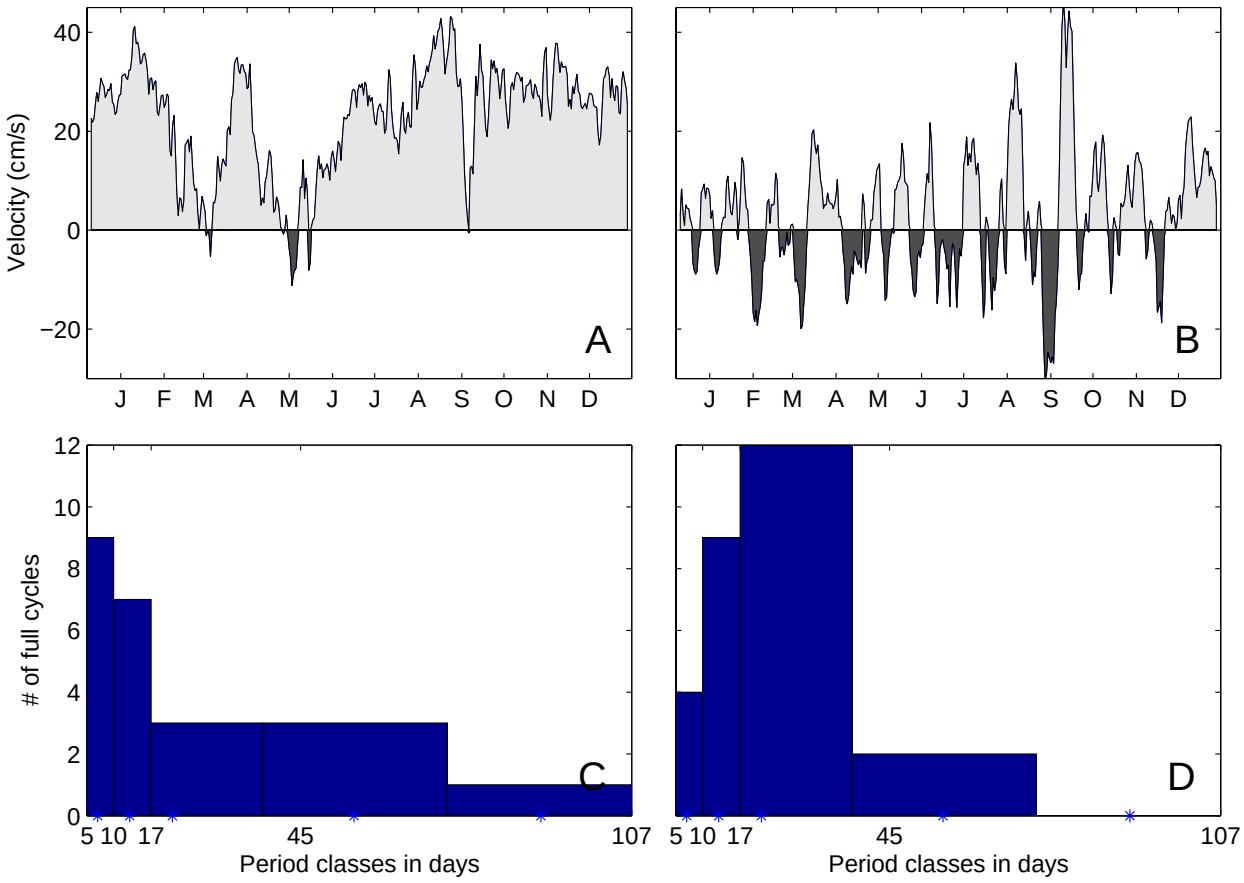

Figure 2: Current-velocity data at 10ºW. *Upper panel*: VACM zonal (left) and meridional (right) velocity components; the depth of the VACM was 154 m. *Lower panel*: Histogram showing the approximate number of full cycles in each period class for the zonal (left) and meridional (right) velocity components of the VACM at 154 m depth.

In order to document the spatial structures associated with the observed velocity fluctuations, Tropical Rainfall Measuring Mission (TRMM) – Microwave Imager (TMI) SST data were examined over the region between 9°S and 9ºN, and 35°W and 10ºE during 2002 (Fig. 1). This SST product is the result of an optimal interpolation with a temporal and a spatial resolution of 1 day and of 0.25º, respectively (http://www.remss.com/sst). Surface wind horizontal velocities were also explored using a daily QuikSCAT product with horizontal resolution of 1/2º which is available at www.ifremer.fr/cersat/en/data/overview/gridded/mwfqscat.htm. SST and wind velocity time series were filtered using a digital Butterworth band pass filter to retain signals

with periods in the band of 5 to 38 days, which is the period band in which all quasi-periodic oscillations in the current-velocity time-series were found.

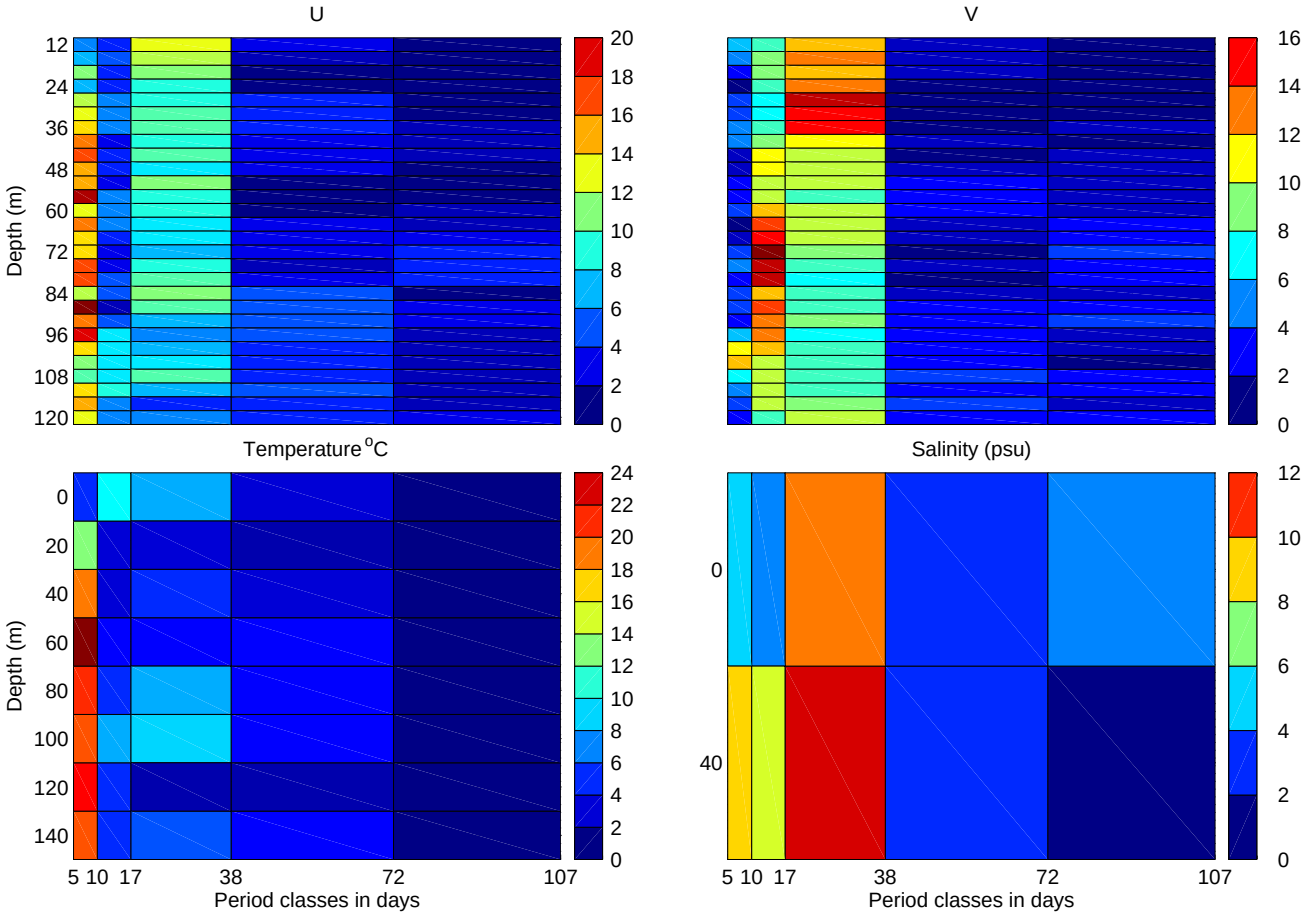

Figure 3: Histograms showing the approximate number of full cycles of each period class, for every measured depth for the different variables measured near the surface at 23º W. *Top-left*: zonal velocity component; *top-right*: meridional velocity component; *bottom-left*: temperature at levels 0, 20, 40, 60, 80, 100, 120 and 140 m. Series at 20, 60 and 120 had gaps. *Bottom-right*: salinity at levels 0 and 40 m.

2.3. Near-Surface (upper 200 m) Variability

2.3.1. In Situ Measurements

The zonal velocity component had few quasi-periodic signals in the intraseasonal time scales when compared to the meridional component. At 23ºW, the zonal velocity component exhibited

20–30-day period oscillations in the mixed layer related to TIWs as described by Grodsky et al. (2005), and fluctuations with a periodicity of approximately 7 days (Fig. 3 ; upper-left panel, period class : 5–10 days). The 7-day signal also had a signature in the temperature record (Fig. 3; lower-left panel). During June and July and at around 60 m depth, close to the thermocline depth, the amplitudes of these 7-day fluctuations reached 25 cm/s in velocity and 2.5ºC in temperature. An increase (decrease) in temperature was associated with a westward (eastward) velocity. Since the strong fluctuations in temperature cannot be surmised to the zonal displacements alone, and since the strongest temperature fluctuations are seen at the thermocline depth, a vertical velocity component at this period must exist. In the record at 10ºW and at 154 m depth, no meaningful 7-day oscillations were observed. During year 2000, intermittent packets of 7-day period oscillations were observed in the zonal velocity component at 10ºW and at 30 m depth (Bunge et al., 2006).

In the meridional component, fluctuations at 23ºW near the surface showed strong similarities with fluctuations observed at 154 m depth at 10ºW. There were two distinguishable signals; the first one had a period of approximately 14 days (period class 10-17 days), it started in mid-February and persisted till the end of April 2002, and was not described in the previous papers using these data (Provost et al., 2004; Grodsky et al., 2005; Giarolla et al., 2005). The second and strongest one had a periodicity of 20–30 days, occurred principally in summer, where it had been associated with the passage of TIWs (Grodsky et al., 2005), but was also observed in December 2001-January 2002 and around November 2002.

The 14-day period signal was coherent in the meridional component throughout the upper 120 m and was also observed in the salinity records for the surface and for the mixed layer (Fig. 3; upper and lower right panels). Maximum meridional velocity amplitudes associated with the

14-day-period fluctuations were found at around 40 m depth, with values of up to 0.45 m/s. There was a time-lag of approximately 5 days between fluctuations at 120 m and at 16 m depths, with the former preceding the latter (Fig. 4; upper panel), implying upward phase propagation. The energy of the signal in the upper 50 m of the water column showed downward radiation (Fig. 4; lower panel). At 10ºW, 14-day-period fluctuations were roughly in phase with those at 23ºW and 120 m. However, one has to be cautious when comparing phases since the two time-series were at different depths and on different isopycnal surfaces. The 14-day signal was consistent with a surface-forced mixed Rossby-gravity wave of vertical mode one or two because a) of its 14-day period, b) lack of variability at that period in the zonal component, c) upward phase propagation and downward energy radiation, and d) an apparent long zonal scale.

TIWs' signatures were observed at both locations during the summer. As for the 14-day period oscillations, the vertical structure of the TIWs presented a phase shift of approximately 5 days between fluctuations at 120 m and at 16 m depths showing upward phase propagation. Zonally, one cannot relate individual TIW-induced fluctuations at 10ºW to fluctuations at 23ºW with in-situ velocity measurements at only these two locations. The reason is that TIWs are generated around 17ºW (Jochum et al. 2004), and akin westward propagating mixed Rossby-gravity waves, the phase velocity propagates westward while the group velocity propagates eastward. TIW-induced fluctuations can thus be observed at 10ºW only if the energy has propagated enough to the east. Such propagation can however easily be documented and tracked with SST data, as shown in the next subsection.

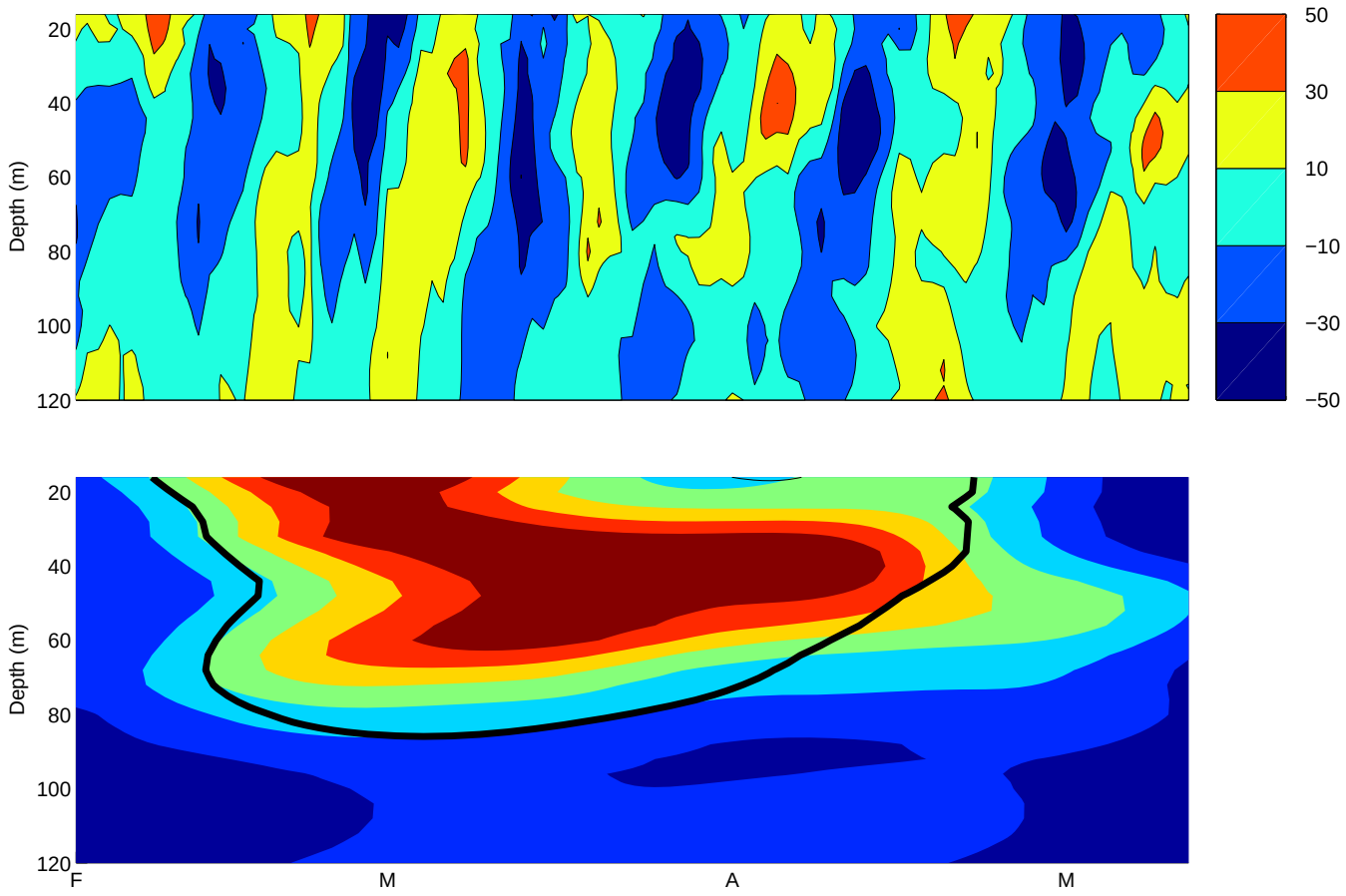

Figure 4: *Upper panel*: meridional current-velocity component (in cm/s) during the 14-day-period fluctuations in the ADCP data at 23W; upward phase propagation is evident. *Lower panel*: normalized wavelet energy of the meridional velocity component for the 12–15-day band; the *black contour* indicates the 95% significance level; downward energy radiation is observed.

2.3.2. Comparison to Satellite SST

TIWs have a strong SST signature and can be easily detected with satellite data. The large spatial and temporal coverage of satellite SST data sets permits to follow the time evolution of SST anomalies and examine their spatial structure. Figure 5 shows two Hovmoller diagrams of filtered SST data at latitude 0.125°N and 1.125°N which describe the time evolution of the SST anomalies. The spatial distribution of the maximum SST gradient is such that, west of 10ºW, it is zonal at ~1ºN and that, east of 10ºW, it is tilted across the equator towards the southeast (Fig. 1).

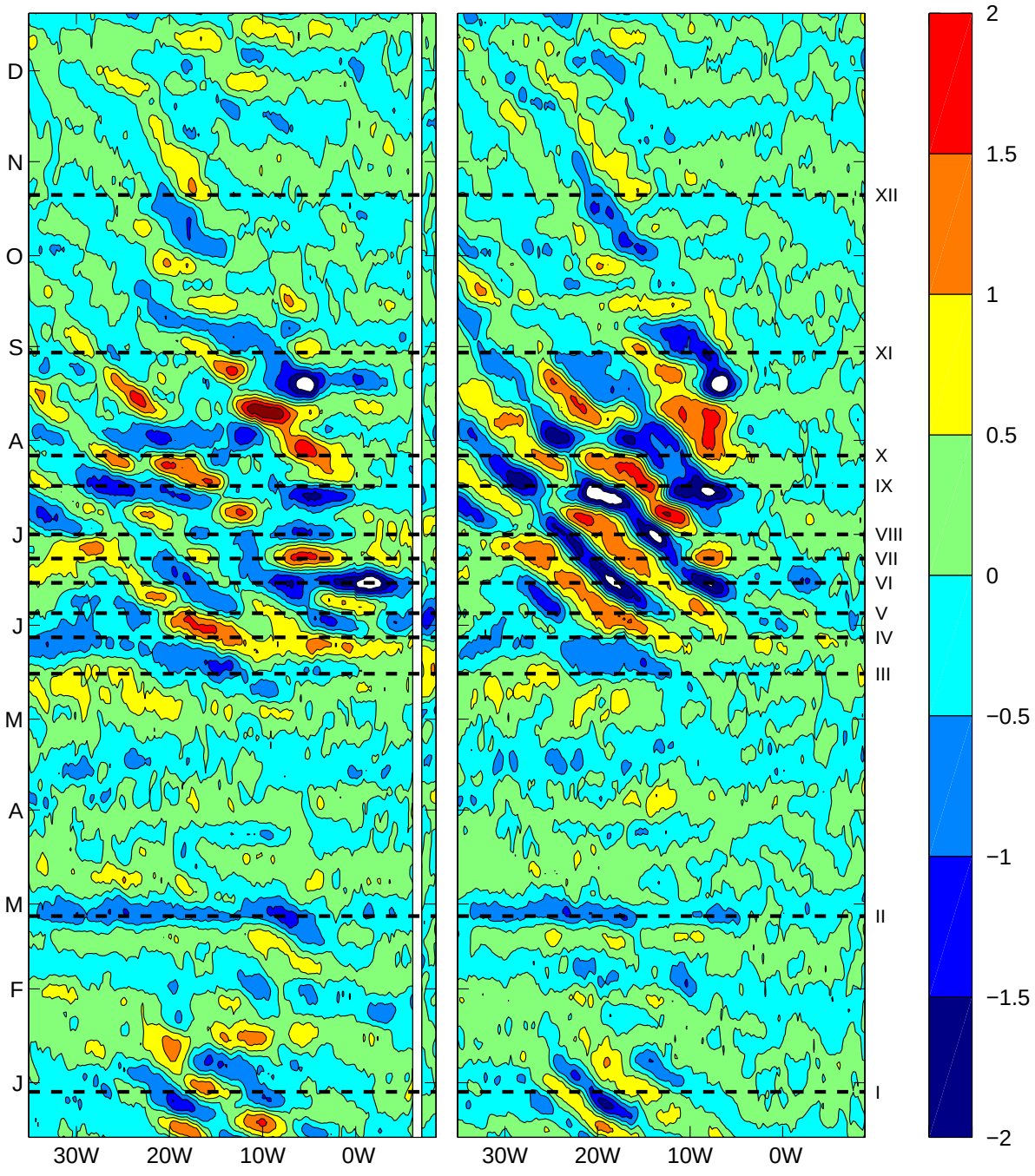

Figure 5: Two SST Hovmoller diagrams at latitudes 0.125º N (left) and 1.125º N (right). SST data has been band pass filter to retain variability in the 5 to 38 day period band. The temperature scale is in º C, the months on the y-axis are set in the first day of each month, and the roman numbers in the right indicate the time for the snapshots on figure 6.

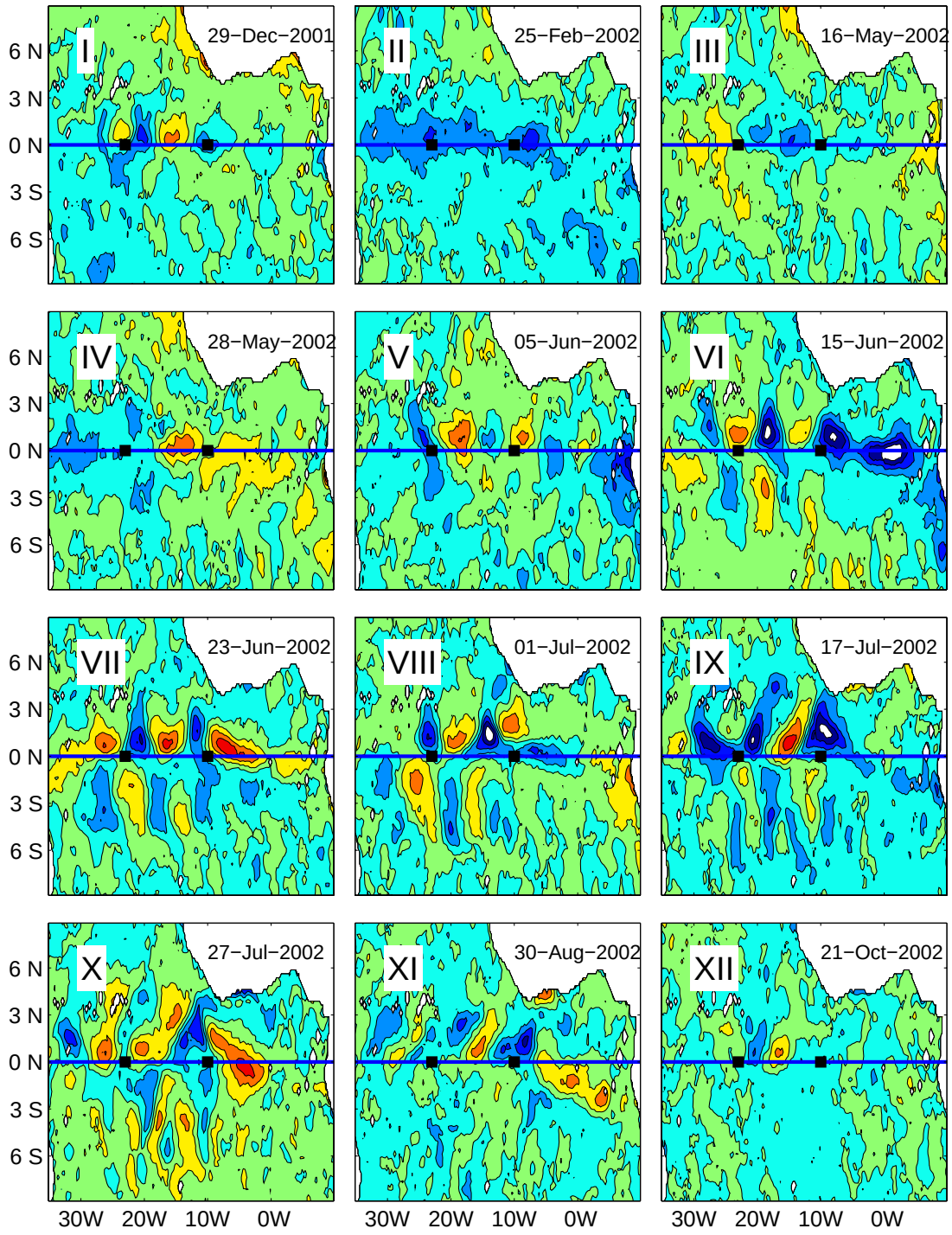

Figure 6: Filtered SST snapshots visualizing the spatial structure of some of the SST anomalies detected in the Howmoller diagrams presented in figure 5. The roman numbers correspond to the marks on the time line in figure 5. For the color code, see the color bar in figure 5.

This implies that variability due to the TIWs in the center of the basin is highly visible in the Hovmoller diagram at 1.125°N while variability taking place in the east of the basin is better illustrated in the Howmoller diagram at 0.125ºN. Both Hovmoller diagrams show TIW-like westward propagating anomalies during December 2001 and January 2002, with a periodicity of 20–30 days and phase propagation of about 0.5 m/s. Between February and beginning of May 2002, basin-scale anomalies showing no propagation and relatively small SST amplitudes were observed. Then, in May, just before the TIW season, eastward propagating anomalies were seen in the west of the basin (Fig. 5). The time period between June and August presented the strongest SST signals. West of 10ºW, there was the unmistakable signature of TIWs. The Hovmoller diagram at 1.125ºN shows the westward phase velocity of TIWs and their eastward energy radiation. TIW events are seen to have originated around 18ºW in early June, and as the energy radiated eastward, their signatures reached 10ºW in mid June. East of 10ºW, however, the

SST anomalies showed no zonal propagation (Fig. 5, left panel). These eastern features could also be the result of instabilities, but, since they present no zonal propagation, they are different from the well known westward propagating TIWs. Both Hovmoller diagrams show westward propagating anomalies from June to mid July in the center of the basin. Afterward, the 1.125ºN diagram shows a discontinuity in the propagation pattern of the SST anomalies and the 0.125ºN diagram shows anomalies which propagated much slower than they initially did. A possible explanation for such changes on the TIW propagating patterns is the coexistence of two different signals at the same time, as it will be discussed in the next section. Later, during October and November, westward propagating TIW-like anomalies were observed again.

In summary, the SST Hovmoller diagrams show westward propagating anomalies with TIWs characteristics at 23ºW during most of the year, except from February to May when the SST

anomalies showed no propagation and large zonal scales. In the eastern part of the basin, the SST anomalies did not propagate.

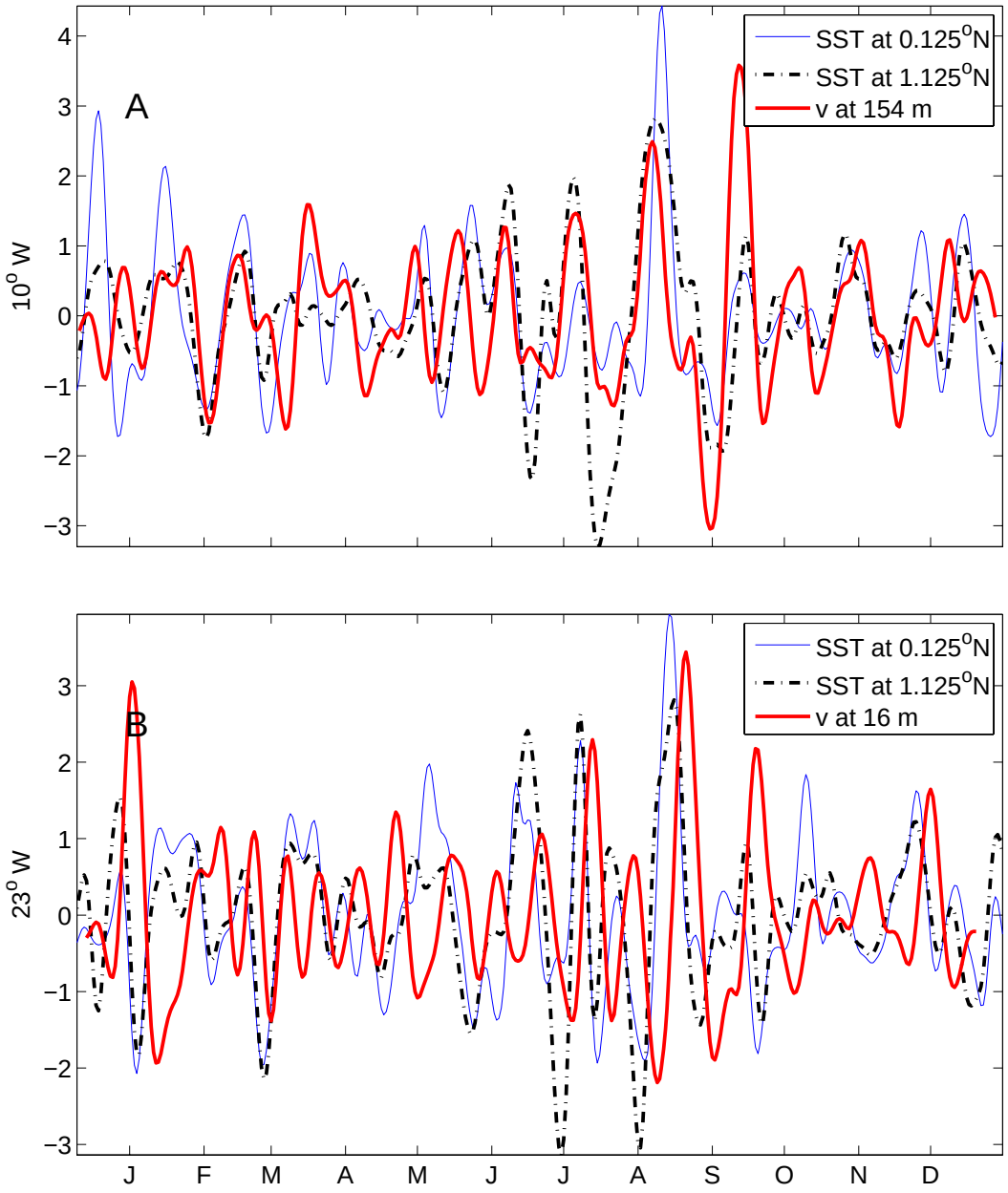

Figure 7: *Panel A:* Normalized and filtered satellite-SST time series from grid points 0.125ºN *(thin line)*, and 1.125N *(dotted lime)* at 10.125ºW, compared to normalized and filtered meridional velocity component data (*thick line*) at 10ºW and 154-m depth. *Panel B*: Same as *panel A*, but for SST time series at 23.125ºW and meridional velocity component at 23ºW and 16-m depth.

The spatial structures of the SST anomalies detected in the Hovmoller diagrams are shown in the 12 panels of figure 6. Panel I illustrates the TIW-like features that occur at the end of December 2001 and beginning of January 2002. During that period, a train of at least three alternate-sign SST anomalies centered at about 1ºN and presenting zonal scales comparable to those of TIWs was observed. The panels II and III (corresponding to February 25 and May 16, 2002) show an example of the non-propagating large scale features detected in Fig. 5.The transition from basin scale anomalies to TIWs is illustrated by the panels IV and V: on May 28, two opposite-sign anomalies were situated at the equator and by June 5, the SST anomalies from the northern hemisphere began to show smaller zonal scales. The SST snapshot of June 15 (panel VI) shows well developed TIWs. West of 10ºW, the SST anomalies exhibit zonal wavelengths of approximately 1,100 km and an antisymmetric phase structure about the equator, both characteristic of TIWs (e.g., Weisberg and Weingartner, 1988; Chelton et al., 2000). The TIW-SST signal was strongest by June 23 (panel VII). East of 10ºW, however, the temperature anomalies are very different, presenting similar periodicities but at larger zonal scales than the SST anomalies west of 10ºW (panels VI, VII and VIII). Around July 17 (panel IX), the antisymmetric structure about the equator of the TIWs became disorganized: in the southern SST anomalies, at about 4ºS, there was a partition of the zonal scale leading to a new zonal scale of roughly 500 km (panels IX and X). In the northern hemisphere, the SST anomalies are no longer round-shaped**,** as it is the case on the July 27 snapshot (panel X). By the end of August (panel XI), the TIW season, as represented in the SST snapshots, was over. Later, in October and November 2002, SST anomalies with the characteristics of TIW were however again observed around 18ºW (panel XII).

The variability in the satellite SST series at 10ºW and 23ºW (Fig. 7) does show similarities to that of the meridional velocity data fluctuations. This is especially true for TIW events at 23ºW (Fig. 7b). At 23ºW, there is a time-lag between the SST and the meridional velocity records at 16 m depth, with the SST leading by 5–10 days, depending on the particular TIW event (Fig. 7b). There is however no phase lag between the SST and the meridional velocity at 120 m (not illustrated). This is not surprising considering that the phase propagation of the meridional velocity component is upward with the TIW- signal in the meridional velocity component at 120 m depth happening to be in phase with the TIW-SST signal. Similarly, at 10ºW, there is also no time-lag between SST-TIWs events and the 154 m depth velocity time series (Fig.7a).

2.4. Discussion and Conclusions

In the near-surface velocity data set at 10ºW and 23ºW, signals at subseasonal time-scales are less conspicuous in the zonal component than in the meridional component. There is, however, one exception at 23ºW: fluctuations with periodicities of 5–7 days which showed a near-surface temperature signature as well. The relation between temperature and zonal velocity component cannot be surmised to the zonal displacements since zonal temperature gradients are unlikely to be important on a 7-day time scale. Since the largest amplitudes in temperature (2.5ºC) are seen at the thermocline depth (~60 m), it is most likely that these near-surface temperature fluctuations are linked to vertical water movements. The temperature fluctuations in the 5- to 10-day range are especially interesting since they mostly occur during June and July simultaneously with the seasonal upwelling and therefore could contribute to the heat exchange at the base of the mixed layer.

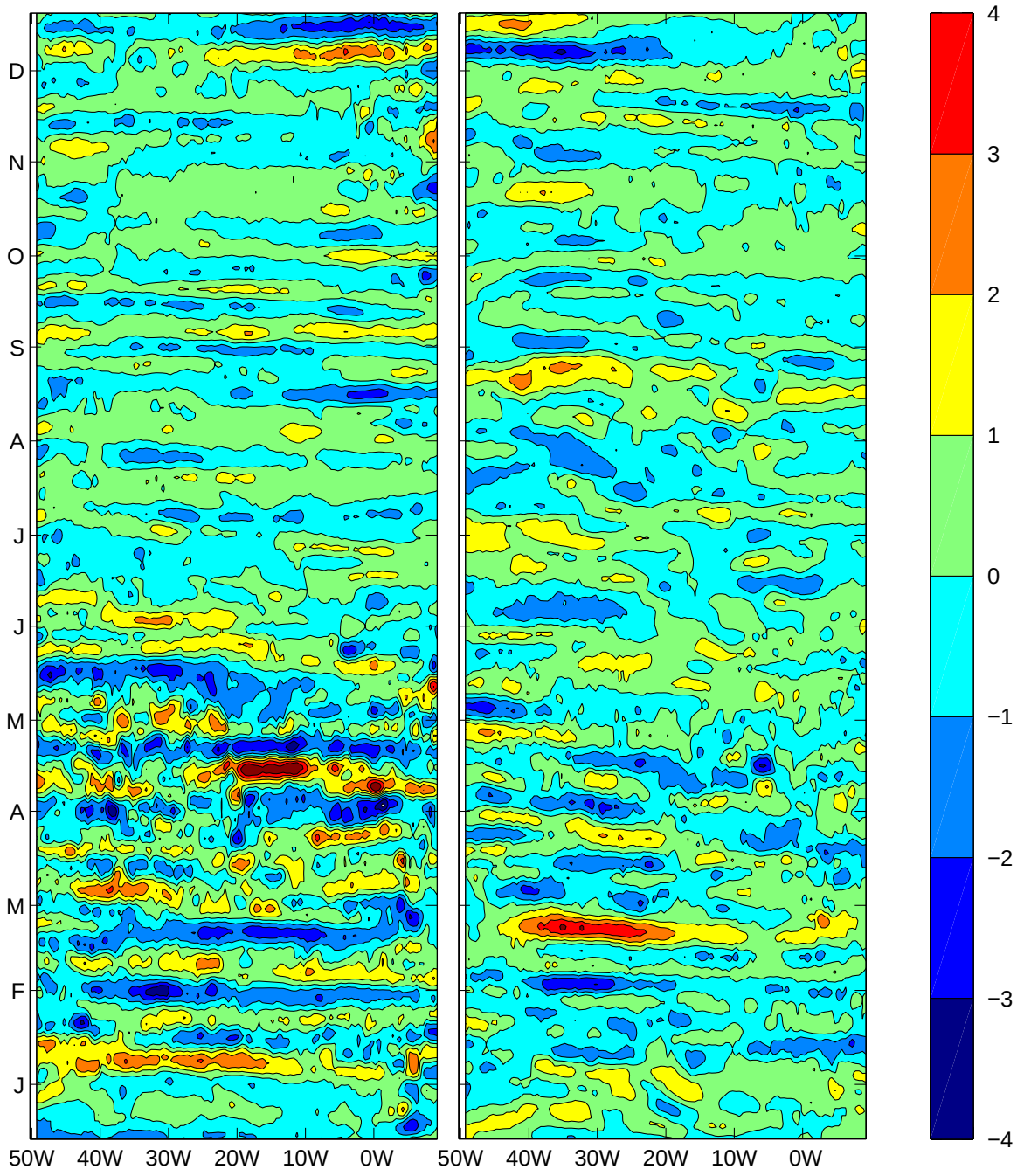

Figure 8: Hovmoller diagrams of zonal (left) and meridional (right) wind velocity components at latitudes 0.25º N. The wind velocity data has been band pass filter to retain variability in the 5 to 38 day band. The velocity scale is in m/s and the months on the y-axis are set in the first day of each month.

An important part of the variability observed at both locations in the near-surface meridional velocity component is due to oscillations with an approximately 14-day periodicity (Fig. 4). These 14-day-period oscillations are present exclusively in the meridional component, show a clear upward phase propagation and downward energy radiation, reminiscent of a first mode mixed Rossby–gravity wave of similar characteristics to what was observed in the western Pacific Ocean by Zhu et al. (1998). In Zhu et al. (1998), the wave resulted from a northerly wind burst crossing the equator. Examination of QuikSCAT surface wind velocity data for the year 2002 in the Atlantic shows great activity at intraseasonal time scales in both horizontal velocity components at large zonal scales (Fig. 8). When comparing the QuikSCAT wind velocity data to the current velocity data, however, we could not find a perfect correspondence for all individual events with either wind velocity component. When there is no correspondence, this does not mean that the 14-day period oscillation in the meridional velocity is not due to wind fluctuations: it could indeed be set in motion by the wind initially and then persists as a free wave by its inherent dynamics. The SST data between February and May 2002 showed non-propagating large scale anomalies and, even though these anomalies occurred simultaneously with the 14-day period oscillation in the meridional velocity component, they could not be directly related to the first baroclinic mode mixed Rossby-gravity wave observed in the velocity measurements. This is because i) the SST time series has larger periods than the meridional current-velocity time series and ii) the SST signature of a mixed Rossby gravity wave should show an antisymmetric temperature structure about the equator and the SST anomalies of boreal spring 2002 have a symmetric structure about the equator.

TIWs can easily be detected in SST snapshots by their equatorially antisymmetric phase structure and by their zonal scale of ~1100 km (e.g., Chelton et al., 2000). This situation is

observed three times in the year, one at the beginning of 2002, one in summer 2002, and another one in fall 2002. The formation of TIWs depends on the intensification of zonal equatorial currents (e.g., Kessler 2004) and, since there is a second intensification of the winds and currents in the Atlantic during the November-December period (e.g., Provost et al., 2004; Okumura and Xie, 2006), it was not surprising to observe TIW-like events during November 2002. The TIW events in early January, however, can only be explained in terms of interannual variability. Indeed, an analysis of interannual variability in the equatorial Atlantic by Provost et al. (2006) showed that the winter 2001-2002 had the coldest SSTs, the strongest westward winds, and the steepest zonal slope anomaly, when compared with other winters from 1993 to 2003. These anomalous conditions could have also led to anomalously stronger equatorial currents which in turn could have favored the generation of TIWs in winter 2001-2002. Overall, variability in both the SST and the meridional velocity component was dominated by TIWs-like events throughout most of the year, except from February to mid May. During the latter, the agreement between the zonal scales of the SST and wind velocity anomalies as well as between the 14-day period in wind and current meridional velocity suggests that the variability was wind forced.

The antisymmetric phase structure of the TIW events during the summer of 2002 was only observed from early June to mid-July. Afterward, the anomalies north of the equator became disorganized and the anomalies to the south reduced their zonal scale by half and disappeared soon after. These changes are accompanied by a reduction of the phase velocity of SST anomalies at the equator (see Hovmoller diagrams on Fig. 6). Despite the fact that the SST anomalies no longer had the antisymmetric shape of TIWs, the SST time-series and the meridional velocity component at 23ºW went on showing perturbations with the same periodicity, therefore implying that the TIWs had not died off. Indeed, SST signatures of TIWs

in the Pacific Ocean have been shown to persist after the velocity perturbations have died off with the propagation of the anomalies resulting from advection by the background flow (Contreras, 2002). Also in the Pacific Ocean, there is an apparent difference in the periodicity of TIWs, depending on the quantity under consideration: SST, altimetric sea surface height, or current velocity (Kessler, 2004). This is not the case in the Atlantic; time-series of SST at 10ºW and 23ºW have oscillations induced by TIWs with the same periodicity as the TIW- induced signatures in the near-surface velocity records (Fig. 7). This fact made the comparison between the velocity and SST data sets straightforward. Lyman et al. (2006) found that the differences in the periodicity of TIWs in the Pacific detected on off-equatorial temperature records and on meridional velocities at the equator, were the result of two types of TIWs coexisting at the same time with distinct periods, dynamical structures, and latitudinal extent. During the deformation of TIWs in mid July, the reduction of the phase velocity of the SST-anomalies at the equator suggests the development of a different TIW. However, there is no change in the period.

Finally, another intriguing set of SST anomalies were the ones found east of 10ºW in the Gulf of Guinea. Although they presented the same periodicities as in the west, their temperature structure had different characteristics: the zonal scale was larger than that of TIWs observed in the west and they did not propagate (Fig. 5 and 6). Whether all these different SST-TIW anomalies expressions share the same dynamics or not, whether they are all part of a single instability process or of different types and/or regions of TIW generation, are questions that remain to be explored.

Chapter 3: Variability at Intermediate Depths at the Equator in the Atlantic Ocean in 2002-2005: Equatorial Deep Jets and Low-Frequency Meridional Flows

Abstract

Simultaneous time-series of high vertical resolution currentmeter measurements were obtained between 600 and 1700 m depths at two locations, 10ºW and 23ºW, on the equator in the Atlantic. The temporal mean zonal velocity component bears the characteristics of equatorial deep jets (EDJ, which have amplitudes of ~8 cm/s and vertical scale of ~500 m), is longitudinally coherent between the two locations and suggests a time-scale of 5 years. The zonal component also presents a downward-propagating signal with amplitude and vertical scale in the EDJ range and with a period of approximately 18 months, and a seasonal cycle with larger vertical scales than those of EDJ. At 23ºW, the meridional component presents low-frequency fluctuations of about 6 cm/s in amplitude and 600 m in vertical scale, which could be linked to EDJ and the presence of the Mid-Atlantic Ridge.

3.1. Introduction

Equatorial Deep Jets (EDJ) are characterized by vertically stacked alternating eastward and westward jets with small vertical scales (400-600 m in the Atlantic)**.** They are confined to a narrow equatorial band (total width less than 3° latitude), and to depths between the thermocline and 2500 m (e.g. Gouriou et al., 1999; Bourles et al., 2003). Their zonal extent in the Atlantic Ocean has been estimated to reach 25º-27º (Gouriou et al., 2001; Schmid et al., 2005). Their

time-scale is controversial. Some authors suggest a periodic wave-like behavior with periods of at least 5 years (Johnson and Zhang, 2002), whereas others suggest an intermittent behavior (Send et al., 2002) of variable duration which may be as short as a few months (Bunge et al., 2006a).

EDJs as well as other semi-permanent currents at intermediate depths are potentially important features in the mass transfer of Antarctic Intermediate Water and North Atlantic Deep Water. Estimates of the transport of these two water masses along the equator by EDJs are difficult because the temporal nature of EDJs is unknown (permanent, oscillatory or intermittent).

We present here the first simultaneous time-series of high vertical resolution current meter measurements at intermediate depths (600-1700 m) at two locations on the equator, 10ºW and 23ºW. This exceptional data set provides some insight into the temporal nature of EDJs as well as allowing new estimates of the amplitude and phase of the annual cycle at intermediate depths. Furthermore, for the first time at these latitudes and depths, low-frequency meridional flows with small vertical scales have been detected.

3.2. Data

The data consist of 2 years of horizontal velocity measurements gathered by Vector Averaged Current Meters (VACMs) at intermediate depths (600-1700 m) at 23ºW and 10ºW. At 10ºW, the two year long time series are continuous from May 2003 to June 2005. At 23ºW, the time series are discontinuous: a first period is from December 2001 to December 2002 and a second period from February 2004 to May 2005. Thus, the two sites were instrumented simultaneously from February 2004 to May 2005.

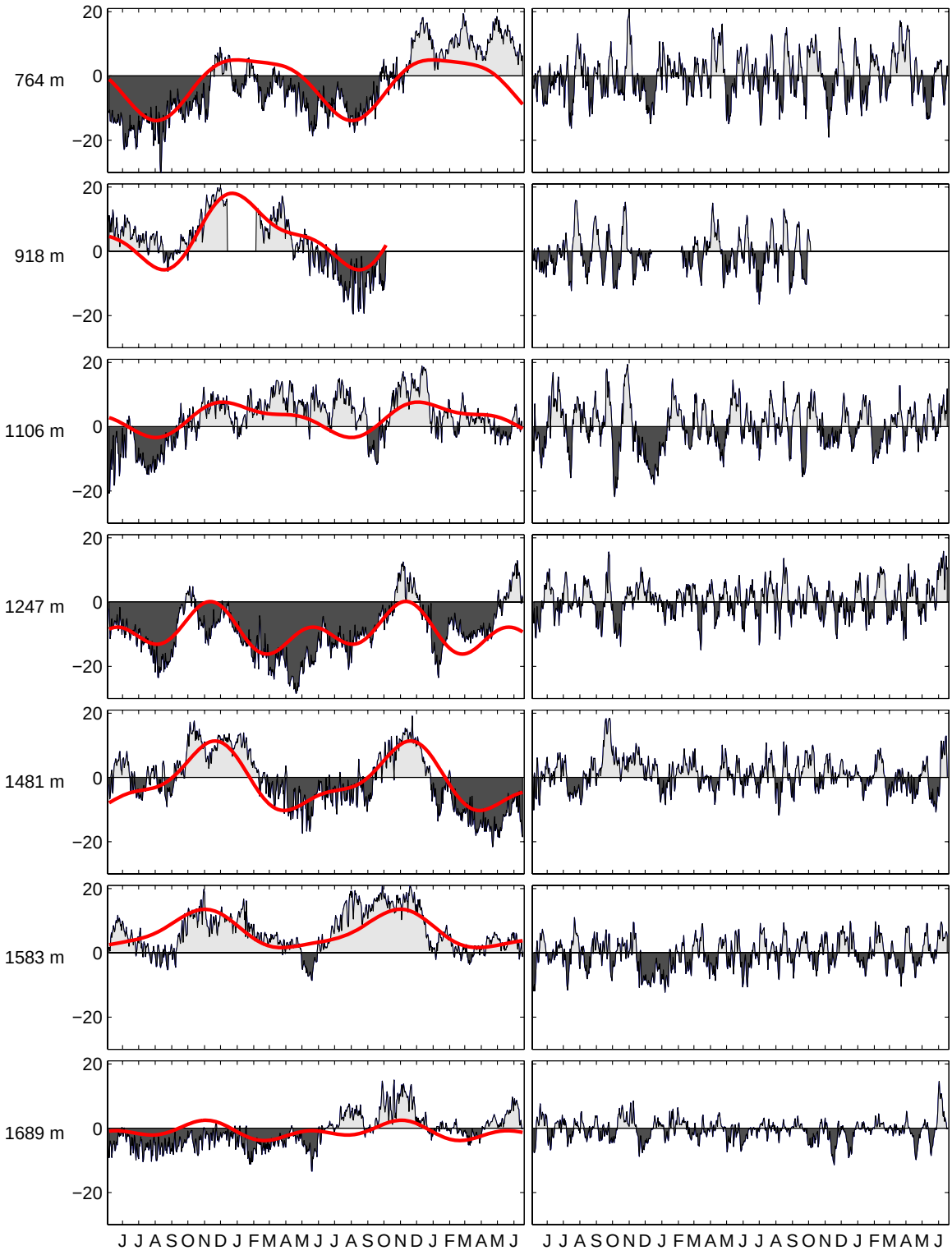

Figure 1: Velocity data from 10º W and the equator. Left panel: zonal velocity component and least square fit (red). Right panel: meridional velocity component. Depth of the instruments is indicated to the left. X-axis indicates time in months starting in May 2003 (duration May 7, 2003 – June 17, 2005). Y-axis indicates velocity in cm/s.

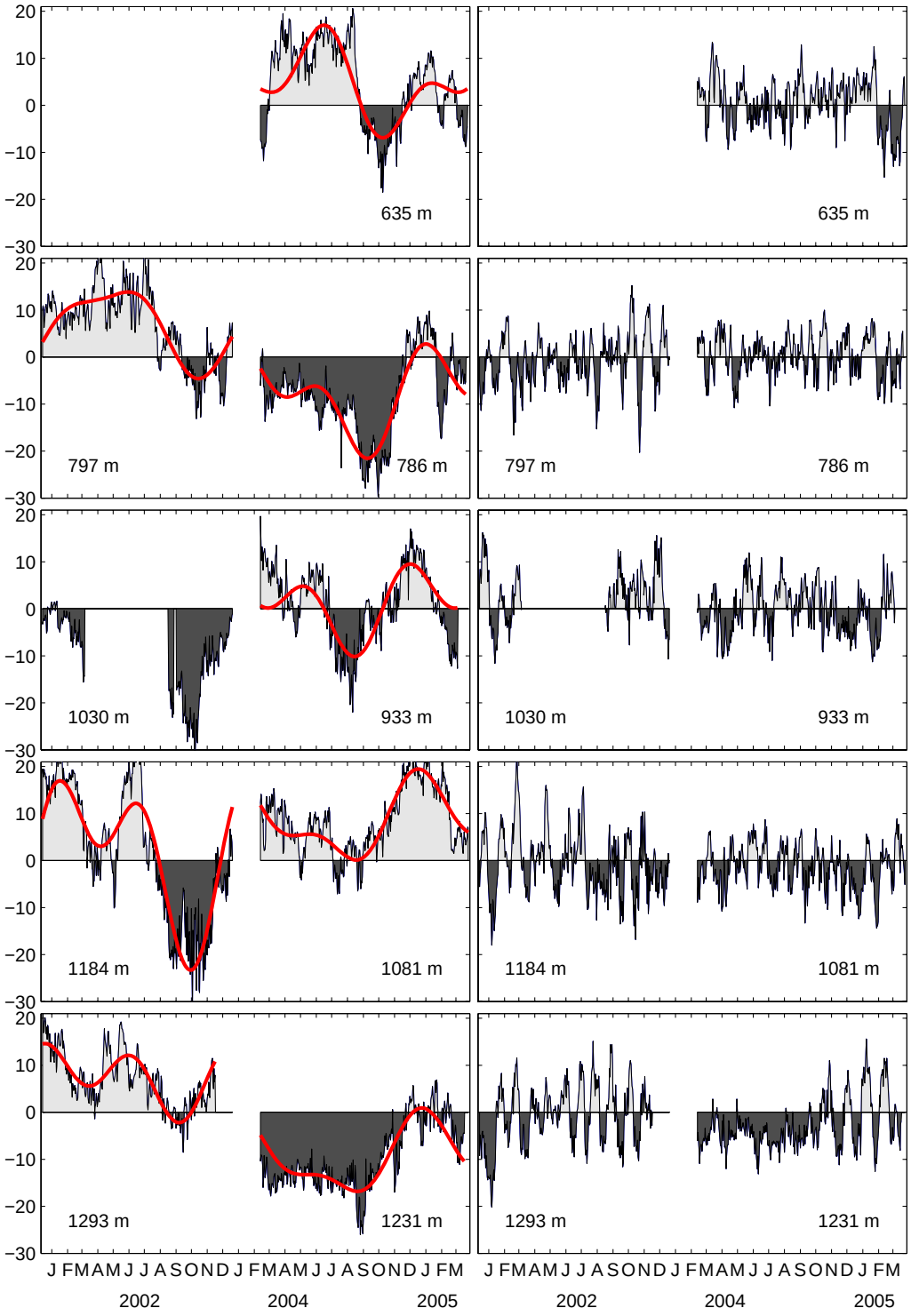

Figure 2: Velocity data from 23º W. Left panel: zonal velocity component and least-square fit (red). Right: meridional velocity component. Depth of the instruments is indicated below each time series. Note that depths of instruments in the same panel may vary. *X*-axis indicates time in months from December 2001 to March 2005. Note that the time line is not linear; there is a gap in the data from December 2002 to February 2004. *Y*-axis indicates velocity in cm/s.

The VACMs were calibrated at the Institut français de recherche pour l'exploitation de la mer (Ifremer), in Brest, for velocity and pressure; details of the data calibration and validation can be found in Kartavtseff (2003), Kartavtseff 2004, and Kartavtseff (2006). The hourly data were averaged over 25 hours to remove tidal frequencies and re-sampled to provide daily resolution (Fig. 1 and 2).

3.3. Zonal Component

3.3.1 Equatorial Deep Jets

The signature of the EDJs, vertically stacked alternating eastward and westward jets with vertical scales of about 500 m and peak-to-peak amplitudes of more than 10 cm/s, was detected in the temporal mean zonal velocity profiles (Fig. 3). Mean zonal velocity profiles at 23ºW and 10ºW for the common period of time (February 2004 to March 2005) presented eastward and westward jets at approximately the same depths, suggesting continuity of the jets between 23ºW and 10ºW, in agreement with previous observations (Gouriou et al. 2001; Schmid et al. 2005). In contrast, the zonal mean velocity profiles at 23ºW (years 2002 and 2004-2005) showed jets with opposite direction at approximately 800 m, 1100 m, and 1300 m, demonstrating the non-permanent nature of the jets. Furthermore, the zonal mean profile using the entire time series at 10ºW (May 2003 to June 2005) showed an intermediate configuration of the jets between 800 m and 1100 m, when compared to the mean profiles at 23ºW for the year 2002 and 2004 (Fig.3). This evolution of the zonal mean profile with time (at 23ºW, jets with opposite direction in 2002 and 2004; at 10ºW, an intermediate configuration of the jets between 800 m and 1110 m in 2003), suggests a time scale for these jets of approximately 5 years, which is consistent with time-scales estimations from LADCP sections (Johnson and Zhang, 2002).

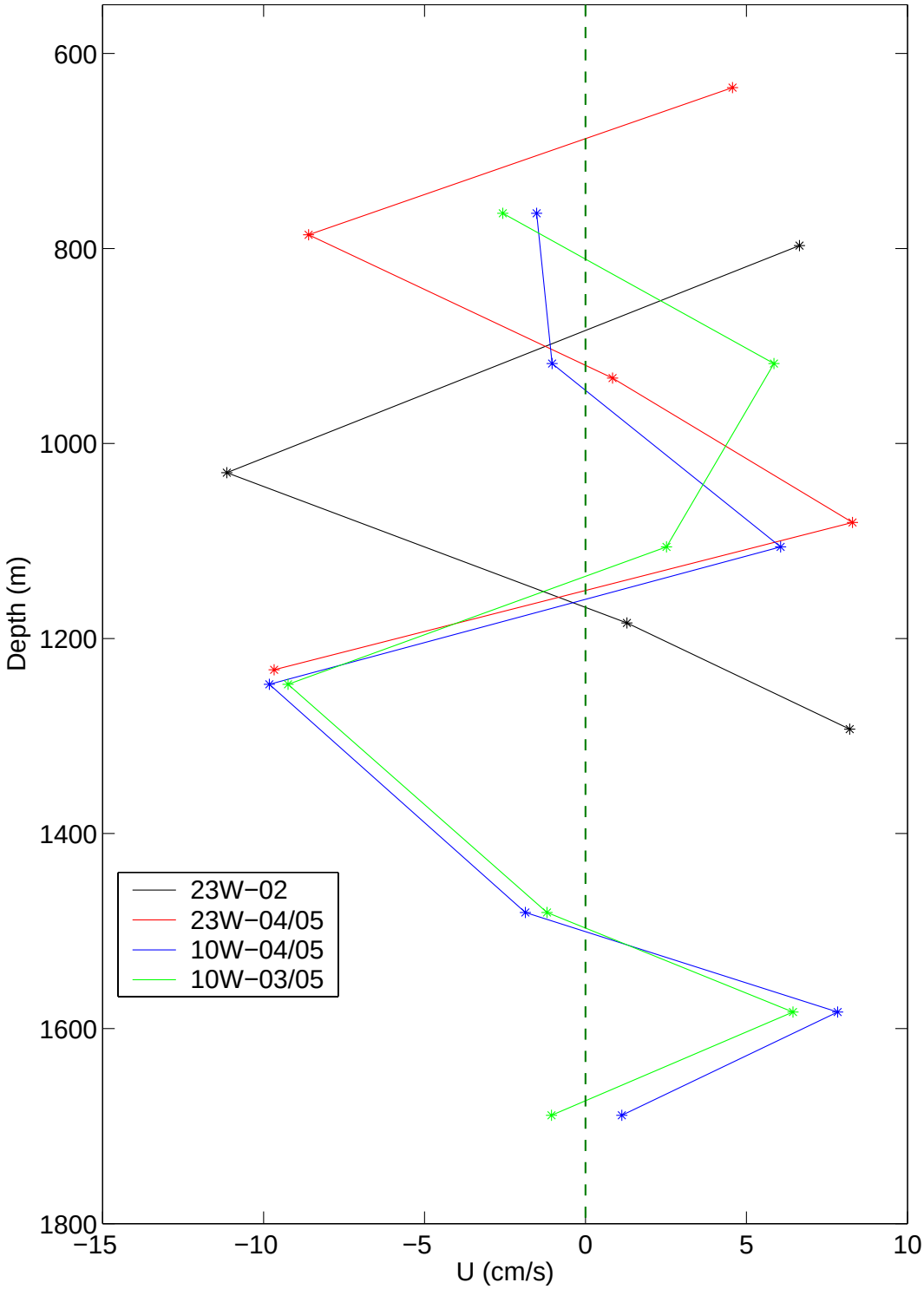

Figure 3: Mean zonal velocity component after extracting the seasonal and semiseasonal harmonics. Green: 10º W for the entire 25-month record; blue: 10º W from February, 2004 to March, 2005; red: 23º W from February, 2004 to March, 2005; black: 23º W for 2002. Positive is westwards, negative eastwards. Note that the time-series from 10º W at 930 m and from 23º W at 1030 m have gaps (cf Fig. 1 and 2); the mean in that case is computed from the available data (blue and green and black curves).

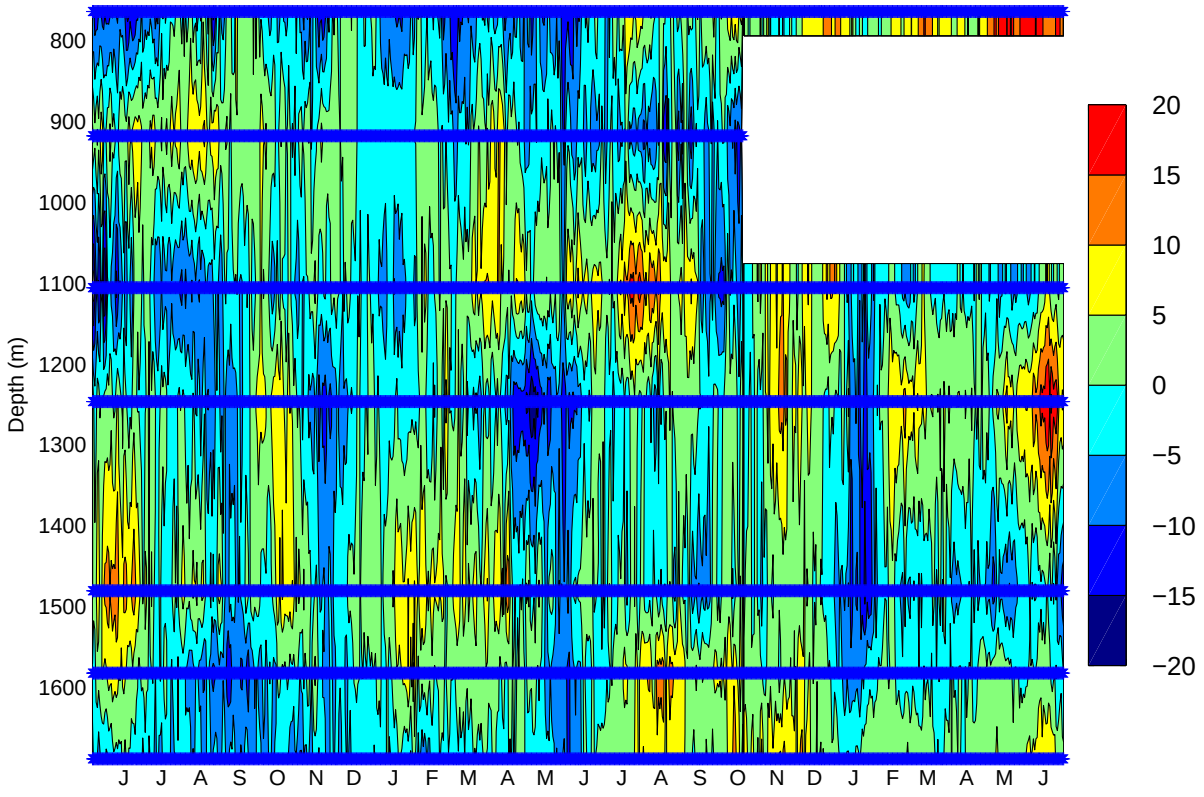

Figure 4: Zonal velocity component anomalies at 10º W. The temporal mean and the seasonal and semiannual signals have been subtracted. Horizontal lines indicate the depth and the length of the time-series. Positive is westwards, negative eastwards. *X*-axis indicates time in months from May 2003 to June 2005.

The other signal with the EDJ imprint in this data set became clear after removing the mean, seasonal, and semiannual signals (Figs. 1 and 2) from the time-series at 10ºW. Figure 4 shows a downward propagating signal with vertical scales of approximately 500 m. The downward phase velocities are reminiscent of the changes in EDJ depths with longitude observed by Schmid et al. (2005), who suggested that vertically propagating, equatorial trapped waves could lead to the alternating sign in the velocity profiles typical of EDJ. The downward propagation began around October 2003 and lasted until the end of the measurements (June 2005). A downward phase speed of roughly 330 m over 12 months (c=1.06×10^{-5} m/s) could be deduced from data as well as

a vertical wave number $m = 2\Pi / 500$ m^{-1} and a frequency $\omega = cm$. Thus, the period of these signals is about 18 months.

At 23ºW, vertical propagation was unclear (not shown). This may be because the data sets at 23ºW are shorter in time as well as in vertical extent than the data set at 10ºW (1 year and 496 m or 596 m, compared to 2 years and 925 m). Instead, the residues at 23ºW suggested variability with time-scales on the order of a few months. Bunge et al. (2006a) found time-scales of ~7 months for the EDJ at 10ºW from a 1-year-long time-series. The propagation pattern observed in Figure 4 is noisy. Note that examination of one year of the 2-year data set at 10ºW, between February 2004 and February 2005 (Fig. 4), for example, could lead to the mistaken conclusion that EDJs lasted only a few months because the propagating signal was only observed during a few months at a particular depth.

3.3.2 Semiannual and Annual Cycle

Together with the EDJs, a seasonal signal of large vertical scale is observed in the zonal velocity component. A sinusoidal curve containing annual and semiannual harmonics was fitted to the data using the least-squares method (Figs. 1 and 2). Table 1 indicates the amplitude, phase and percentage of variance explained by each harmonic and by their sum. Even though time series are short for the estimation of an annual signal, the phase of the annual signal estimates present a coherent structure in the vertical, providing confidence to the analysis.

With a few exceptions, the annual harmonic was more important than the semiannual harmonic in both locations (the exceptions are at 10ºW and 1247 m and at 23ºW and 1293 m – see Table 1). The annual harmonic had maximum amplitudes of about 10 cm/s, and presented upward phase propagation in all three datasets. This upward phase velocity propagation was

consistent with a downward-propagating odd meridional-mode Rossby beam, as already observed in models and other data (e.g. Brandt and Eden, 2005; Thierry et al. 2006).

Instrument depth (m)	Amplitude (cm/s) semi- annual	annual	Phase (days) semi- annual	annual	Percentage of explained variance semi- annual	annual	total
10ºW 2003-2005							
764	2	9	-109	29	2	39	42
918	4	10	-50	17	10	56	67
1106	2	4	-97	12	3	18	22
1247	5	4	-91	-67	20	13	35
1481	3	9	-58	-56	5	54	62
1583	1	6	-99	-68	1	40	43
1689	2	2	-102	-80	6	6	13
23ºW 2004-2005							
635	6	8	-9	139	19	38	58
786	6	8	-23	44	18	42	67
933	6	6	-81	25	23	26	51
1081	4	8	-41	2	13	56	72
1231	3	8	-24	5	8	53	65
23ºW 2002							
797	3	9	16	111	6	61	67
1030	-	-	-	-	-	-	-
1184	11	13	0	80	34	46	81
1293	6	4	-43	50	41	25	67

Table 1: Semiannual and annual cycle: amplitude, phase and amount of explained variance (in percent). The first number in each principal column refers to the semiannual fit and the second number to the annual fit. In the last column the third number refers to the percentage of explained variance combining the semiannual and annual fits. The phase is estimated in days with respect to January 1, 2003. The percentage of explained variance is computed as one minus the ratio of the variance of the residuals over the variance of the original series.

In velocity data from 2003-2005, at depths where the seasonal signal was important (i.e. explaining a large amount of the variance (see Table 1), phases varied similarly with depth at both locations (a phase of about 30 days at ~800 m; 10, at ~ 1100 m; and 70, at 1600 m), suggesting a coherence in the signal between 10ºW and 23ºW. The coherence failed, however, for the record at 635 m and 23°W. The 635-m zonal velocities were eastward during the boreal winter as in all other 23ºW time-series. However, unlike the other 23ºW time series, the 635-m

zonal velocities presented a very energetic eastward event of 6- months duration in the boreal spring and summer, which we believe biased the resulting phase of the annual cycle fitting. The 6-month eastward flow was most probably not related to an annual cycle, since it showed no coherence with the annual signals in the data from greater depths (Fig. 2). The seasonal cycle in 2002 at 23ºW also showed different phase when compared with the seasonal cycle in years 2004-2005 at the same location. Those differences are of about 60 days when comparing similar depths between the two intervals of time. We cannot be certain on whether those differences are the result from incertitude on the method or from intraseasonal variability. However, the consistency among phase shifts in the vertical between the two intervals of time at 23ºW, suggests that the observed differences could be the result of interannual variability.

In summary, at about 800 m depth, the data from 2003-2005 bore a seasonal cycle with maximum eastward velocity during the boreal winter and maximum westward velocity during the boreal summer. Below, at about 1600 m depth, maximum eastward velocities occurred in the boreal fall and maximum westward velocities occurred in boreal spring. At 23ºW in 2002, the phase of the seasonal signal at 800 m showed maximum eastward velocities during boreal winter-spring and maximum westward velocities during boreal summer-fall. Other observations of the annual cycle at 800m depth in the center and the west of the basin indicate eastward velocities during the boreal winter and westward velocities during the boreal fall (Ollitrault et al., 2006) and eastward velocities in the boreal summer and westward velocities in the boreal fall (Schott et al., 2003). Comparisons of our results with the results of these two papers are difficult since 1) we have a difference of about 60 days in the annual cycle phase estimation depending on the year analyzed and 2) the annual cycle in the papers mentioned above is not symmetric along the year (i.e. maximum eastward and westward flows do not occur on opposite seasons of the

year). Nonetheless, below 1300 m, the seasonal cycle certainly varies from the west to the east of the Atlantic Basin. Indeed, the two-year-long series of VACM measurements between 1300 m and 1900 m depths at 35ºW discussed by Send et al. (2002) showed no annual signal at all whereas Thierry et al. (2006), in a 2-year VACM series at 1700 m and 15ºW, found similar amplitude and phase to the signal derived here from the record at 1689 m at 10ºW. Finally, a linear regression using values from Table 1* led to rough estimates of the parameters of the annual cycle: a phase velocity between 9.7×10^{-5} ms^{-1} and 6.9×10^{-5} ms^{-1} and a vertical scale between 2190 m and 3066 m, a much larger vertical scale than that of the EDJs.

The semiannual signal was more important at 23ºW than at 10ºW (Table 1). The vertical phase structure was complicated, since it changed direction with depth (Table 1). For example, at 23ºW for the measurements of 2004-2005, the phase propagation was upwards between 635 m and 933 m and downwards between 933 m and 1231 m. Thierry et al. (2006) found similar phase changes in the water column, but the reason for that behavior remains unclear.

3.4. Mean and Low-Frequency Signal in the Meridional Velocity Component

The mean meridional velocity component was small (less than 1.5 cm/s), except at 1231 m at 23ºW, where it reached 3 cm/s. Indeed, the meridional velocity component at 1231 m in the year 2004 showed southward velocities for over 7 months (Fig. 2). Although periods less than 50 days dominated the variations in the meridional velocity at both locations, vertically coherent flows at longer time-scales were observed at 23ºW, especially on data from 2004-2005. A 50-day low pass filter was applied to the residual meridional velocity, once the mean was taken out. The low-pass filtered time series (Fig. 5), revealed fluctuations with amplitudes reaching 6 cm/s, an

* Values corresponding to VACM at 630 m at 23ºW and at 1247 m at 10ºW were not used for the linear regression.

upward phase propagation, a vertical scale of ~600 m and a period of about 10 months. The values for the time and vertical scales are rough estimations, since the time duration of the series as well as the vertical extent are not long enough to resolve those scales properly. With these cautionary remarks in mind, to our knowledge, no such flows in the meridional component with such small vertical scales have been reported yet.

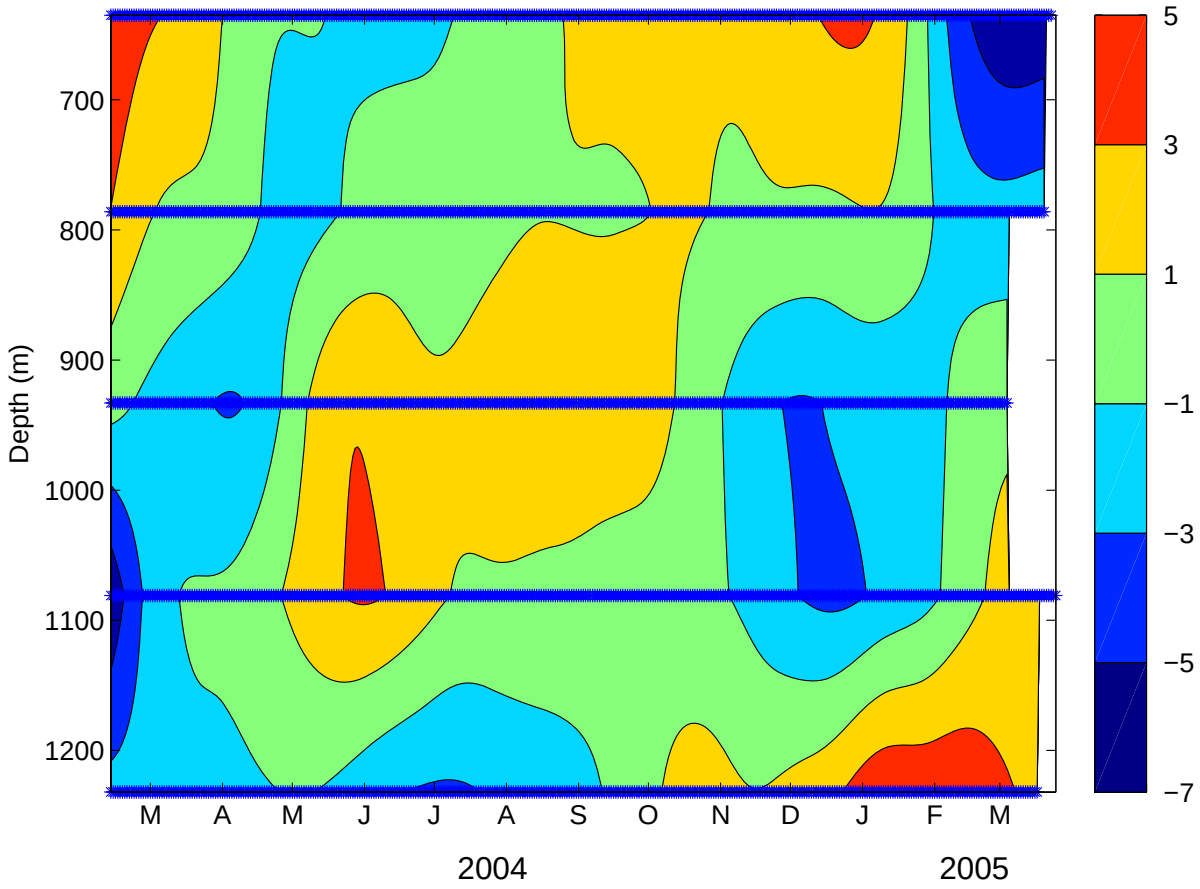

Figure 5: 50-day low pass filtered meridional velocity component anomalies at 23º W for the years 2004-2005. The temporal means have been subtracted. Horizontal lines indicate the depth and the length of the time series. Positive is northwards, negative southwards. *X*-axis indicates time in months from February 2004 to March 2005.

One of the differences between 10ºW and 23ºW is the presence of the Mid-Atlantic Ridge at 23ºW. McPhaden and Gill (1986) studied the scattering of low-frequency, equatorial Kelvin-wave energy by a submarine ridge. They found that the presence of a submarine ridge in the path

of propagation of a Kelvin wave induced meridional motions. The model they used was of very low vertical resolution and their results cannot be compared with these data. However, we suggest that more work on the lines of McPhaden and Gill's (1986) could help to explain the low-frequency fluctuations observed in the meridional component.

3.5. Discussion

The difficulties in establishing an appropriate time-scale for assessing the variation in the parameters of EDJs through observations resides in the lack of long time-series of data with high vertical resolution. The mooring at 10ºW provided the data set with the longest duration and high vertical resolution for the depths sampled at the equator. The results from these data suggested that different features sharing similar vertical scales and amplitudes and different time scales coexist, along with a seasonal cycle with a much larger vertical scale. A numerical model (D'Orgeville et al., 2006) based on a recent theory of the mechanism of EDJ formation (Hua at al., 2006) suggests that the instability of mixed Rossby–gravity waves at the equator forced by the Deep Western Boundary Current may trigger small vertical-scale zonal flows. In the model presented by D'Orgeville et al. (2006), the structure of the jets can have a standing-mode pattern or a vertical propagating pattern, depending on the amplitude of the excited mixed Rossby-gravity wave. They also found that the time scales of these EDJs corresponded roughly to equatorial basin modes (~5 years in the Atlantic for a first equatorial basin mode of vertical number 20) and that these basin modes may also present horizontal patterns corresponding to a second or higher equatorial basin mode, in which cases, the period would be drastically reduced (e.g., ~2.5 years for the second equatorial basin mode). In that sense, EDJs in the Atlantic would have time scales of 5 years and less, in agreement with the time scales estimated from observations. Moreover, the meridional structure of the EDJ presented in D'Orgeville et al.

(2006) corresponds to Kelvin and Rossby waves. This information, combined with the results of McPhaden and Gill (1986), suggests that there is a possible link between EDJs, the Mid-Atlantic Ridge and the low-frequency flows of small vertical scale in the meridional component observed at 23ºW.

Chapter 4: 13-Day Period Oscillations in Spring 2004

Abstract

13-day period oscillations were observed in the first half of the year 2004 in equatorial ocean velocity records at 23°W and at 10°W. Two distinguishable 13-day period oscillations were identified; one was subsurface intensified and occurred from February to March and the other was surface intensified and occurred from April to May. A 13-day period oscillation in SST was also detected from March to May. The conspicuous SST 13-day period signal permitted to relate the velocity oscillations with SST variations and then to estimate the meridional structure and the zonal scale of the waves. The 13-day period oscillation in March-May was consistent with a second baroclinic mode standing mixed Rossby-gravity wave, forced by meridional winds presenting the same periodicity. Preliminary results indicate that waves with 13-day periodicities are well represented in high horizontal resolution model simulations (MICOM) where the waves could be inferred from velocity and sea surface height anomalies.

4.1 Introduction

Oscillations with biweekly periodicity have been observed in the three equatorial oceans (e.g., Zhu et al., 1998 in the Pacific; Miyama et al., 2006 in the Indian; and Houghton and Colin, 1987 in the Atlantic). In all the cases the oscillations have been associated with wind-forced mixed-Rossby gravity waves. In the Indian Ocean, these biweekly waves have a temperature signature as well; the wave is associated with intermittent off-equator upwelling and downwelling throughout the year (Sengupta et al. 2004). Since upwelling followed by mixing is

an irreversible process, these authors suggest that the biweekly oscillations might have an impact on subsurface temperature and in biology, and eventually in climate.

Meridional velocity observations in 2000, (Chapter 1) and 2002, (Chapter 2) showed 11-15 day period fluctuations during boreal spring. Spring 2004 also showed 11-15 day period oscillations (hereafter 13-day period oscillations) in the meridional velocity component (Fig. 2) and in SST. The characteristics of the 13-day period oscillations in 2004 bore similarities and differences with the waves observed in other years. In this chapter we will not address those comparisons. Instead, we will focus on the 13-day period oscillation observed in 2004. This chapter is organized in four sections. Section two provides a brief description of the data and data processing. Section three studies some of the characteristics of the 13-day period oscillation in current velocities, SST and wind velocity data, and the fourth section discusses the results and compares them with the model results.

4.2. Data

To study the upper equatorial circulation in the equatorial Atlantic, the PIRATA (Pilot Research moored array in the Tropical Atlantic) program deployed moorings with ADCPs (Acoustic Doppler Current Profilers) on top, at 10ºW and 23ºW (see table below for the duration of the deployments). A mooring at 10ºW equipped with an upward looking ADCP NB150 sampling the upper 300 m was deployed on May 2003. The mooring was recovered and redeployed on February 2004, along with a second mooring at 23ºW equipped with an upward looking ADCP observing the upper 120 m. The two moorings were recovered in May and June 2005. The hourly data were averaged over 25 hours to remove tidal frequencies and re-sampled to provide daily resolution (Figure 1).

In this chapter, we also make use of satellite sea surface temperature and surface wind velocity data. Tropical Rainfall Measuring Mission (TRMM) – Microwave Imager (TMI) SST data were examined over the region between 9°S and 9ºN, and 35°W and 10ºE during the years 2000 to 2005. This SST product is the result of an optimal interpolation with temporal and a spatial resolutions of 1 day and 0.25º, respectively. SST data is available at http://www.remss.com/sst. QuikSCAT surface wind horizontal velocities were explored over the region bounded by 10°S and 10ºN, and by 50°W and 10ºE in the year 2004. These data is daily, has a horizontal resolution of 1/2º, and is available at www.ifremer.fr/cersat. SST and wind velocity time series were filtered using a digital Butterworth band pass filter to retain signals with periods in the band of 5 to 38 days.

The computational domain of the Miami Isopycnic Coordinate Ocean Model (MICOM) simulation used in this study is the North and Equatorial Atlantic Ocean basin from 28ºS to 70ºN, including the Caribbean Sea, the Gulf of Mexico, and the Mediterranean Sea. The horizontal grid is defined on a Mercator projection with resolution given by $1/12º \times 1/12º \cos(\Phi)$, where Φ is the latitude and is approximately 9 km at the equator. The vertical density structure is represented by 19 isopycnic layers topped by an active surface mixed layer that exchanges mass and properties with the isopycnic layers underneath. After a six-year spinup with monthly climatological forcing, the model was integrated using surface boundary conditions based on European Centre for Medium-Range Weather Forecasts (ECMWF) daily atmospheric data from 1979 to 1986. The high horizontal grid resolution drastically improved the model's behavior in comparison to that of previous coarse-resolution simulations (Paiva et al., 1999).

We analyzed the horizontal velocities, SST, and sea surface height (SSH) from the output model by computing a frequency dependent polarization analysis. This method is based on a

singular value decomposition of a matrix of eigenspectra at a given frequency (Park et al. 1987). As a result, we were able to obtain the spatial structure and phase propagation associated with the 13-day periodicity.

Location	Depth	Starting date	End date	Days of good data
23ºW	ADCPs (10-120m)	13.Feb.04	28.May.05	471
10ºW	ADCP (26-286 m)	7.May.03	17.Jun.05	773

Table 1: Location, depth, and number of days of good data of the ADCPs from PIRATA moorings.

4.3. 13-Day Period Oscillations

From February to March, 13-day period oscillations were seen in the subsurface, at the depth of the Equatorial Undercurrent (EUC); from April to May, these fluctuations were surface-intensified. Subsurface 13-day period oscillations had maximum amplitudes of approximately 20 cm/s in both locations while surface-intensified oscillations reached amplitudes up to 50 cm/s at 10ºW, and did not exceed 10 cm/s at 23ºW. SST and surface wind velocity data also showed oscillations with periods in the 11-15 day band. In SST data, the 13-day period signal started to be observed in mid March, was confined to the equatorial region (Fig. 3, bottom panel), showed large zonal scales and had amplitudes of up to 2ºC. Sometimes, the spatial structure of the SST anomaly was anti-symmetrical about the equator and sometimes was symmetrical (e.g., fig. 4, snapshots of April 7 and May 10). There was no sign of zonal propagation.

In spring 2004, satellite surface wind data presented 13-day period fluctuations simultaneously in both horizontal velocity components. The 13-day period fluctuation in the zonal wind velocity component had the form of a strong zonal jet (amplitudes of up to 7 m/s)

localized mainly between the equator and 5ºN, and between 20ºW and 0ºE (Fig. 5). The variance at periods between 11 and 15 days (Fig. 3) shows that there was also some energy in this period range off the coast of Gabon. Grodsky et al. (2001) reported strong quasi-biweekly fluctuations in surface winds and rainfall during boreal spring and summer of 2000. The disturbances they described are mostly zonal and are the result of a cycle of continental heating, convection, and cooling. The zonal wind observations in boreal spring of 2004 presented here are equivalent to the ones observed by Grodsky et al. (2001). In contrast, the meridional wind velocity component at this period had smaller amplitude (3 m/s) and a more complicated structure. The strongest meridional winds with this periodicity were found off the coast of Brazil (Fig. 3). However, the meridional winds relevant for the observed SST structures are the ones observed over the equatorial region. In spring 2004, meridional winds in the equatorial region with periods of ~13 days often presented different signs on each side of the equator (e.g., Fig 6, snapshots from March 24 and April 7) and sometimes there was even a three band structure like the one shown in the May 10 snapshot (Fig. 6).

As observed in figures 5 and 6, the spatial structure of the 13-day period fluctuation in each wind velocity component does not bear much acquaintance. For that reason, the spatial structure of the 13-day period fluctuation is difficult to interpret in terms of the combination velocity components. However, both, zonal and meridional wind velocity fluctuations can potentially explain the SST anomalies observed in figure 4 separately. The zonal component is consistent with upwelling and downwelling at the equator due to Ekman pumping; the meridional component is consistent with convergent and divergent flows at the equator due to direct wind drag. The problem with the zonal wind velocity component is that there is a lag with respect to the SST signal, with the zonal wind leading by 7 days. This means that in the series at zero time-

lag, a westward wind anomaly corresponds to a warm SST event at the equator and an eastward wind anomaly corresponds to a cold SST event, which is the opposite of what is expected. The meridional wind velocity component on the other hand, presents the right phase with respect to the SST signal; divergent velocities on the equator correspond with cold SST anomalies (e.g., figs. 4 and 6, snapshots corresponding to March 23 and April 13) and convergent velocities to warm SST anomalies (Figs. 4 and 6 snapshots corresponding to April 7 and May 4). There is even a case when the meridional component showed a three-band structure about the equator (fig. 6, snapshot of May 10) presenting northward wind anomalies at each sides of the equator and a southward wind anomaly right at the equator. The temperature snapshot for that same day shows an anti-symmetrical SST structure with a cold SST anomaly north of the equator and a warm SST anomaly south of the equator, which is consistent with the idea of converging and diverging flows due to direct wind drag. 9 days later, however, the SST anti-symmetrical structure changes sign; the warm anomaly is north of the equator and the cold anomaly is south of the equator, and there is no consistent change of sign in the meridional winds (figs. 4 and 6, snapshots corresponding to May 19).

Another possible explanation for the temperature 13-day period signal is that the SST anomalies are the signal of an oceanic equatorial wave. The wave could have been initially forced by the winds. The observed SST anomalies, especially those with antisymmetric structure about the equator, can be explained as the result of oceanic mixed Rossby-gravity waves in the ocean. In the following paragraphs we will explore that possibility.

A correlation analysis using SST data and the meridional current velocity component series at 26 m depth, at 10º W, shows that SST series precede the current meridional velocities by 3 days (Fig. 7). At the same time, the correlation map shows that the areas of good correlation

between current and SST data agree with the SST structure attributed to the 13-day period oscillation and that the corresponding zonal scale is of over 30 degrees of longitude (~3300 km). The dominance of the meridional component over the zonal component in current measurements at the equator, the period of the wave and the anti-symmetrical SST structure about the equator, indicate that the 13-day oscillation in the ocean can be surmised to a mixed Rossby-gravity wave. The large zonal scale ($k \rightarrow 0$) and the lack of evidence of zonal propagation suggest a standing wave which surface moves up and down, but with opposite sign on each side of the equator (to the extent that velocity streamlines coincide with isotherms, this would explain the anti-symmetrical SST structure about the equator). All these characteristics are consistent with a second baroclinic mode mixed Rossby-gravity wave as shown in the dispersion relationship diagram of figure 8.

4.4. Conclusions and Comparisons with Model Outputs

In conclusion, there are two different signals presenting ~13-day periodicities in the meridional velocity component. The first one is subsurface intensified and appears to be related in someway to the EUC. The second is surface intensified and is well correlated with SST fluctuations. We do not know if these two signals are related. However, at 10°W where the EUC is close to the surface, the differences between the two 13-day period oscillations are almost imperceptible.

SST signals are well related to fluctuations in the meridional wind velocity component and in the current meridional velocity component. The SST signal could be the result of both, divergent and convergent meridional winds about the equator and a remotely wind-forced oceanic mixed Rossby-gravity wave. At times when the SST 13-day period signal is symmetrical about the

equator, the meridional wind would be the main factor controlling the observed SST signal; when the SST 13-day period signal is antisymmetrical about the equator, the inherent dynamics of the mixed Rossby-gravity wave are responsible for the observed SST anomalies.

As mentioned before, other velocity observations have shown 11-15 day period oscillations in the meridional velocity component in boreal spring. However, the corresponding SST signal was not always present or did not last long enough to enable any significant correlation between velocity and SST fluctuations. For instance, in 2002, 2003 and 2005, no 13-day period signal was observed in SST at the equator, and in 2000 and 2001, only one or two full cycles of 13-day period fluctuations in SST could be detected. The presence or absence of the 13-day period signal in the SST may be related to the nature of the wave (surface or subsurface intensified) and to the pre-existing background SST field and the depth of the mixed layer. Further analysis is needed to understand the dynamics of the different types of 13-day period oscillations, examine whether they are related to each other or not, and investigate the main factors playing a role in the 13-day period SST signal.

Preliminary analysis of 8-years of model data (1979-1986, MICOM- forced with realistic daily winds) did not show similar SST structures at 13-day period. Nonetheless, the sea-surface height and the horizontal velocity components in the surface oceanic layer at 13-day period showed mixed-Rossby gravity waves characteristics; symmetric spatial structure in the meridional component and antisymmetric spatial structure in the zonal velocity component and in the pressure field (fig. 7). The analysis of the model outputs was done over the entire time series and one needs to repeat this analysis on a year by year basis to find out if the lack of SST 13-day period signature is over the whole time period or if some are present on a yearly basis as it is the case for the observations.

Velocity observations at intermediate depths at the equator have shown the presence of 13-day period oscillations at 1000 m depths during boreal spring (chapter 1). Further analyses are needed to know whether the 13-day period oscillations observed at 1000 m depth are the deep expression of the 13-day period oscillations observed at the surface or not. If they are related, then how 13-day period oscillations penetrate that far in the water column has to be understood.

The model outputs are interesting. They provide another way to continue studying this 13-day period oscillation near the surface and at depth. We shall compare the simulation products with data from other years in the Atlantic and to the biweekly oscillations found in the Indian (e.g., Miyama et al., 2006) and Pacific Oceans (e.g., Zhu et al., 1998).

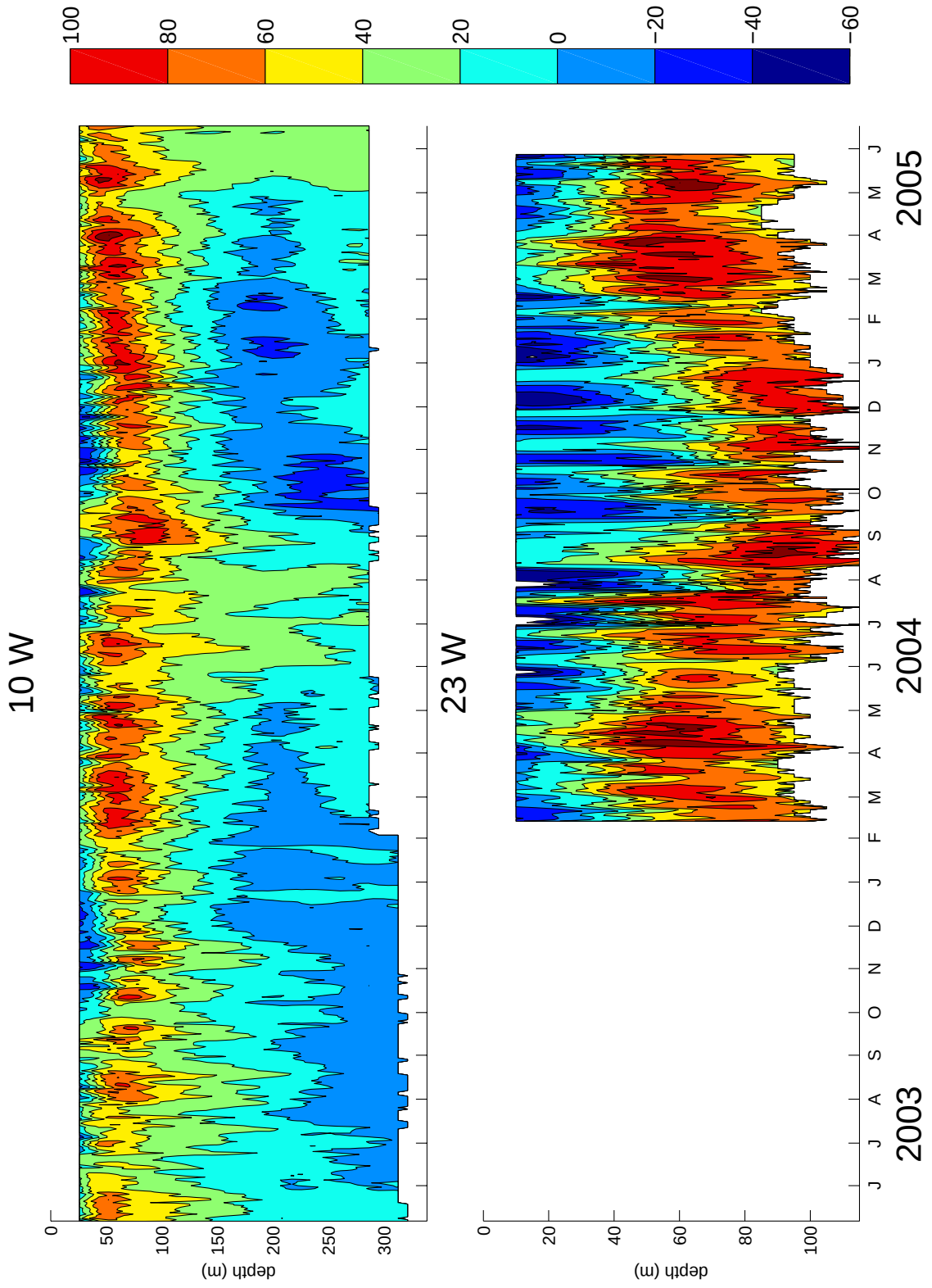

Figure 1: Zonal (first panel) and meridional (second panel) velocity components from the ADCP at 10ºW (top) and the ADCP at 23ºW (bottom).

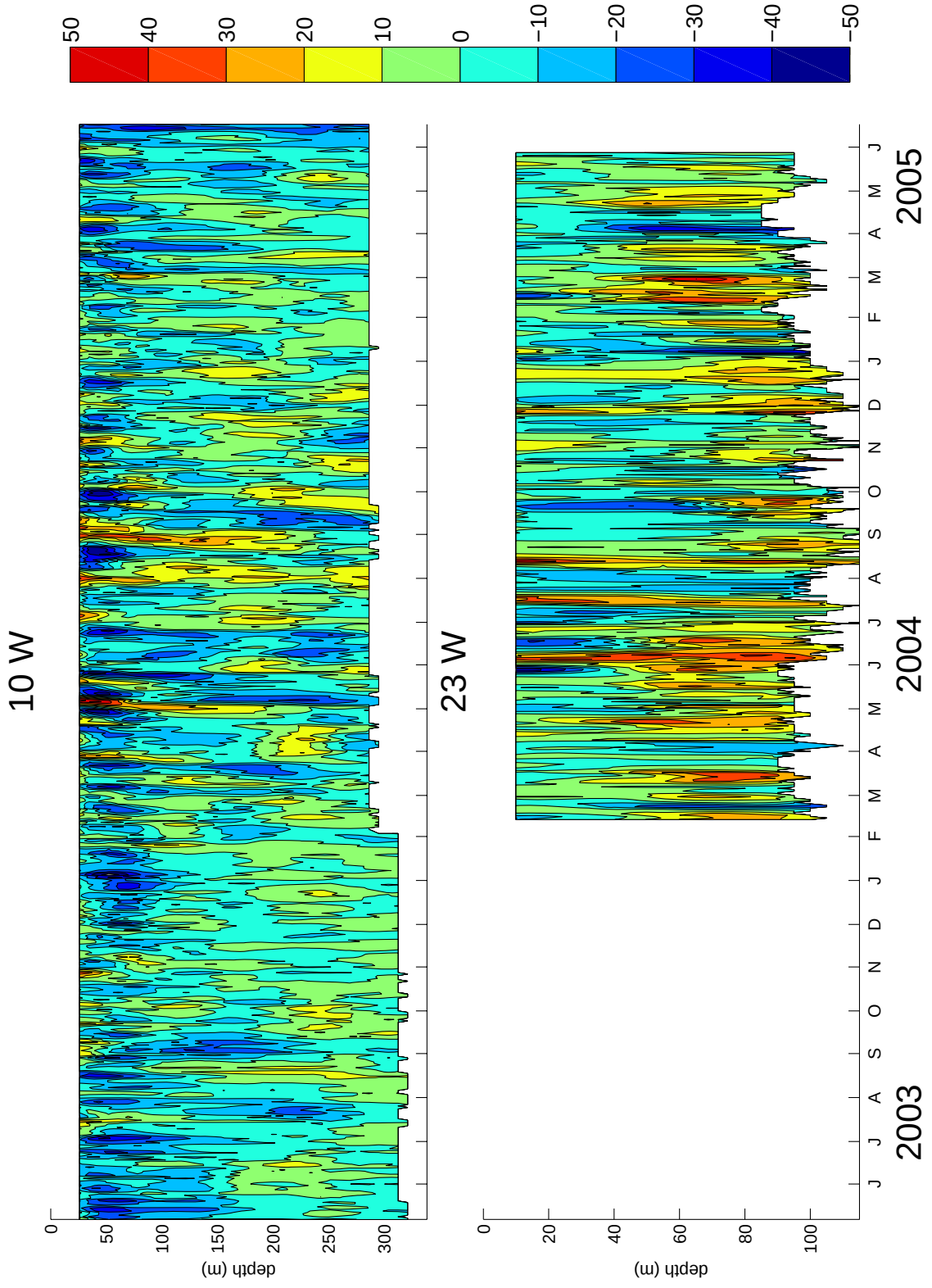

Figure 1: (continued).

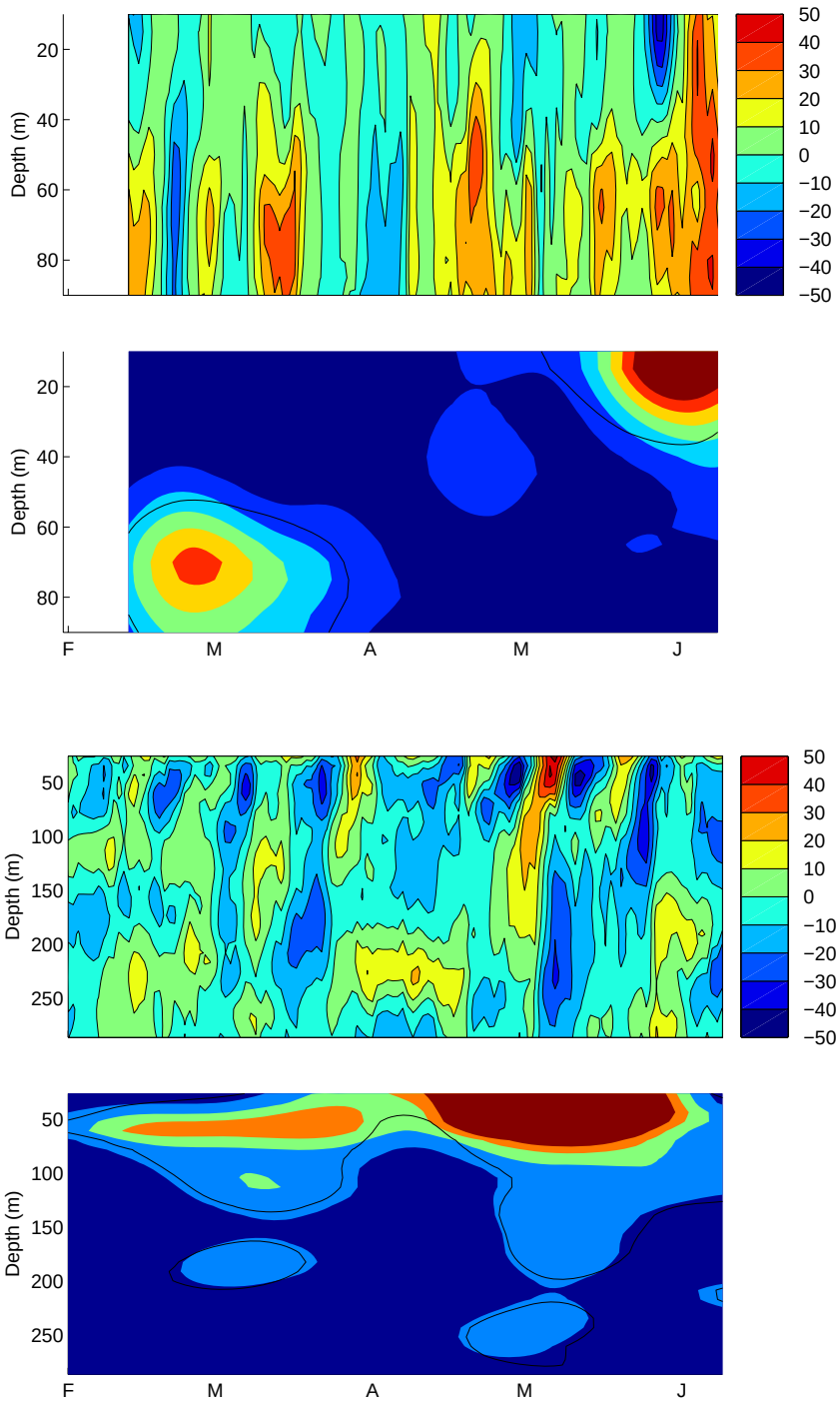

Figure 2: Meridional current-velocity component (in cm/s) during the 13-day-period fluctuations in the ADCP data at 23ºW (top panel) and 10ºW (middle-upper panel) and normalized wavelet energy of the meridional velocity component for the 12–15-day band for 23ºW (middle-lower panel) and 10ºW (bottom panel) ; the *black contour* indicates the 95% significance level. Roughly, from February to March the signal is subsurface intensified and from April to June the signal is surface intensified.

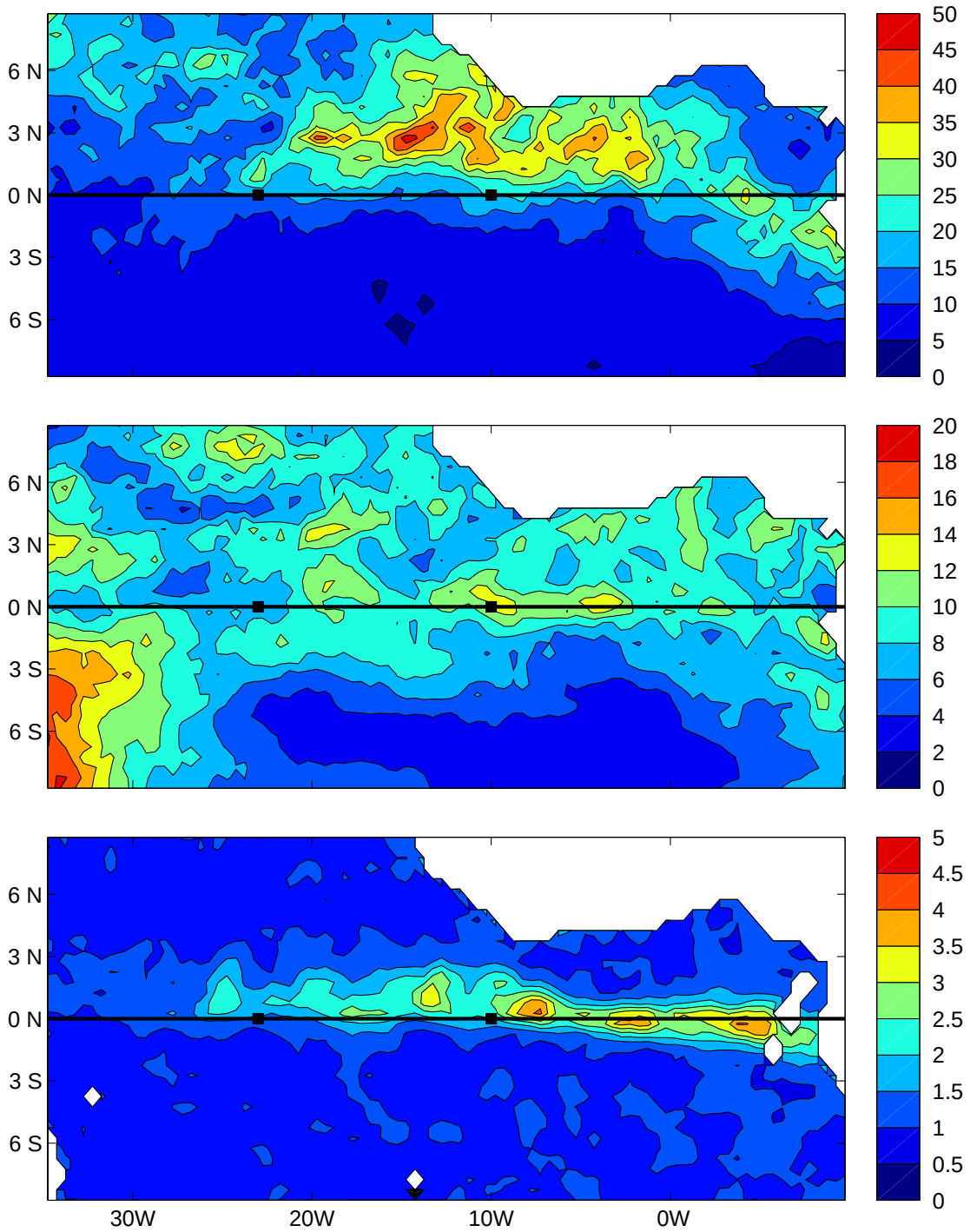

Figure 3: Variance over the year 2004, corresponding to the period band 11-15 days for the zonal and meridional wind velocity components (in m^2/s^2 - upper and middle panels respectively) and for the SST (in $ºC^2$ – lower panel).

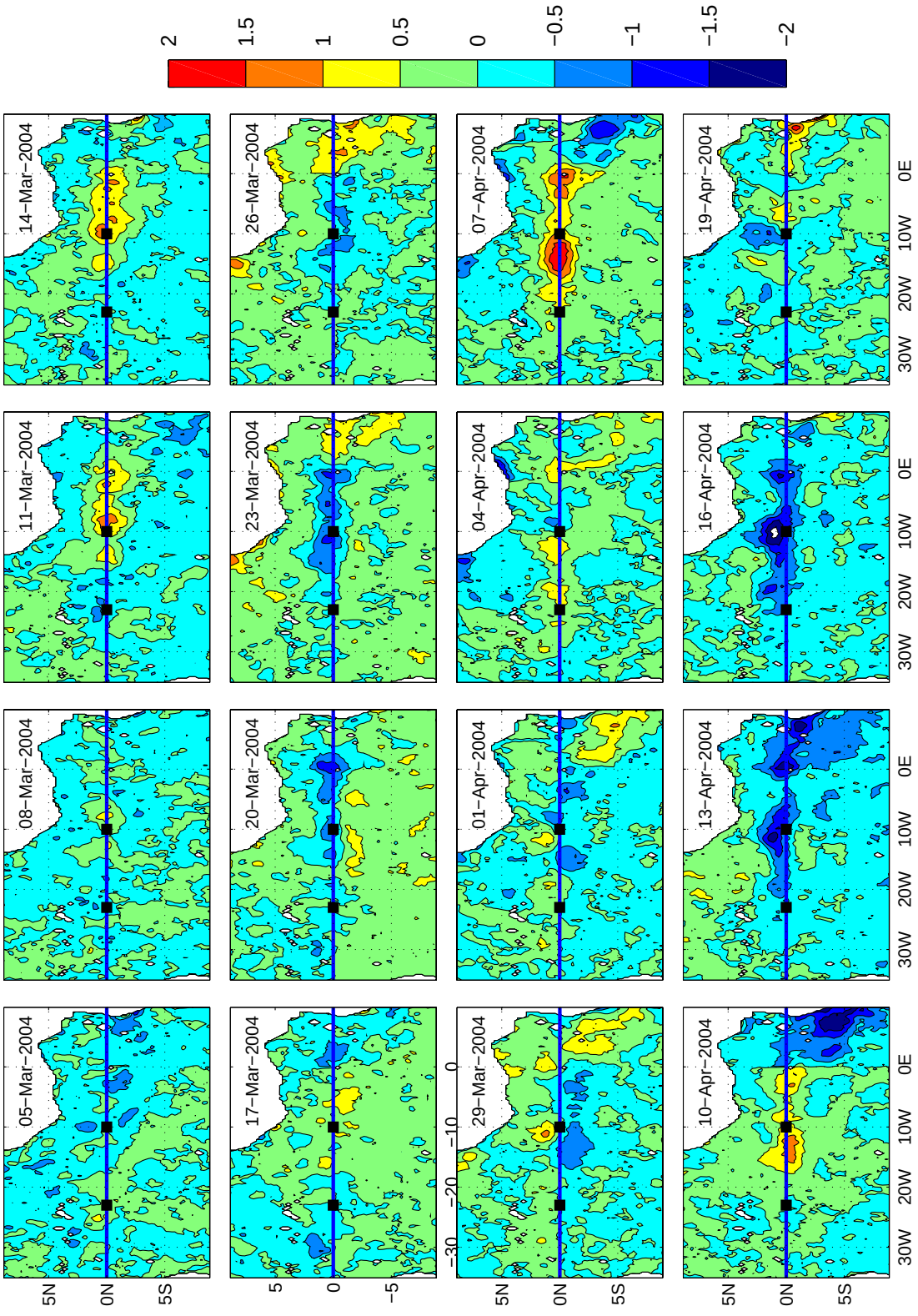

Figure 4: Snapshots of SST in spring 2004. Time series were filtered to retain variability in the 9 to 45 day period band.

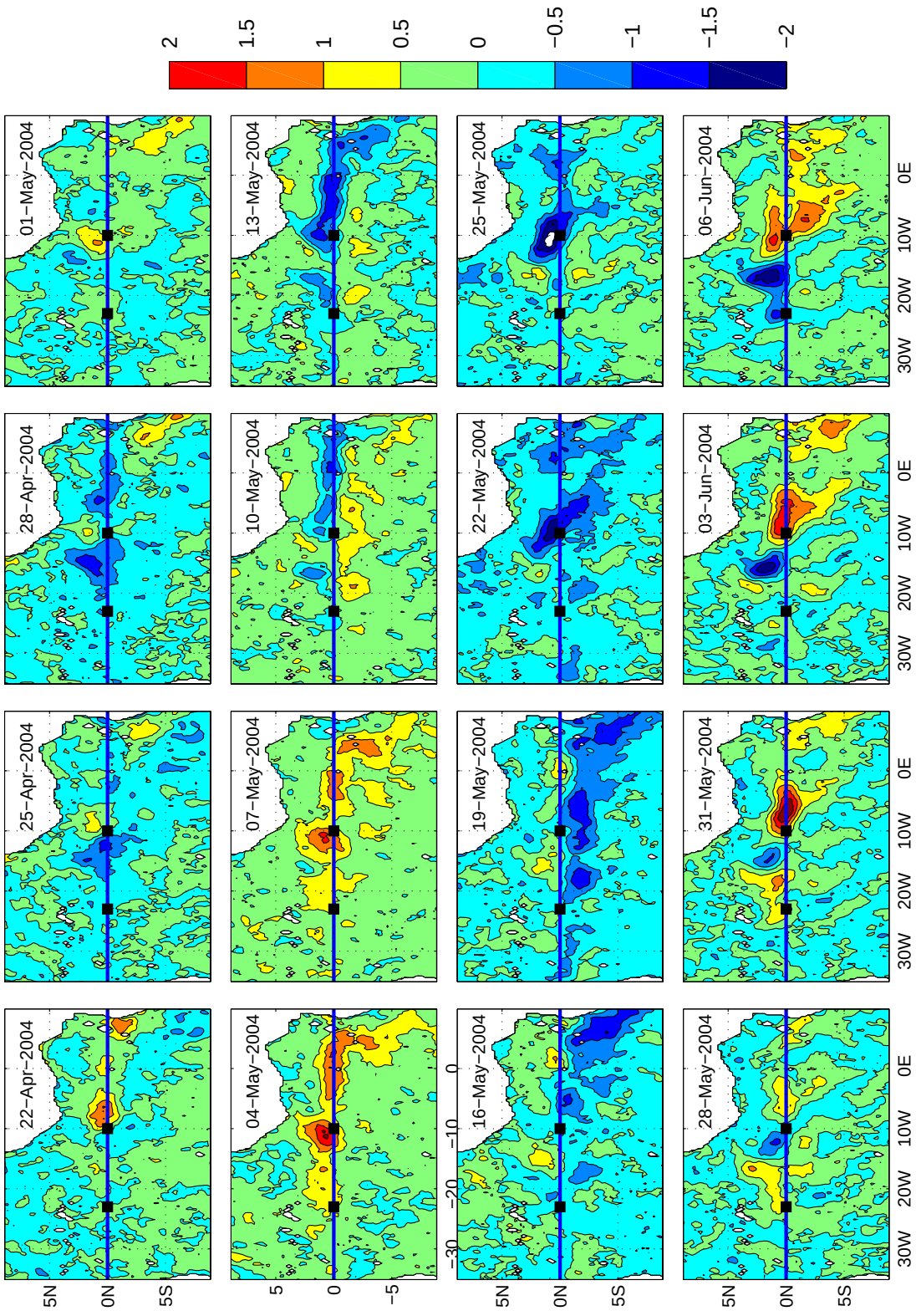

Figure 4: (continued).

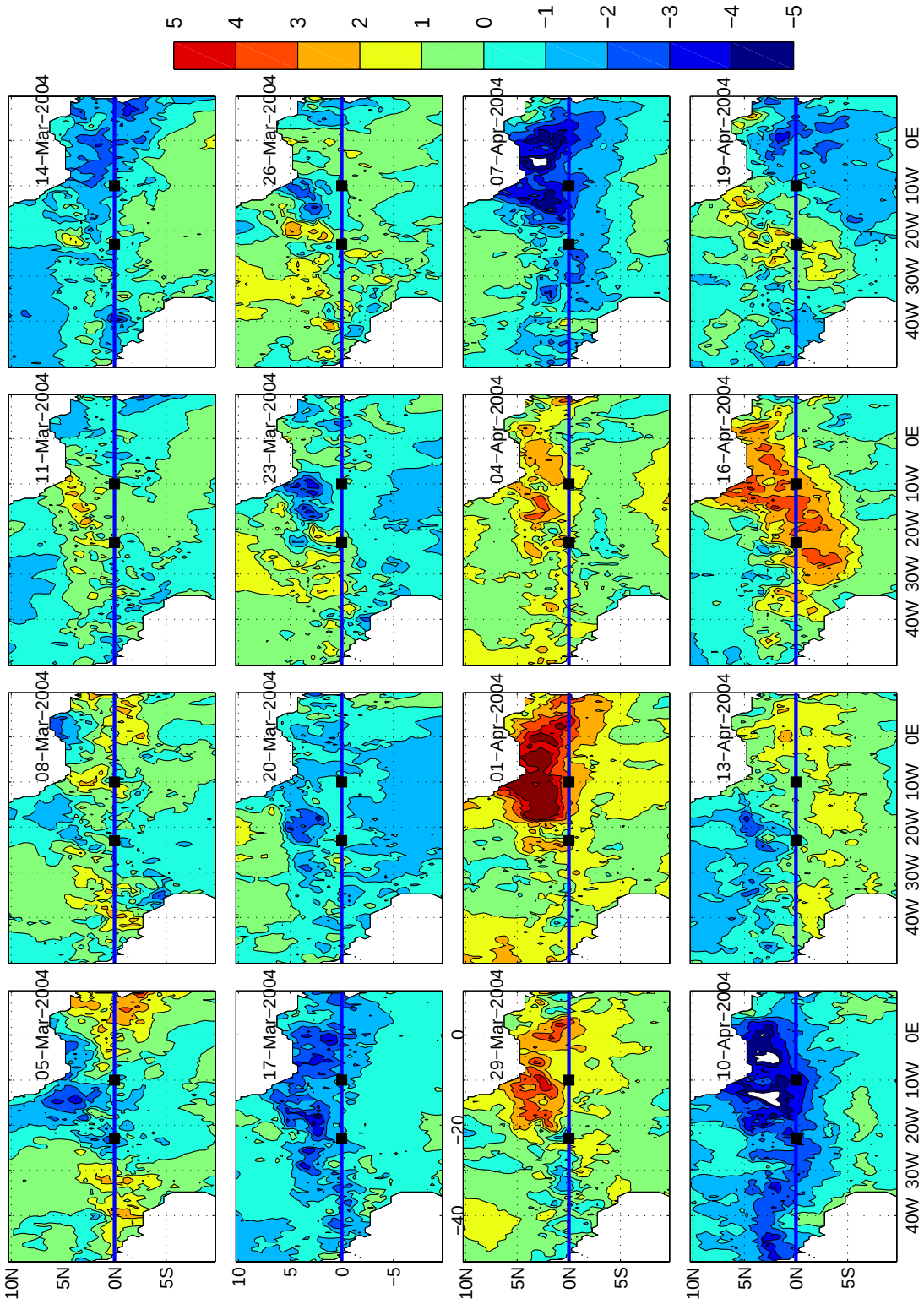

Figure 5: Snapshots of the zonal wind velocity component in spring 2004. Time series were filtered to retain variability in the 9 to 45 day period band.

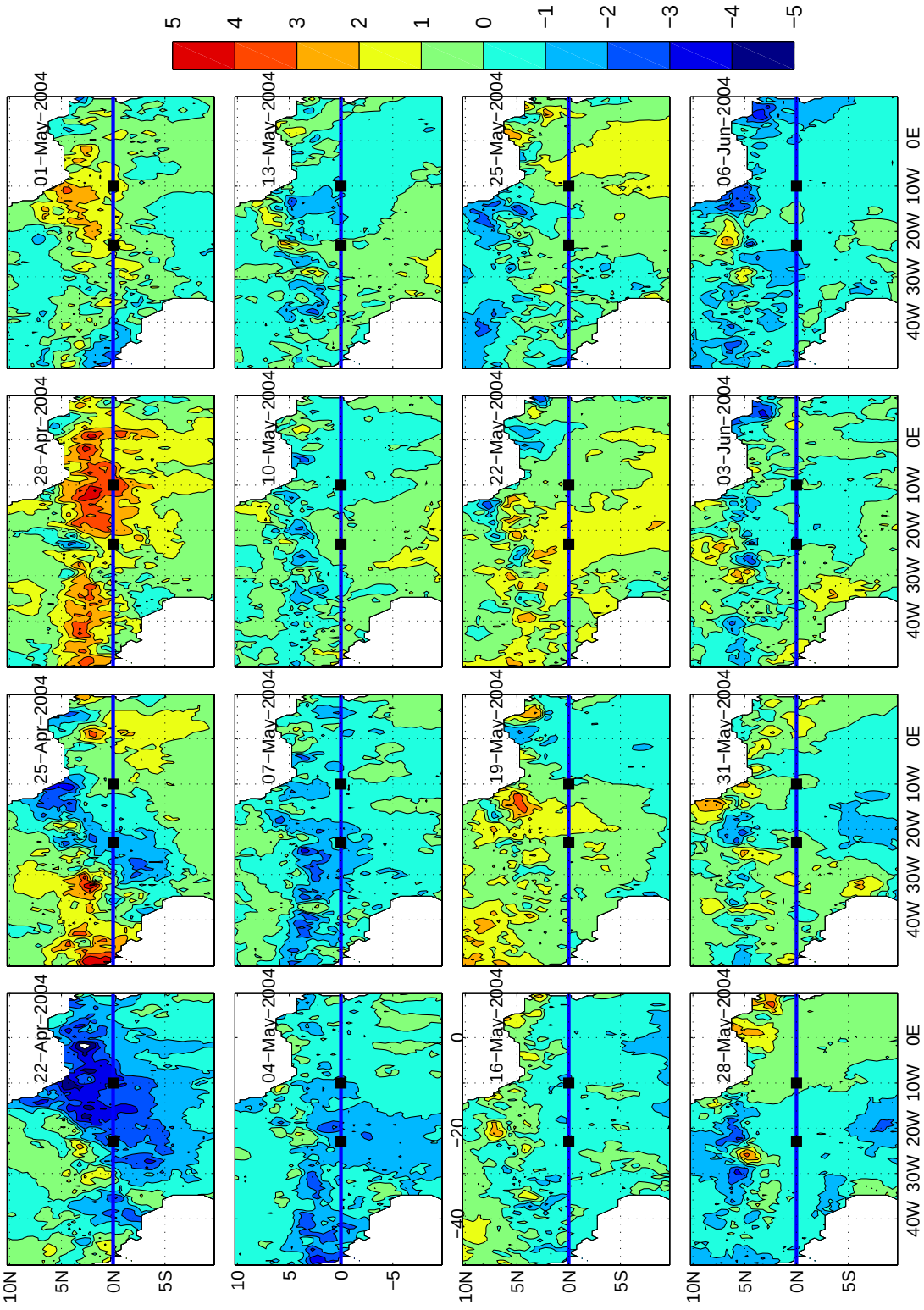

Figure 5: (continued).

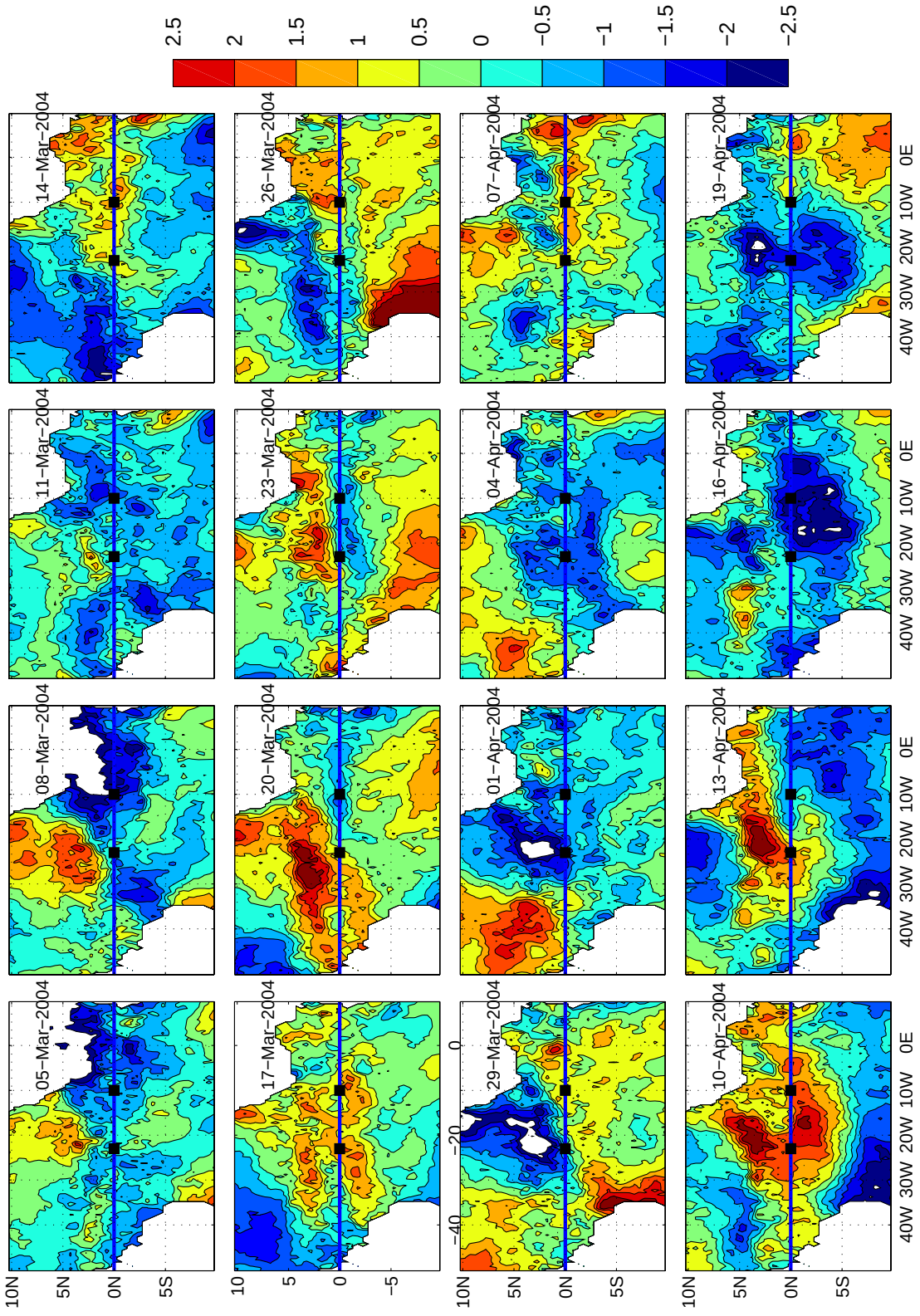

Figure 6: Snapshots of the meridional wind velocity component in spring 2004. Time series were filtered to retain variability in the 9 to 45 day period band.

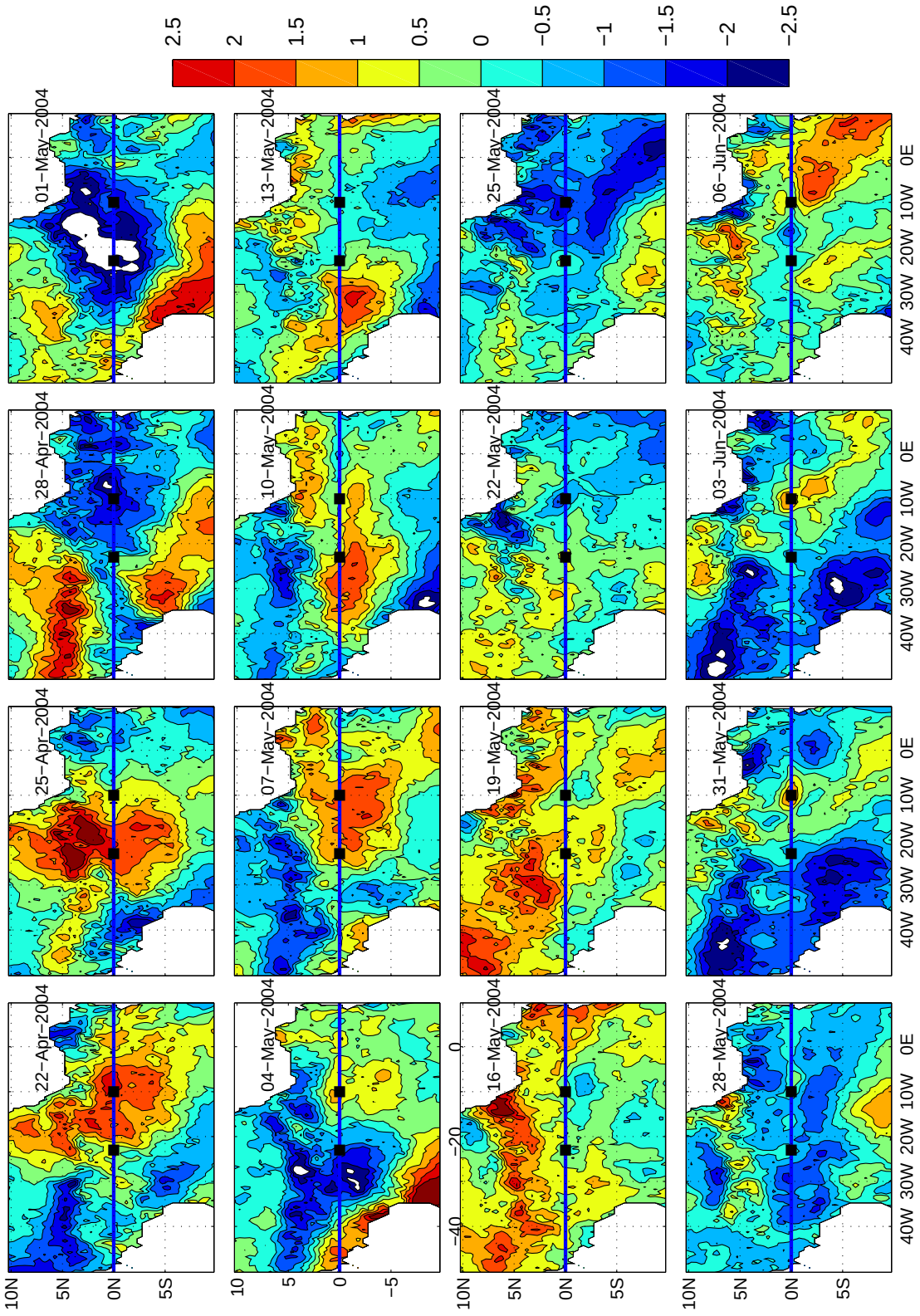

Figure 6: (continue).

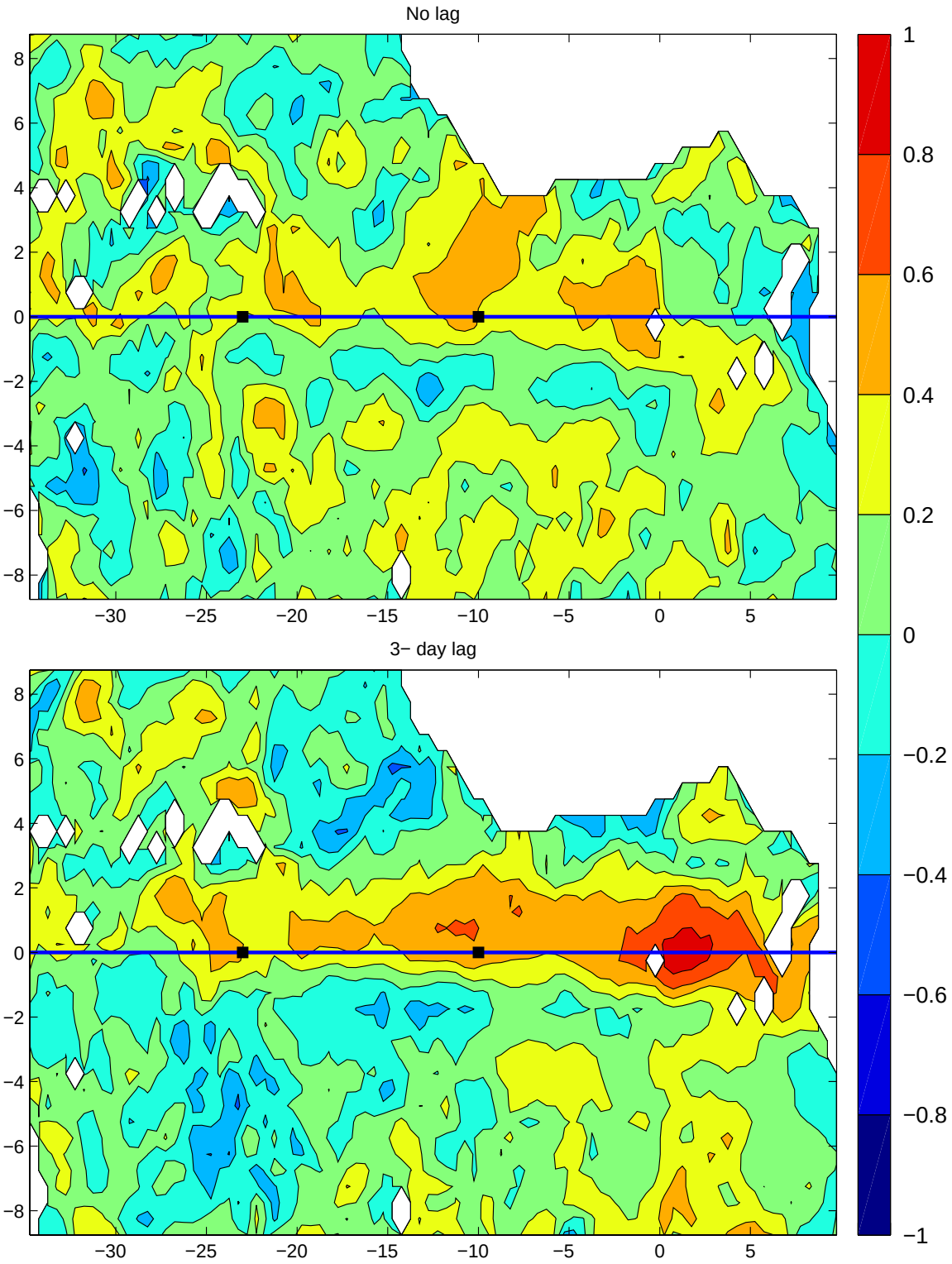

Figure 7: Correlation between 5-38 day band pass filtered SST time series and meridional current velocity at 26 m and 10ºW. The correlation was performed over 101-day time series around boreal spring 2004.

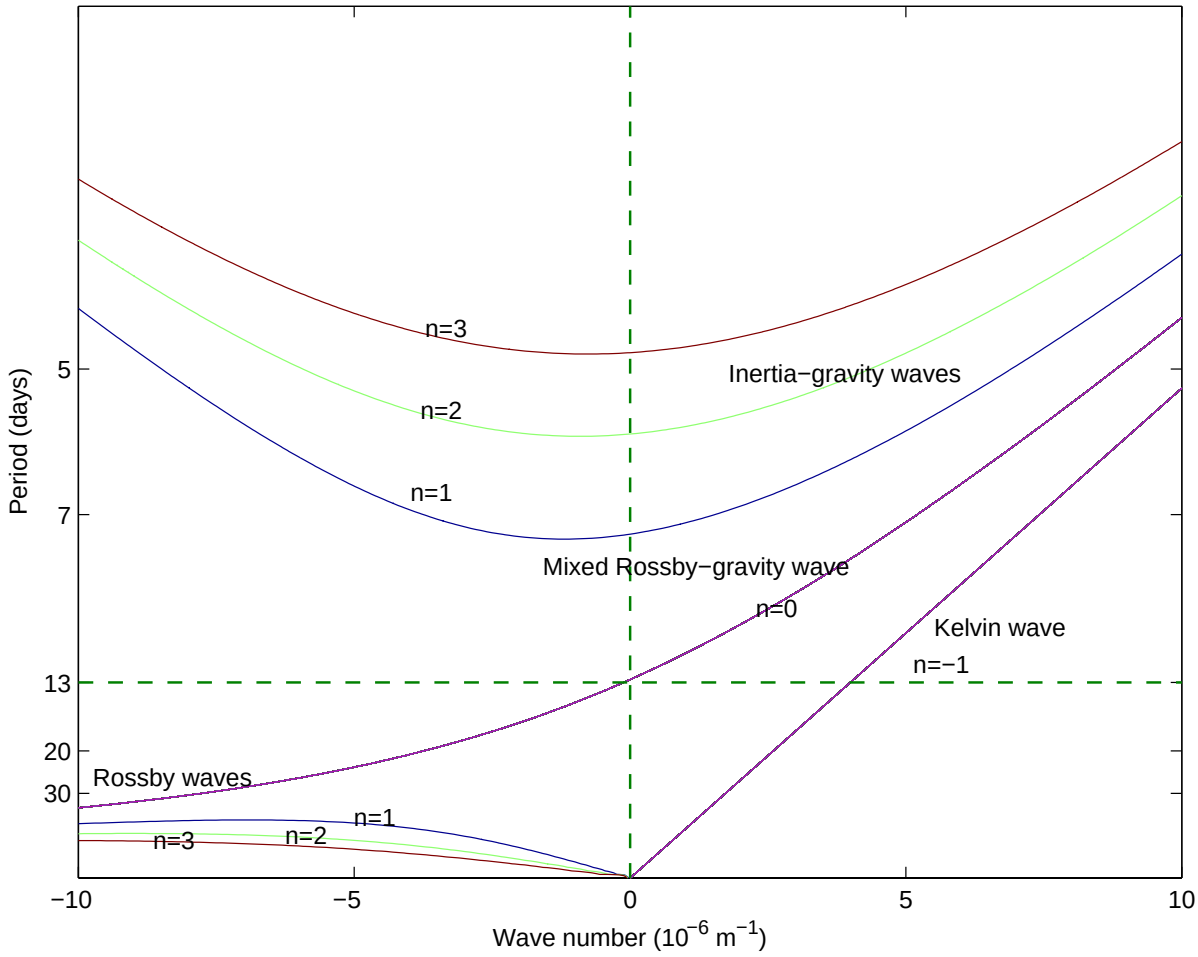

Figure 8: Dispersion relation for the second baroclinic mode with c_2=1.4 m/s (Philander 1990). The horizontal dotted line indicates the period at 13 days.

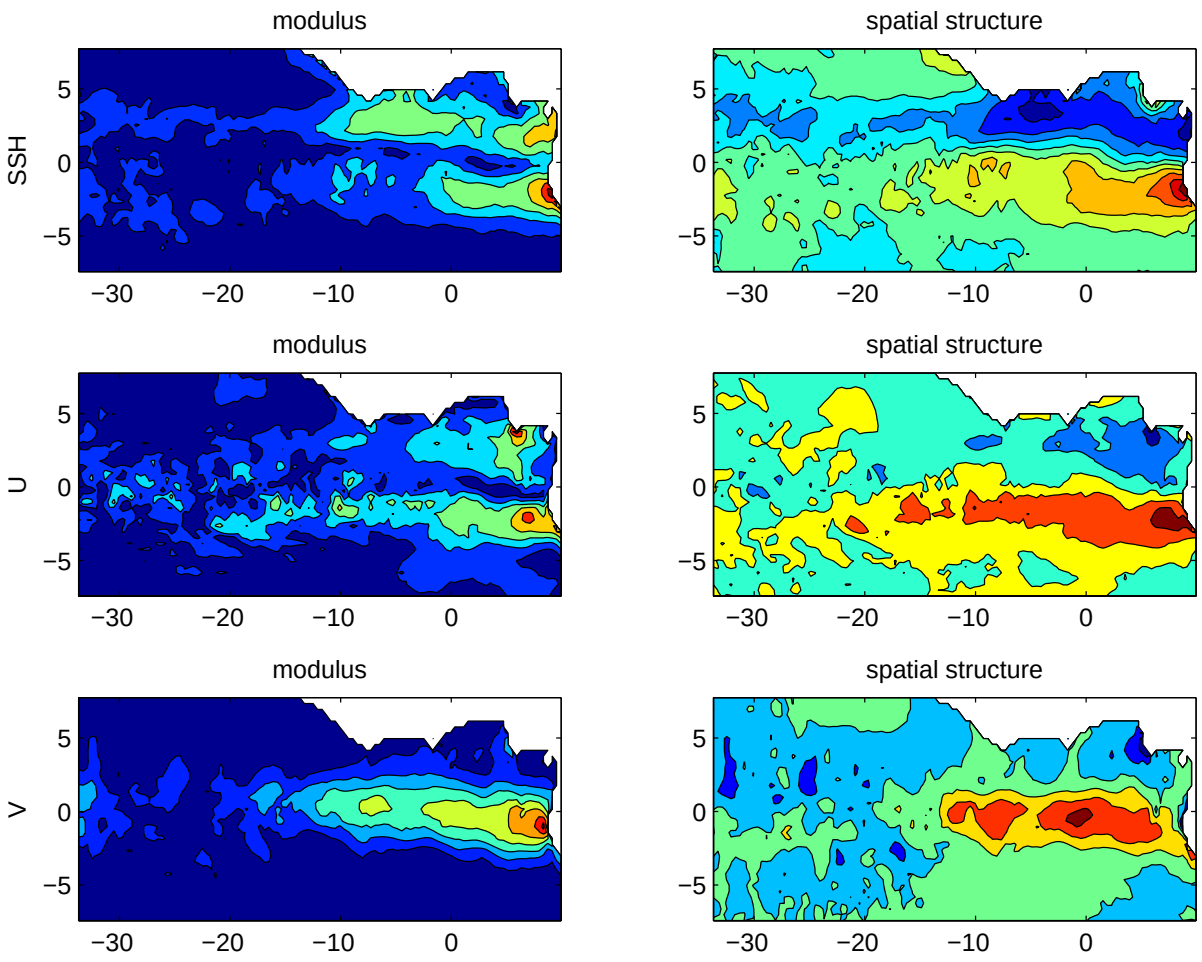

Figure 9: Modulus and spatial structure of the 13-day period oscillation in sea surface height (top pannels), zonal velocity component (middle panels) and meridional velocity component (bottom pannels). In the modulus panels yellow-red colors indicate regions of strong 13-day period activity. In the spatial structure panels, positive values are in red and negative values in blue. These results were obtained performing a polarization analysis over 8-years of MICOM data (see Park et al. 1987 for details on this method). Scales of the variables are missing but will be added in another version.

General Conclusions and Perspectives

The analysis of more than 4 years of velocity data at the surface in two locations, 23ºW and 10ºW, showed three principal types of quasi periodic oscillations in the intraseasonal band. The first oscillation was observed in the zonal velocity component near the surface as well as at intermediate depths, had a period of about 7 days, and occurred indistinctly along the year. In 2002, the 7 day period oscillations were particularly interesting since they had a strong signature in temperature records as well. The temperature 7-day period oscillation was strongest at the thermocline depth, suggesting the existence of a vertical component in the 7-day period signal.

The second oscillation had a period between 11 and 15 days, occurred in boreal spring and was forced by winds presenting the same periodicity. In 2000, the signature of this wave is detected as deep as 1000 m. Depending on the year, the 11 to 15 day period oscillation showed a SST signature as well. In 2004, the SST signature was particularly strong and we were able to estimate a zonal scale of about 30 degrees of longitude and to see a clear antisymmetric SST structure about the equator. This particular oscillation in 2004 presented no propagation and was consistent with a standing, second baroclinic mode, mixed Rossby-gravity wave.

The third type of intraseasonal quasi-periodic oscillation had a period of about 20 to 30 days. They occurred principally in boreal summer and fall but under exceptional conditions they were also observed in winter. These waves, better known as TIWs, presented a strong SST signature. The simultaneous analysis of SST and velocity data in the year 2002 showed that unlike the Pacific Ocean, the TIW in the Atlantic share the same period in temperature and current velocity time series. The TIW-SST signature was not the same at all locations: east of 10ºW the SST anomalies showed no propagation and larger zonal scales than west of 10ºW. Moreover, the

propagation patterns at the equator, in the center of the basin, changed with time. These variations in the TIW-SST anomalies suggest the possibility of different types of TIWs.

The three quasi-periodic oscillations mentioned above presented variations from year to year. A full comparison between similar oscillations at different years is planned. Several questions arise. Is the 7-day period oscillation in the zonal component always related to fluctuations in subsurface temperature? What are the differences between 13-day period oscillations at the surface and at the subsurface? Are they all forced by the winds? Are they related? How deep do they reach? When do the 13-day period oscillations have an SST signature as well? Do we observe the same kind of TIW-SST anomalies detected in 2002 in other years? How do results about TIW from 2002 compare with datasets at 23ºW and 10ºW for the years 2004-2005? Indeed, the signals in the last data set (2003 to 2005) have only been partially explored.

The analysis of velocity measurements at intermediate depths (600 m-1700 m) showed a wide range of variability, and different spectral contents for the two horizontal velocity components, with zonal motions being dominated by larger periods than the meridional motions. The meridional component presented quasi-periodic oscillations with 14-day periods in spring and with 20-30 day periods in fall. The simultaneity with oscillations presenting the same periods in the surface suggests that these deep quasi periodic oscillations are the deep expression of forced surface waves. Other oscillations in the meridional component presented periods of approximately 60 days and had no apparent seasonal pattern. The 60-day period oscillations are consistent with mixed Rossby-gravity waves forced by the Deep Western Boundary Current as found by D'Orgeville et al. (2006). The meridional velocity component also showed long period fluctuations (~ 10 months) but only at 23ºW. These flows had vertical scales of about 600 m and

upward phase propagation. Their presence, restricted to 23ºW, suggest that they could be the result of scattered Kelvin waves in the presence of the Mid Atlantic Ridge.

The zonal velocity component presented a seasonal cycle of large vertical scale (between 2190 m and 3066 m) and maximum amplitudes of 10 cm/s. On top of the seasonal cycle, EDJ were detected. Estimations of the time scales for EDJ gave three different values; 7 months, 18 months and 5 years. The two last ones were detected simultaneously, with the 18 months EDJ signal showing downward phase propagation. The diversity of time scales as well as vertical structures (standing mode vs. vertically propagating waves) implies a rather complex vertical and temporal behavior for the EDJs system. Again, several questions arise. Are all intermediate depths subject to the same EDJ time scales? The data suggests that EDJ around 1000 m have shorter time scales than EDJ at around 1500 m, but results are not conclusive. Does the Mid Atlantic Ridge affect the EDJ? What are the implications of meridional flows at 23°W in the interhemispheric water exchanges? Since data at intermediate depths are scarce, these questions will have to be addressed either by new data sets of long duration or by models capable of reproducing realistic EDJs.

References

Boebel, O., C. Schmid and W. Zenk, 1999: Kinematic elements of Antarctic Intermediate Water in the western South Atlantic. *Deep-Sea Res*. II, **46**, 355-392.

Böning, C. W., and J. Kröger, 2005: Seasonal variability of deep currents in the equatorial Atlantic: a model study. *Deep-Sea Res.* I, **52**, 99-121.

Bourlès, B., M. D'Orgeville, G. Eldin, Y. Gouriou, R. Chuchla, Y. DuPenhoat and S. Arnault, 2002: On the evolution of the thermocline and subthermocline eastward currents in the Equatorial Atlantic. *Geophys. Res. Lett.*, **29,** No. 16, doi:10.1029/2002GL015098.

Bourlès, B., C. Andrié, Y. Gouriou, G. Eldin, Y. du Penhoat, S. Freudenthal, B. Dewitte, F. Gallois, R. Chuchla, F. Baurand, A. Aman, and G. Kouadio, 2003: The deep currents in the Eastern Equatorial Atlantic Ocean. *Geophys. Res. Let*., **30**, 5, doi:101029/2002GLO15095.

Brandt, P., and C. Eden, 2005: Annual cycle and interannual variability of the mid-depth tropical Atlantic Ocean. *Deep-Sea Res*. I, **52**, 199-219.

Brandt, P., F. Schott, C. Provost, A. Kartavtseff, V. Hormann, B. Bourlès and J. Fischer, 2006: Circulation in the central equatorial Atlantic: Mean and intraseasonal to seasonal variability. *Geophys. Res. Lett.*, **33**, L07609, doi:10.1029/2005GL025498.

Bunge, L., C. Provost, J. M. Lilly, M. D'Orgeville, A. Kartavtseff and J.-L. Melice, 2006: Variability of the horizontal velocity structure in the upper 1600 m of the water column on the equator at 10°W. *J. Phys. Oceanogr*., **36**, 7, 1287-1304.

Caltabiano, A. C. V., I. S. Robinson, and L. P. Pezzi, 2005: Multi-year satellite observations of instability waves in the Tropical Atlantic Ocean. *Ocean Science Discussions*, **2**, 1-35.

Chelton, D. B., F. J. Wentz, C. L. Gentemann, R. A. de Skoeze and M. G. Schlax, 2000: Satellite microwave SST observations of transequatorial tropical instability waves. *Geophys. Res. Lett.,* **27**, 1239-1242.

Chiang, J.C.H., Y. Kushnir, and A. Giannini, 2002: Deconstructing Atlantic ITCZ variability: influence of the local cross-equatorial SST gradient, and remote forcing from the eastern equatorial Pacific. *J. Geophys. Res.*, **107**, 10.1029/2000JD000307.

Colin, C., and S. Garzoli, 1998: High frequency variability of in situ wind, temperature and current measurements in the equatorial Atlantic during the FOCAL/ SEQUAL experiment. *Oceanologica Acta,* **11,** 139-148.

Contreras, R. L., 2002: Long-term observations of tropical instability waves. *J. Phys. Oceanogr*., **32**, 9, 2715-2722.

Delprat, N., B. Escudié, P. Guillemain, R. Kronland-Martinet, P. Tchamitchian, and B. Torrésami, 1992: Asymptotic wavelet and Gabor analysis: extraction of instantaneous frequencies. *IEEE Trans. Inform. Theory,* **38**(2), 644-665.

Dengler, M., F. A. Schott, C. Eden, P. Brandt, J. Fischer, and R. J. Zantopp, 2004: Break-up of the Atlantic deep western boundary current into eddies at 8ºS (letter). *Nature*, **432** (7020), 1018-1020.

D'Orgeville, M., B. L. Hua, and H. Sasaki, 2006: Equatorial deep jets triggered by a large vertical scale variability within the western boundary layer. *J. Mar. Res.*, submitted.

Eriksen, C. C., 1985: Moored observations of deep low-frequency motions in the central Pacific Ocean: vertical structure and interpretation as equatorial waves. *J. Phys. Oceanogr*., **15**, 1085-1113.

Firing, E., 1987: Deep zonal currents in the central equatorial Pacific. *J. Mar. Res*., **45**, 791-812.

Foltz, G.R., and M. J. McPhaden, 2004: 30-70 day oscillations in the tropical Atlantic. *Geophys. Res. Lett.*, **31,** L15205, doi:10.1029/2004GL020023.

Garzoli, S. L., 1987: Forced oscillations on the equatorial Atlantic basin during the Seasonal Response of the Equatorial Atlantic Program (1983-1984). *J. Geophys. Res*., **92**, 5089-5100.

Ghil, M., R. M. Allen, M. D. Dettinger, K. Ide, D. Kondrashov, M. E. Mann, A. Robertson, A. Saunders, Y. Tian, F. Varadi, and P. Yiou, 2002: Advanced spectral methods for climatic time series, *Rev. Geophys.*, **40** (1), 1003, doi:10.1029/2000RG000092.

Giarolla, E., P. Nobre, M. Malagutti, and L. P. Pezzi, 2005: The Atlantic Equatorial Undercurrent: PIRATA observations and simulations with GFDL Modular Ocean Model at CPTEC. *Geophys. Res. Lett.*, **32**, L10617, doi:10.1029/2004GL022206

Gill, A. E., 1982: Atmosphere-Ocean Dynamics, Academic Press, New York, 661p.

Gouriou, Y., B. Bourlès, H. Mercier, R. Chuchla, 1999: Deep jets in the equatorial Atlantic Ocean. *J. Geophys. Res.*, **104**, C9, 21217-21226.

Gouriou Y., C. Andrié, B. Bourlès, S. Freudenthal, S. Arnault, A. Aman, G. Eldin, Y. du Penhoat, F. Baurand, F. Gallois, and R. Chuchla, 2001: Deep circulation in the Equatorial Atlantic ocean. *Geophys. Res. Letters*, **28**, 819-822.

Grodsky, S. A., and J. A. Carton, 2001: Coupled land/atmosphere interactions in the West African Monsoon. *Geophys. Res. Letters*, **28**, 1503-1506.

Grodsky, S. A., J. A. Carton, and S. Nigam, 2003: Near surface westerly wind jet in the Atlantic ITCZ. *Geophys. Res. Letters*, **30,** 19, 2009, doi: 10.1029/2003GL017867.

Grodsky, S. A., J. A. Carton, C. Provost, J. Servain, J. A. Lorenzzeti, and M. J. McPhaden, 2005: Tropical instability waves at 0ºN, 23ºW in the Atlantic: A case study using Pilot Research Moored Array in the Tropical Atlantic (PIRATA) mooring data. *J. Geophys. Res*., **110**, C08010, doi: 10.1029/2005JC002941

Han, W., 2004: Impact of Atmospheric Intraseasonal Variability in the Indian Ocean: Low-Frequency Rectification in Equatorial Surface Current and Transport. *J. Phys. Oceanogr.*, **34**, 6, 1350–1372.

Hastenrath, S., 1984: Interannual variability and annual cycle: mechanisms of circulation and climate in the Tropical Atlantic sector, *Mon. Weath. Rev.,* **112**, 6, 1097-1107.

Houghton R. W., and C. Colin, 1987: Wind driven meridional eddy heat flux in the Gulf of Guinea. *J. Geophys. Res.*, **92**, 10777-10786.

Hua, B. L., M. D'Orgeville, C. Menesguen, and H. Sasaki, 2006: Destabilization of mixed Rossby-gravity waves and equatorial zonal jets formation. *J. Fluid Mech.* (submitted).

Hua, B.L., D. W. Moore, and S. Le Gentil, 1997: Inertial non-linear equilibration of equatorial flows. *J. Fluid. Mech.*, **331**, 345-371.

Jochum, M, P. Malamotte-Rizzoli and A. Busalacchi, 2004: Tropical instability waves in the Atlantic Ocean. *Ocean Modelling*, **7**, 145-163.

Johnson G. C., and D. Zhang, 2002: Structure of the Atlantic Ocean equatorial deep jets. *J. Phys. Oceanogr.*, **33**, 600-609.

Kartavtseff, A., 2002: Mouillages EQUALANT, Rapport interne LODYC n. 2002-02.

Kartavtseff, A., 2003: Mouillages courantométriques à l'équateur à 23W et 10W Déc. 2001 – Jan 2003. Rapport interne LODYC, Université de Paris VI.

Kartavtseff, A., 2004 : Mouillage courantométrique PIRATA 10º W, Rapport interne LODYC n. 2004-04.

Kartavtseff, A., 2006: Mouillages courantométriques PIRATA 10º W et 23º W, Rapport interne LOCEAN n. 2006-03.

Kessler, W.S., 2004: Intraseasonal variability in the oceans. In: *Intraseasonal Variability of the Atmosphere–Ocean System*. W.K.M. Lau and D.E. Waliser (eds.). Praxis Publishing.

Legeckis, R. and G. Reverdin, 1987: Long waves in the equatorial Atlantic Ocean during 1983. *J. Geophys. Res*., **92**, 2835-2842.

Lumpkin, R., and S. L. Garzoli, 2005: Near-surface Circulation in the Tropical Atlantic Ocean. *Deep-Sea Res.* I, **52** (3), 495-518, 10.1016/j.dsr.2004.09.001.

Luther, D.S. and E.S. Johnson, 1990: Eddy energetics in the upper equatorial Pacific during the Hawaii-to-Tahiti shuttle experiment, *J. Phys. Oceanogr.*, **20**, 913-944.

Luyten, J. R., and J. C. Swallow, 1976: Equatorial undercurrents. *Deep-Sea Res*., **23**, 999-1001.

Lyman, J. M., G. C. Johnson and W. S. Kessler, 2006: Distinct 17-day and 33-day Tropical Instability Waves in subsurface observations. *J. Phys. Oceanogr*., accepted.

Madden, R. A., and P. R. Julian, 1994: Observations of the 40-50 day tropical oscillation: a review. *Mon. Wea. Rev.*, **122,** 814-837.

Mallat, S., 1999: A wavelet tour of signal processing, Academic Press, 2nd edition, San Diego, 637p.

McCreary J.P. and Z. Yu, 1992: Equatorial dynamics in a 2½-layer model. *Prog. Oceanogr.*, **29**, 61-132.

McPhaden, M. J. and A. E. Gill, 1986: Topographic scattering of equatorial Kelvin waves. *J. Phys. Oceanogr.*, **17**, 82-96.

McPhaden, M.J. and X. Yu, 1999: Equatorial waves and the 1997-98 El Nino. *Geophys. Res. Lett.*, **26**, 2961-2964.

Menkes, C. E., S. C. Kennan, P. Flament, and coauthors, 2002: A whirling ecosystem in the equatorial Atlantic. *Geophys. Res. Lett*., **29**, 48, 1-4.

Mercier, H., and K. G. Speer, 1998: Transport of bottom water in the Romanche fracture zone and the Chain fracture zone. *J. Phys. Oceanogr.*, **28,** 779-790.

Merle, J., 1980: Variabilité thermique annuelle et interannuelle de l'océan Atlantique équatorial Est - l'hypothèse d'un « El Niño » Atlantique. *Oceanol. Acta*, **3**, 2, 209-220.

Miyama, T., J. P. McCreary, D. Sengupta, and R. Senan, 2006: Dynamics of biweekly oscillations in the equatorial Indian Ocean. *J. Phys. Oceanogr.*, in press.

Molinari R.L., S.L. Garzoli, and R.W. Schmitt, 1999: Equatorial currents at 1000 m in the Atlantic Ocean. *Geophys. Res, Lett.*, **26**, 361-363.

Muench, J. E., E. Kunze, and E. Firing, 1994: The potential vorticity structure of equatorial deep jets. *J. Phys. Oceanogr.*, **24,** 418-428.

Nobre P. and J. Shukla (1996), Variations of sea surface temperature, wind stress, and rainfall over the tropical Atlantic and South America, *J. Climate, 9*, 2464-2479.

Okumura, Y. and S. Xie, 2006: Some overlooked features of tropical Atlantic climate leading to a new Niño-like phenomenon. *J. Climate*, in press.

Olhede, S. C., and A. T. Walden, 2002: Generalized Morse wavelets. *IEEE Trans. Sig. Proc.* **50**, (11), 2661-2670.

Ollitrault, M., M. Lankhorst, D. Fratantoni, P. Richardson, and W. Zenk, 2006: Zonal intermediate currents in the equatorial Atlantic Ocean. *Geophys. Res. Lett.*, **33**, L05605, doi: 10.1029/2005GL025368, 2006.

Paiva, A.M., J.T. Hargrove, E.P. Chassignet, and R. Bleck, 1999: Turbulent behavior of a fine mesh (1/12 degree) numerical simulation of the North Atlantic. *J. Mar. Sys.*, **21**, 307-320.

Park, J., C. R. Lindberg and F. L. Vernon III, 1987: Multitaper spectral analysis of high frequency seismograms. *J. Geophys. Res.*, **92**, B12, 12675-12684

Percival, D. B., and A. T. Walden, 1993: Spectral Analysis for Physical Applications –Multitaper and Conventional Univariate Techniques, Cambridge Univ. Press, New York, 580 pp.

Philander, S. G. H., 1990: El Nino, La Nina, and the Southern Oscillation, Academic Press, 289 pp.

Picaut, J., 1983: Propagation of the Seasonal Upwelling in the Eastern Equatorial Atlantic, *J. Phys. Oceanogr*., **13**, 18-37.

Ponte, R.M., J. Luyten, and P. L. Richardson, 1990: Equatorial deep jets in the Atlantic Ocean. Deep-Sea Res., 37, 711-713.

Provost, C., S. Arnault, N. Chouaib, A. Kartavtseff, L. Bunge and E. Sultan, 2004: Equatorial pressure gradient in the Atlantic in 2002: TOPEX/Poseidon and Jason versus the first PIRATA current measurements, *Mar. Geodesy*, **27**, 13774-13769.

Provost C., N. Chouaib, A. Spadone, L. Bunge, S. Arnault, and E. Sultan, 2006: Interannual variability of the zonal sea surface slope at the equator in the Atlantic in the 1990's. *J. Adv. Space Res*., **37**, 4, 823-831. doi:10.1016/j.asr.2005.06.018

Richardson, P.L., and D. Walsh, 1986: Mapping climatological seasonal variations of surface currents in the tropical Atlantic using ship drifts. *J. Geophys. Res.*, **91**, 10,537-10,550.

Richardson, P.L., and W.J. Schmitz, 1993: Deep cross-equatorial flow in the Atlantic measured with SOFAR floats. *J. Geophys. Res.*, **98**, 8371-8387.

Richardson, P. L., and D. M. Fratantoni, 1999: Float trajectories in the deep western boundary current and deep equatorial jets of the tropical Atlantic. *Deep-Sea Res. II*, **46**, 305-333.

Schmid, C, Z. Garraffo, E. Johns, and S.L. Garzoli, 2003: Pathways and variability at intermediate depths in the tropical Atlantic. In "Interhemispheric Water Exchange in the Atlantic Ocean", edited by G. Goni and P. Malanotte-Rizzoli, 233-268.

Schmid, C., B. Bourlès, and Y. Gouriou, 2005: Impact of the equatorial deep jets on estimates of the zonal transports in the Atlantic. *Deep-Sea Res. II*, **52,** 409-428.

Schott, F.A., M. Dengler, P. Brandt, K. Affler, J. Fischer, B. Bourlès, Y. Gouriou, R.L. Molinari, and M. Rhein, 2003: The zonal currents and transports at 35ºW in the tropical Atlantic. *Geophys. Res. Lett*. **30**, 7, 1349, doi: 10.1029/2002GL016849.

Send, U., C. Eden, and F. Schott, 2002: Atlantic equatorial deep jets: Space-time structure and cross-equatorial fluxes. *J. Phys. Oceanogr*., **32**, 891-902.

Sengupta, D., R. Senan, V.S.N. Murty, and V. Fernando, 2004: A biweekly mode in the equatorial Indian Ocean, *J. Geophys. Res*., doi: 10.1029/2004JC002329.

Thierry, V., 2000: Observation et modélisation de la variabilité saisonnière dans l'océan Atlantique équatorial profond, PhD Thesis, Université de Bretagne Occidentale, 203p.

Thierry, V., A. M. Treguier, and H. Mercier, 2006: Seasonal fluctuations in the deep central equatorial Atlantic Ocean: a data-model comparison. *Ocean Dynamics*, doi: 10.1007/s10236-005-0045-y.

Thomson, D. J., 1982: Spectrum estimation and harmonic analysis, Proc. IEEE, 70, 1055-1096.

Vangriesheim, A., A. M. Treguier and G. Andre, 2005: Biweekly current oscillations on the continental slope of the Gulf of Guinea. *Deep-Sea Res.*, **52**, (11), 2168-2183.

Wacongne, S., 1989: Dynamic regimes of a fully non linear stratified model of the Atlantic Equatorial Undercurrent. *J. Geophys. Res.*, **94,** 4801-4815.

Weisberg, R. H., A. M. Horigan, and C. Colin, 1979: Equatorially trapped Rossby-gravity wave propagation in the Gulf of Guinea. *J. Mar. Res.*, **37**, 1, 67-86.

Weisberg, R. H., and A. M. Horigan, 1981: Low-frequency variability in the equatorial Atlantic. *J. Phys. Oceanogr.*, **11**, 913-920.

Weisberg, R. and Colin, 1986: Equatorial Atlantic ocean temperature and current variations during 1983 and 1984. *Nature*, **322**, 240-243.

Weisberg, R. H., 1984: Instability waves observed on the equator in the Atlantic Ocean during 1983. *Geophys. Res. Letters*, **11**, 753-756.

Weisberg, R. H., and T. J. Weingartner, 1988: Instability waves in the equatorial Atlantic Ocean. *J. Phys. Oceanogr.*, **18,** 1641-1657.

Xie, S.–P., and J. A. Carton, 2004: Tropical Atlantic variability: patterns, mechanisms, and impacts. In *Ocean Atmosphere Interactions and Climate Variability*, edited by C. Wang, S.-P. Xie and J. A. Carton, AGU Press.

Zhu, X. H., A. Kaneko, N. Gohda, H. Inaba, K. Kutsuwada and M. H. Radenac, 1998: Observation of mixed Rossby-gravity waves in the western Equatorial Pacific. *J. Oceanogr*., **54**, 133-141.